

UNIVERSITA' DEGLI STUDI DI VERONA



DEPARTMENT OF

Neurosciences, Biomedicine and Movement Sciences

GRADUATE SCHOOL OF

Life and Health Sciences

DOCTORAL PROGRAM IN

Life and Health Applied Sciences

WITH THE FINANCIAL CONTRIBUTION OF

Aptuit Verona, an Evotec Company

Cycle / year (1° year of attendance) XXXIII/ 2017

TITLE OF THE DOCTORAL THESIS

**Characterization of an *in vitro* 3D Human Small Airway
Epithelia model for the application of integrated
strategies in inhaled drug development**

S.S.D. BIO13

(Please complete this space with the S.S.D. of your thesis – mandatory information)*

Coordinator: Prof. Giovanni Malerba

Signature _____

Tutor: Prof.ssa Maria Grazia Romanelli

Signature _____

Doctoral Student: Dott./ssa Illaria Masotto

Signature _____

*When your determination changes,
everything will begin to move in the direction you desire.
The moment you resolve to be victorious, every nerve and fiber
in your being will immediately orient itself toward your success.
On the other hand, if you think, "This is never going to work out,"
then at that instant every cell in your being will be deflated and give up the fight.*

Daisaku Ikeda

Table of Contents

1	ABSTRACT	9
2	INTRODUCTION AND BACKGROUND	11
2.1	The 3Rs principles and integrated approaches to testing and assessment (IATA).....	13
2.2	Respiratory tract anatomy and physiology.....	17
2.3	<i>In vivo</i> models for inhaled compounds studies	24
2.4	<i>In vitro</i> cell-models	25
2.5	Lung Toxicity.....	33
2.6	Factors affecting drug delivery to the lungs	34
2.6.1	The Muco-ciliary Clearance (MCC)	35
2.6.2	Phagocytosis by Alveolar Macrophages.....	37
2.6.3	Lung metabolism.....	37
2.7	Mechanisms of drug transport across the lung barrier....	39
2.8	Exposure System.....	44
3	AIM OF THE PROJECT	49
4	MATERIALS AND METHODS	50
4.1	Materials	50
4.2	Test System	51
4.2.1	<i>SmallAir™ 3D Model</i>	51
4.2.2	<i>A549 Cell Model</i>	52
4.3	Methods	52
4.3.1	<i>Acute Toxicity Assay Protocol</i>	52
4.3.2	<i>Viability Assay – Resazurin Test</i>	55
4.3.3	<i>Trans-epithelial electrical resistance (TEER) measurement</i>	56
4.3.4	<i>SmallAir™ Hystology</i>	57
4.3.5	<i>Permeability Assay</i>	58
4.3.6	<i>Phospho-SMAD2 (p-SMAD2) measurement</i>	66
4.3.7	<i>Cytokines and pro-inflammatory mediators measurement</i>	67
4.3.8	<i>Lactate Dehydrogenase (LDH) assay</i>	67
4.3.9	ROS measurement	68
4.3.10	<i>Muco-ciliary Clearance Assay</i>	70
4.3.11	<i>MPPD prediction analysis</i>	73
5	RESULTS	75
5.1	Acute Toxicity Assessment	75
5.1.1	Histology Observation	86
5.2	Transport Evaluation (Permeability)	88
5.2.1	Permeability studies in <i>SmallAir™</i> - liquid treatment	90
5.2.2	Permeability studies in <i>SmallAir™</i> - aerosol treatment...	92
5.2.3	Permeability studies in <i>SmallAir™</i> - powder treatment...	96
5.3	Inflammatory mediators assessment.....	97
5.3.1	pSMAD2 assessment.....	97
5.3.2	Cytokines release, ROS and LDH release	98
5.3.3	pSMAD2 analysis.....	99
5.3.4	Cytokines, LDH release and ROS evaluation.....	100

5.4	Muco-ciliary Clearance Assessment	104
5.4.1	Results of Automatic and Manual methods evaluation.	105
5.4.2	Effect of agonists and inhibitor on MCC	109
5.4.3	Effect of drug compounds on MCC	113
5.4.4	MPPD simulation	120
6	DISCUSSION	123
6.1	Acute toxicity Assessment.....	123
6.2	Transport Evaluation (Permeability)	124
6.3	Inflammatory Mediators assessment.....	126
6.4	Muco-ciliary clearance	127
6.5	In silico Prediction	129
7	CONCLUSION	132
8	AKNOWLEDGMENTS	135
9	REFERENCES.....	136

List of Abbreviation

3D	Three dimensional
ADME	Absorption Distribution Metabolism
ALI	Air-Liquid Interface
AM	Alveolar Macrophages
AO	Adverse Outcome
AOP	Adverse Outcome Pathway
ASL	Air Surface Liquid
AT-I	Alveolar Type I Cells
AT-II	Alveolar Type II Cells
BEAS-2B	Bronchial Epithelial Cell Line
BCRP	Breast cancer resistance protein
BCA kit	Bicinchoninic Acid Assay protein
CaCl ₂	Calcium Chloride
cAMP	Adenosine 3,5-Cyclic Monophosphate
Ca ²⁺	Calcium Ions
CBF	Cilia Beating Frequency
CCH	Carbachol
CdCl ₂	Cadmium Chloride
CF	Cystic fibrosis
CFTR	Cystic fibrosis transmembrane conductance
CFTR	Cystic fibrosis transmembrane conductance Inhibitor-172
cGMP	Guanosine 3,5-cyclic monophosphate
COPD	Chronic obstructive pulmonary disease
CYP450	Cytochrome P450
cldn	Claudin
DMSO	Dimethyl sulfoxide
DPI	dry-powder inhaler
EMA	European Agency for the Evaluation of
ENaC	Epithelial sodium channels
EPDExS	Electrostatic Particulate Dosage and Exposure
ER	Efflux Ratio
EXTN	Eotaxin
FDA	Food and Drug Administration
FMO	Flavin-Containing Monooxygenases
FRSK	Forskolin
GAM- plate	Goat Anti Mouse plate

GRO	Growth-regulated oncogene chemokines
HBSS	Hank's Balanced Salt Solution
HBSSH	Hank's Balanced Salt Solution with HEPES
HPLC-MS/MS	high performance liquid chromatography coupled with mass spectrometry analysis
HPLC-UV	high performance liquid chromatography coupled with ultra violet analysis
IATA	Integrated Approaches to Testing and
ICH	International Conference on Harmonization
IL-4	Interlukine-4
IL-6	Interlukine-6
IL-8	Interlukine-8
MIP-1 β	Macrophage inflammatory protein-1 β
ICRP	International Commission on Radiological Protection
IP-10	Interferon gamma-induced protein 10
IS	Integrated Strategy
ITS	Integrated Testing Strategy
LDH	Lactate Dehydrogenase
LY	yellow luciferase marker
LPS	Lipopolysaccharide
LC-MS/MS	liquid chromatography coupled with mass
L/min	Liter per minute
MAO	Monoamine Oxidase
Mg ²⁺	Magnesium Ions
MCC	Muco-ciliary Clearance
MIE	Molecular Initiating Event
MIP-1 β	Macrophage inflammatory protein 1 β
MOA	Mode of Action
MRP	Multidrug resistance-related protein
MSD-based assay	Meso Scale Discovery's Assay
MPPD	multiple-path particle dosimetry model
NACIVT	Nano Aerosol Chamber for In Vitro Toxicity
NAD ⁺	Nicotinamide adenine dinucleotide oxidized
NADH	Nicotinamide adenine dinucleotide reduced
NCEs	New Chemical Entities
NCRP	National Council on Radiation Protection and Measurements
NGI	Next Generation Impactor
OAT	Organic anion transporters

OATP	Organic anion transporting polypeptides
OCT	Organic cation transporters
OCTN	Organic cation/carnitine transporters
OECD	Organisation for Economic Co-operation and
Papp	apparent permeability
p-SMAD2	Phospho- Small Mothers Against
PEPT	Oligopeptide transporters
PNECs	Pulmonary neuroendocrine cells
P-gp	P-glycoprotein
PK	Pharmacokinetic
QSAR	Quantitative Structure Activity Relationship
RFU	relative fluorescence unit
RANTES	Regulated upon Activation, Normal T cell
RPMI	Roswell Park Memorial Institute 1640
SAECs	Small Airway Epithelial Cells
SLC	Solute carrier
SMAD	Small Mothers Against Decapentaplegic
SD	standard deviation
SMGs	Submucosal glands
TBST	Tris Buffer Saline with Tween 20
TB Clearance	tracheal-bronco clearance
TEER	Trans-epithelial electrical resistance
TGF- β	Transforming growth factor beta
tSMAD2	Total SMAD2
TJ	Tight junctions
Ω	Ohm

1 ABSTRACT

Drug Inhalation is one of the most effective administration routes; in fact, first pass metabolism is bypassed, rapid action onset is enabled and drug doses can be kept relatively low compared to other administration routes.

The most recent 3D *in vitro* models allow to mimic some of the pulmonary tissue functionalities. These models reproduce the air-liquid interface, with beating cilia and mucus production, since different types of cells are present. Therefore, these models could be possibly applied to multi-disciplinary investigations following liquid, dry powder or aerosol treatment.

In this thesis, an integrated strategy is proposed, with the aim to increase the rate of success in the drug candidate selection phase. Ideally, safety data should be integrated with early pharmacokinetics (PK) and efficacy indications in order to increase chances to select the candidate with the highest safety margins. With this ambitious objective in mind, a human-based 3D model were evaluated as model for the toxicity assessment and drug permeability evaluation; some examples of the initial work previously conducted by other authors under the supervision of myself and other colleagues will be discussed (Pomari, 2019; Sembeni, 2020).

In particular, a commercially available 3D respiratory model SmallAir™ has been qualified for: a) sensibility and specificity in the evaluation of lung toxicity potential of new compounds; b) permeability to test drug transport through tissues for formulation screening purposes; c) quantitative cytokine secretion on cell supernatant; d) cilia beating and muco-ciliary clearance evaluation by image analysis.

These tests performed on a human tissue could provide more reliable results also because all tests were performed in the same model and this could be helpful in data integration. This approach could allow to fill gaps in drug discovery for human-relevant screening of new chemical entities (NCEs), best formulation selection, including physiochemical equivalence evaluation generic drug development. *In vitro* and *in silico* data can be helpful in predicting PK and toxicity profiles prior to

preclinical and clinical studies. This allows to respect the 3Rs principle of replacement, reduction and refinement of *in vivo* studies. The proposed integrated testing strategy (ITS) has the potential to reduce the attrition in drug development, to optimize the inhaled formulation, to screen compounds for candidate selection and to reduce *in vivo* studies.

For the toxicity tests, well-known respiratory toxic compound were tested both in the SmallAir™ model and in the A549 cell line model. On the basis of results, the SmallAir™ model seemed to be less sensitive than A549, probably due to the 3D structure physiological features. Cilia beating and mucus production can indeed protect the cells from the toxic effect miming the *in vivo* response.

For the permeability study, well-known inhalation compounds with very different permeability values were evaluated both in SmallAir™ model and in the standard Caco2 cell model. For low and high permeable compounds results obtained were comparable in the two test considered systems. The most evident difference was observed with medium permeable compounds, suggesting that the SmallAir™ model should express different efflux pumps on their surface form the standard Caco2 cell model.

The SmallAir™ model was also evaluated as *in vitro* model for the inflammatory mediators assessment. The treatment with TGF- β allowed to confirm the activation of the signalling via Smad2 while, inconclusive results were obtained with regards to cytokines and ROS release following Bleomycin treatment.

The SmallAir™ model was finally evaluated as *in vitro* model for the assessment of the Muco-ciliary Clearance (MCC). Results obtained in this project, showed that the SmallAir™ can be a promising model to assess the MCC *in vitro* after treatment with compound acting on ATP release and Cystic fibrosis transmembrane conductance Inhibitor-172 (CFTR172inh).

More test considering different compound, study design and end points has to be conducted, in order to identify a human relevant *in vitro* lung model to be applied in many fields of analysis.

2 INTRODUCTION AND BACKGROUND

Respiratory drug delivery has raised a very strong interest within the pharmaceutical field. Inhalation therapy has been primarily applied for the treatment of respiratory diseases. Inhalation therapies are extensively used in asthma, chronic obstructive pulmonary disease (COPD) and cystic fibrosis therapies. For local effects, inhaled drugs are delivered directly to the site of action in the lung, providing fast onset of action (within 5 minutes) (Hou et al., 2015). The lung has been used as an administration route for systemic delivery of anesthetics and many other therapeutic and recreational drugs (Gonda, 2000). Different reasons lead to an increased interest in the respiratory administration route, including the emergence of biotherapeutics that have delivery issues (i.e. their large molecular size, hydrophilicity and lability make difficult their formulation in traditional oral dosage forms such as tablets and capsules) (Agu et al., 2001) and a better understanding of the absorption properties of the lungs. Great exposure surface, high permeability, relatively low metabolic capacity and a rich blood supply make the lungs a suitable alternative non-invasive route for systemic drug administration (Chan et al., 2014; Forbes et al., 2011). Small molecules can be rapidly adsorbed from the lungs, with high bioavailability. Fast drug delivery is particularly effective to relieve acute symptoms such as pain, migraine and nausea (Farr & Otulana, 2006; Patton & Byron, 2007). For example, in January 2006, the Food and Drug Administration (FDA) and the European Agency for the Evaluation of Medicinal Products (EMA) approved the first inhaled therapeutic macromolecule for systemic delivery, the human insulin (Exubera™), to treat patients with type 1 and type 2 diabetes (Lenzer et al., 2006).

The advances in aerosol and formulation technology, as well as inhaler device technology, now allow to deliver therapeutic molecules to defined lung regions (Anderson et al., 2005). Commercial manufacturing processes are now in place for the production of delivery systems to overcome issues such as high costs and therapeutic limitations of biologics. The inhalation route has been evaluated also for low molecular weight drugs, previously administered by injection, for a faster induction, or to improve the therapeutic ratio for drugs acting in the lung (Gonda, 2000).

Drug discovery to reach the candidate selection is challenging, time consuming and an expensive process. Also, the drug development process is articulated through several stages to assess safety, efficacy, and regulatory compliance (**Error! eference source not found.**).

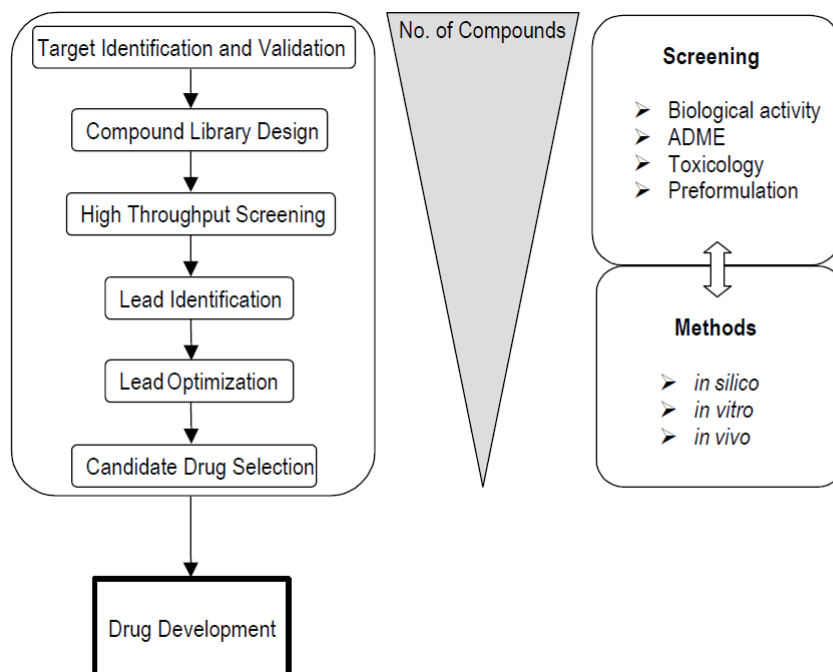


Figure 1. Steps of a generic drug discovery process. A considerable number of compounds discovered in the early phase are screened by appropriate screening models to select the potential candidate drug (Lead Optimization) for possible progression into drug development. The screening process consists of the integration of data obtained with *in silico*, *in vitro* and *in vivo* models (taken from A. Tronde, 2002)

The first step in developing a new drug is the target identification and validation. Thousands of compounds may be potential candidates for the development of a new drug. However, after early testing on a specific target (Hit to Lead phase), only a small number of compounds show to be promising and can proceed for further studies. At this stage, the aim is to maintain the desired properties of lead compounds while improving on possible deficiencies of their structures, with a view to produce a preclinical drug candidate (Lead Optimisation phase). For this process, an integrated approach is recommended. The combination of specialists in

computational chemistry, medical chemistry, drug pharmacokinetic and metabolism, and other research areas can provide unique insights into this late stage of the process (Hughes et al., 2011). Once a compound has proved to be with the desired characteristics, usually described by Target Product Profile, it can be progressed to a development phase. The package of studies in the development phase consists of Absorption/Distribution/Metabolism/Excretion (ADME) studies, physico-chemical characterisation, formulation feasibility studies, toxicity and mutagenicity, dose selection and route of administration. Only if the compound passes all the preclinical test, it is then moved to the first in human clinical trial.

The evaluation of all these properties of the new compound requires *in silico*, *in vitro* and *in vivo* studies.

A large amount of drug discovery programs fails in bringing novel compounds to the market. In particular, unacceptable toxicity in the respiratory tract represents a major issue in the development of inhaled therapies and it has been reported to account for approximately 30% of inhaled project failure (Cook et al., 2014). Usually, respiratory toxicities have been identified at a relatively late stage in preclinical testing (Sivars et al., 2018). Therefore, an early assessment and prediction of toxicity potential can reduce late stage attrition with an impact on the number of animals used.

2.1 The 3Rs principles and integrated approaches to testing and assessment (IATA)

Since drug development is a long and costly process, in order to avoid wasting time, resources and animals, it is desirable to screen out drug candidates that are not suitable for development as potential medicines. Within the drug discovery and development process, laboratory animals' use occurs in a step-wise manner. Pharmacokinetics and pharmacodynamic properties are assessed first, then followed by efficacy studies, before proceeding into candidate selection and regulatory safety testing.

The different stages of the drug development are regulated by the International Conference on Harmonization (ICH) guidelines (e.g., ICH M3(R2)). The aim of

these guidelines is to harmonize the regulatory studies for medicines between the European Union, Japan and the United States. Respiratory drug development entails the standard preclinical toxicology tests, including genotoxicity studies and carcinogenic potential evaluation. In addition to safety assessment studies, *in vivo* pharmacokinetics studies in animals provide data on the outcome of a drug and its metabolites in the body by measurement of the drug concentrations in plasma or tissues. The information obtained during the early characterization of toxic effect is used to estimate an initial safe starting dose and dose range for the human clinical trials. These data together with the toxicological data, are needed for the regulatory submission, prior to starting Phase I clinical trials.

The preclinical studies for the inhalation toxicity evaluation are technologically challenging and expensive. In fact, to expose animals to drugs by inhalation, special equipment, facilities, specific knowledge and skills are needed. Furthermore, the administration via inhalation route requires amounts of test compound larger than that for other routes of administration due to the continuous fresh aerosol delivery and the significant compound waste in the inhalation device.

The conduction of *in vivo* studies is highly regulated. Directive 2010/63/EU (which revises the Directive 86/609/EEC on the protection of animals used for scientific purposes) was adopted on 22nd September 2010. This Directive is firmly based on the principle of the 3Rs, to replace, reduce and refine the use of animals used for scientific purposes, in all aspects of the development, manufacture and testing of medicines.

The adoption of the 3Rs principle not only has an impact on animals, but in some cases, also offers scientific and business benefits by reducing costs and improving efficiency.

Both *in vivo* and *in vitro* models have advantages and disadvantages. The term “model” implies an approximation of the human patho-physiology. The cell culture technologies are the basis of the so-called “alternative” methods. The critical question about the *in vitro* models is how well the cells in culture can mimic the cell behaviours in the organism; similarly, the extent of human relevance needs to be considered also for laboratory animals on a case-by-case basis.

Up to now, models holistic enough to recapitulate the complexity of a tissue or organ as stand-alone are extremely rare, therefore, an integration of different approaches is currently considered as the way forward; in toxicology, this approach is called Integrated Testing Strategies (ITS) (Hartung et al., 2013).

Extrapolation of animal data to predict a human outcome presents numerous challenges due to physiological, anatomical, and metabolic differences across species.

Both scientific and ethical considerations have conducted to significant interest and investment in developing and using reliable human-relevant approaches without the use of animal to assess the toxicity of inhaled substances.

A workshop on “Alternative Approaches for Acute Inhalation Toxicity Testing to Address Global Regulatory and Non-Regulatory Data Requirements” (Clippinger, Allen, Jarabek, et al., 2018) considered current testing requirements and the usefulness of using integrated approaches that combine existing data with *in vitro* and/or computational approaches.

The integration of existing information, the physico-chemical properties of the substances, the expected human exposure, and data from *in vitro* and *in silico* models implemented in the inhaled drug development could help in optimizing the research approach with an impact on 3Rs principle. Furthermore, tiered testing can help in an early identification of highly toxic substances using assays that have higher throughput and are less expensive than *in vivo* studies, followed by more in-depth testing of the remaining substances with more sophisticated *in vitro* methods. The report “Toxicity Testing in the 21st Century: A Vision and Strategy” suggests to transform toxicity testing from a system based on studies in laboratory animals to one established primarily on *in vitro* methods that evaluate changes in normal cellular signalling pathways using human-relevant cells or tissues (Krewski et al., 2010).

Transition to these more predictive approaches requires the production and acquisition of mechanistic data to better characterize biological systems in formalized descriptions. Considerable progress is being made in the explanation of cellular-response networks and connections between pathways consisting of complex interactions of genes, proteins, and small molecules that maintain normal

cellular function and are involved in the cellular response to compound treatment (Krewski et al., 2010). Cellular response pathways that, given a perturbation, are expected to lead to adverse health effects are termed toxicity pathways.

This concept of pathway-based approaches in risk assessment has further evolved in the concept of ‘Adverse Outcome Pathways’ (AOPs). An AOP is a conceptual framework that describes a logical sequential chain of causally linked events at different levels of biological organisation, which follows exposure to a chemical and leads to an adverse health effect (Allen et al., 2014).

Conceptually, an AOP can be considered as a series of essential, measurable events starting with the initial interaction of a stressor with a molecule in a target cell or tissue (i.e., the molecular initiating event, MIE), progressing through an interconnected series of key events at different levels of biological organization (cell, tissue, organ), leading to the manifestation of a toxic event (adverse outcome, AO) in single individuals or in populations (**Error! Reference source not found.**). AOPs showed as a linear series of key events, in fact they constitute interdependent networks of events with feedback loops in which disease outcomes are initiated or modified (Bal-Price & Meek, 2017).

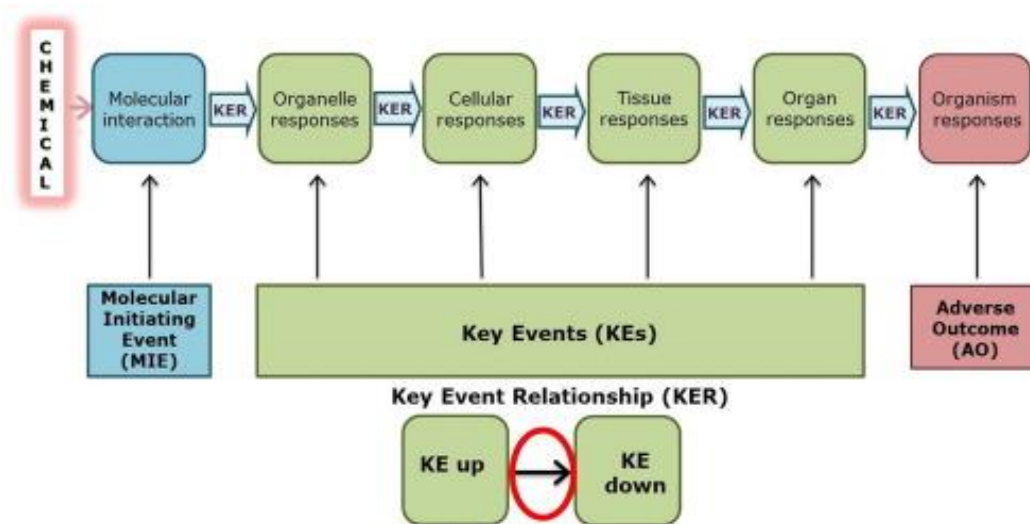


Figure 2. An AOP consists of key events (KEs) and key events relationships (KERs) starting from an initial interaction of a chemical with the biological system (molecular initiating event; MIE) through a sequence of KEs leading to an adverse outcome (AO) of regulatory relevance (taken from Bal-Price A., 2017).

In 2012, the OECD launched a Development Program (<http://www.oecd.org/chemicalsafety/testing/adverse-outcome-pathways-molecular-screening-and-toxicogenomics.htm>) with the subsequent release of a guideline for the description of AOPs (OECD, 2013) and a Handbook (OECD, 2016), which describes best practices for defining, documenting and assessing AOPs in an associated AOP knowledge base (AOP-KB), based on background experience. The AOP approach is conceptually similar to that of mode of action (MOA) defined as a “biologically plausible series of key events leading to an adverse effect”.

Well characterized AOPs may therefore provide a helpful support in data evaluation and integration in targeted and efficient testing strategies, commonly defined as integrated approaches to testing and assessment (IATA) (Worth & Blaauboer, 2018).

IATA are structured approaches that integrate and weight different types of data for the purposes of hazard identification and characterization and/or risk assessment of a chemical (Tollefsen et al., 2014). Based on the phase a IATA is intended for (compound screening and prioritization, risk assessment etc), its composition might be different. In fact, different data requirements, nature of tests (e.g. *in vitro*, *in chemico*, *in vivo*), use of possible non-testing methods (e.g., QSAR, read-across), data integration approaches and acceptable level of uncertainty considerations will drive the IATA.

2.2 Respiratory tract anatomy and physiology

The structure of the mammalian lung is optimized to fulfill its main function of gas exchanging. It is a complex organ and its function as a gas exchanger is directly determined by its microstructure (Weibel, 2017).

The respiratory tract in humans and animals is a complex structure that can be divided into two functional regions: the conducting airway and the respiratory region. The conducting airways consists of: nasal cavity, nasopharynx, larynx, trachea, bronchi and bronchioles. In these regions the air is transported to/from the

lung, filtered, warmed and humidified. The respiratory unit is composed by the lungs with their millions of alveoli and capillaries where the gas exchanging occurs. From trachea to the periphery of the airway tree, the airways repeatedly branch dichotomously into two daughter branches with smaller diameters and shorter length than the parent branch (Weibel, 2017). The whole pulmonary tree is lined by a continuous layer of epithelial cells. The distribution of the epithelial cell types differs significantly, not only between species, but also within the various airway regions of each species (**Error! Reference source not found.**) (Bustamante-Marin Ostrowski, 2017).

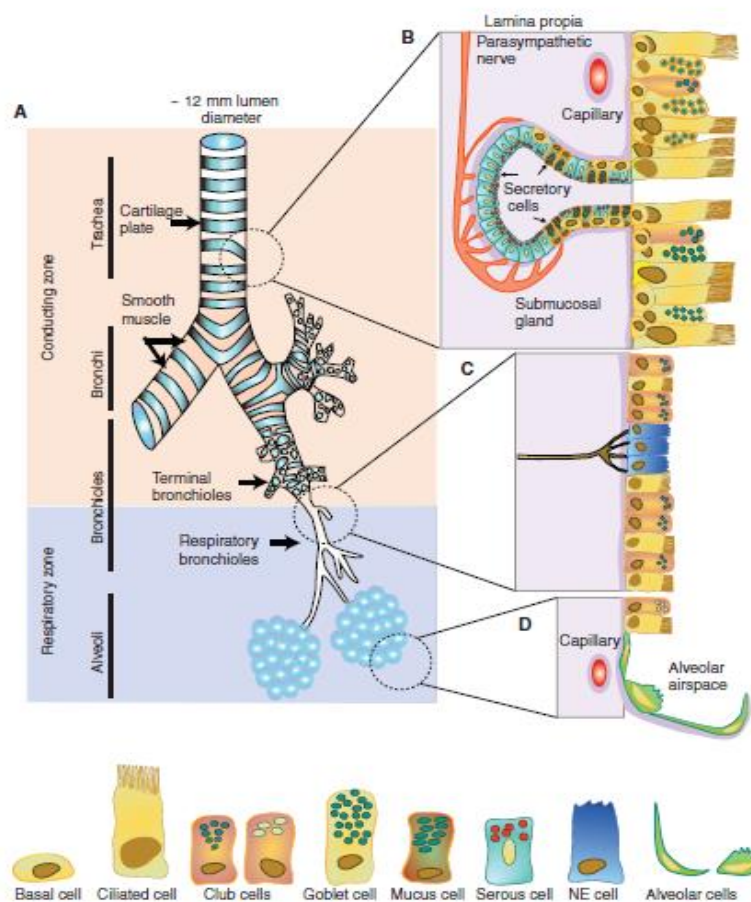


Figure 3. A. Structure of the airways; B. The trachea and most proximally airways are lined by a pseudostratified epithelium formed by ciliated and secretory cells. (C) The small airways are lined by a simple cuboidal epithelium with fewer goblet cells. (D) The alveolar region is made of type I and type II alveolar cells (taken from Bustamante-Marin X.M., 2017).

Air enters the respiratory system through the nose and mouth, travelling to the pharynx and the larynx which opens into the trachea. From the trachea, the air

passes to the bronchi, where branches into the right and left bronchi. Inside the lungs, the bronchi branches into smaller bronchioles until they reach the alveoli.

The air-blood barrier of the gas exchange area is composed of the alveolar epithelial cells (surface area 140 m²) on one side and the capillary bed (surface area 130 m²) on the other side of a thin basement membrane (Tronde, 2002).

The pulmonary epithelium is important for maintaining the normal functions of the respiratory system. As one of the primary interfaces between the organism and the environment, the respiratory system is constantly exposed to airborne particles, potential pathogens, and toxic gases in the inspired air (Plopper, 1996). Therefore, different defense mechanisms are involved, comprising mechanical (i.e. air filtration and muco-ciliar clearance), chemical and immunological defense mechanisms (Tronde, 2002).

Epithelium

The airway consists of more than 40 different cell types and the thickness of epithelial cell layer also varies within different airway regions along with the presence of different cell types (Upadhyay & Palmberg, 2018).

In general, the epithelial cells of the proximal airway can be divided into the surface epithelial cells of the tracheal and bronchial regions and the cells of the submucosal glands.

The epithelium at the level of tracheobronchial tract is composed of ciliated cells, non-ciliated secretory cells, and basal cells. Pulmonary neuroendocrine cells (PNECs) are present both as single cells and in clusters throughout the proximal airway. Submucosal glands (SMGs), characterized by a variable proportion of ciliated cells, mucous cells and serous cells (Chang et al., 2008) is a unique structure of the proximal cartilaginous airway.

Ciliated cells constitute the main element in the conducting airway epithelium. They are covered with cilia and are roughly columnar in shape, with little variations in morphological appearance between species. The ciliated cells are attached to the basal lamina via desmosomes. In humans, the cilia are 0.25 µm in diameter and range from 6 µm in length in the proximal airway to 3.6 µm in seventh generation

airway. Each cilium is anchored to the cell cytoplasm by a basal body through an axoneme (Chang et al., 2008). On their apical surface, the cilia remove inhaled particles trapped in the mucus creating a mucociliary flow.

The ciliated cells are involved in the restoration and regeneration of bronchiolar epithelium after injury (Park et al., 2006).

Basal Cells. The basal cells form a monolayer along the basement membrane and are responsible for the pseudostratified appearance of the epithelium. Basal cells are connected to the basement membrane through hemidesmosomes and provide the base for the attachment of ciliated and non-ciliated columnar cells to the basal lamina. The distribution of basal cells in airway epithelium is different in various airway tracts and in different animal species. Airways larger in diameter have a taller epithelium and more basal cells than airways smaller in diameter with a shorter epithelium.

The first role of the basal cells is to repopulate all the major cell types acting as a stem cell (Hong et al., 2004). Furthermore, evidence indicates that basal cells are involved in regulating physiologic and inflammatory responses of the airway. In response to various inhaled agents, axons in the airway epithelium release neuropeptides into the lateral intercellular space, initiating the process of neurogenic inflammation (increased vascular permeability, neutrophil adhesion, vasodilatation, gland secretion; ion transport; smooth muscle contraction; increased cholinergic transmission; cough) (Van Winkle & Fanucchi, 2009).

Non-ciliated secretory cells: The distribution of non-ciliated secretory cells in tracheobronchial epithelial cell types differs a lot among the species. In humans, ciliated cells predominate and are interspersed with mucus-secreting (goblet) cells (with approximately five ciliated cells for every goblet cell) (Chang et al., 2008). In rats, the most present secretory cell is the serous cell, whereas in rabbits and mice, the Clara cell is the only type of secretory cell in the entire conducting airway (Plopper et al., 1983).

- The Goblet cells are the principal secretory cells situated in the epithelium of the conducting airways, with their apical surfaces protruding into the

lumen. They are intercalated among ciliated cells and connected to adjacent cells by tight junctions; together these cells form a selective barrier lining along the respiratory tract. The morphology of goblet cells is highly polarized, with the nucleus and other organelles localized at the base of the cell. Under healthy conditions, goblet cells, together with submucosal glands, secrete high molecular weight mucous glycoproteins that allow it to properly capture and remove particles, and therefore to protect the epithelial surface. Once trapped, the particles are removed from the airways by the ciliated cells, by a process named muco-ciliary clearance (Alvarado & Arce, 2016; Rogers et al., 1993).

- Another secretory type of cell are the Clara cells (Club cells or non-ciliated bronchiolar secretory cells), which are predominantly present in the terminal and respiratory bronchioles epithelium of mammals including man, and in the upper airways of some species such as mice. Their primary function is to secrete the lung surfactants and other specific proteins that contribute to the ASL (Air Surface Liquid), to serve as progenitor cells for ciliated and secretory epithelial cells and to metabolize xenobiotic compounds. Indeed, Clara cells are able to metabolize xenobiotics through their cytochrome p450 monooxygenase activity, a function that makes them susceptible to injury by lipophilic compounds (Baron et al., 1988).
- The predominant secretory cells in rat surface epithelium are the Surface Serous Cells (Rogers et al., 1993). They morphologically resemble the serous cell type of the submucosal gland, and they have been identified in the human for the first time by Rogers AV et al. in 1993.

In the alveolar region, four cell types are present: the epithelial type I and II cells, alveolar brush cells (type III) and alveolar macrophages (Plopper, 1996).

- Alveolar type I cells (AT-I). The AT-I are large and flat squamous cells. They comprise 95% of the alveolar epithelium and their relatively simple structure allows them to act as a thin, gas-permeable membranes (Rozycki, 2014). These cells are also involved in the maintenance of ion and fluid

balance. The AT-1 contains a number of ion transport channels, including the amiloride-sensitive epithelial sodium channels (ENaC), Cystic fibrosis transmembrane conductance regulator chloride channels (CFTR), and a variety of potassium channels, which help to maintain the electrochemical gradient needed for ion movement (Hollenhorst et al., 2011).

- Alveolar type II cells (AT-II). The AT-II cells, which cover 3–5% of the alveolar surface area, are cuboidal epithelial cells and have been labelled defenders of the alveolus for their immunomodulatory functions. The AT-II cells can produce cytokines and chemokines, such as TNF- α , IL-6, IL-1 β , monocyte chemoattractant protein 1 (MCP-1), macrophage inflammatory protein 1 α (MIP-1 α), growth related oncogene α (GRO- α) and granulocyte-macrophage colony stimulating factor (GM-CSF) in response to various forms of lung injury induced by bacteria, viruses, or mechanical ventilation. AT-II cells also produce, secrete, and recycle surfactants, which can enhance chemotaxis, bacterial uptake and phagocytosis by alveolar macrophages, but can also inhibit cytokine production in response to LPS (Wong & Johnson, 2013).
- Alveolar macrophages. The alveolar macrophages are a type of white blood cells and take part in the cellular components of the immune system, they are the first response to invading respiratory pathogens. They originate from monocytes in the blood and evolve in the lungs. Since inhaled drug particles may be recognized as pathogens, these cells play an important role in the drug's pharmacokinetic. Furthermore, alveolar macrophages are capable of producing a wide range of pro- and anti-inflammatory cytokines. They are cleared from the alveoli to the bronchioles by the lining fluid, and then from the airways by the muco-ciliary escalator (Sibille & Reynolds, 1990; Stanke, 2015).

The Airway Surface Liquid

The airways are lined with an Airway Surface Liquid (ASL) film in two layers. Around the cilia is the aqueous layer (sol phase); over this, a viscous mucus layer

(gel phase) can be found. The low viscosity of the sol phase allows the cilia to beat, while the gel phase traps inhaled particles. The ASL has a crucial role in protecting the airways and alveoli from any potentially inhaled particles. The mucus comes predominantly from the mucus gland and goblet cells in the surface epithelium (Widdicombe, 2002).

The major macromolecular constituents of the mucous layer are the mucin glycoproteins. The mucin proteins are encoded by *MUC* genes, and many of them are expressed in the airways, including the gel-forming mucins MUC5AC, MUC5B, MUC2, MUC8, and MUC19. In healthy airways, the goblet cells typically express MUC5AC, whereas mucosal cells of the submucosal glands express primarily MUC5B (Groneberg et al., 2002). The secretion of mucin can be stimulated by many factors, including paracrine and autocrine mediators, especially ATP. Increased production and secretion of mucins is a feature of many chronic airway diseases, including asthma, Chronic Obstructive Pulmonary Disease (COPD), and cystic fibrosis (CF) (Rose & Voynow, 2006).

Water transport across epithelia is secondary to active trans-epithelial transport of solutes, which creates local concentration gradients across the epithelium and results in water movement by osmosis.

The regulation of the relative rates of Na versus Cl ions transport occurs in the apical domain of the airway epithelial cell. The relevant ion channels, e.g. epithelial Na channel and CFTR, and most of their intracellular regulators, are localized within the apical plasma membrane (P. Huang et al., 2001).

The surfactants

Between these two layers of ASL, there are the surfactants. Lung surfactants have a complex composition of unique phospholipids and proteins secreted by Clara cells and AT-II cells.

Their specific function is to reduce the surface tension at the pulmonary air-liquid interface.

About 80% of surfactants are glyceropholipids, with a minor contributions of sphingomyelin. Roughly 10% of mammalian surfactant is cholesterol. The phospholipids composition assure function under dynamic changes of the air-liquid

interface area during respiration. A 2-5% of surfactant is composed by surfactant proteins (SP-a, -B, -C and -D) (Bernhard, 2016). The two hydrophilic proteins SP-A and SP-D are calcium-dependent lectins and are important for primary defense mechanism of the lung as well as in alveolar surfactant homeostasis (Haagsman & Diemel, 2001). The two hydrophobic surfactant proteins SP-B and SP-C are essential to optimize alveolar surfactant function. The presence of surfactants in the alveolar fluid can promote the solubility of drugs, and consequently the dissolution of poorly water-soluble drugs. Furthermore, the pulmonary surfactants have good capabilities in spreading, facilitating transport and preventing adhesion of inhaled particles (Velaga et al., 2018).

2.3 *In vivo* models for inhaled compounds studies

For the purposes of assessing toxic end points and ADME/PK of inhaled compounds, animal-based studies have limitations in a variety of aspects. These include not only ethical considerations relating to animal experiments, but also, and above all, their biological relevance; their high costs and technical complexity need to be also considered. Airways in rodent and in human are anatomically very different. These variations modify air flow rates and air speed in the airways which affect the deposition the clearance and the retention of inhaled agents (Clippinger, Allen, Jarabek, et al., 2018).

There are evident differences in the anatomy and geometry of airways. Rodents have less extensive airway branching than humans. In the mouse, there are six to eight generations of intra-pulmonary branches with a stereotypical branching pattern. While in humans, there are more generations of intrapulmonary branches, with cartilage plates and smooth muscle surrounding the intrapulmonary airways at the the lung level (Clippinger, Allen, Jarabek, et al., 2018; Matute-Bello et al., 2011). The trachea of a mouse has an internal diameter of approximately 1.5 mm as opposed to the average human trachea that has an internal diameter of approximately 12 mm (Lacroix et al., 2018). Also, the cells type composition differs between non clinical species and humans (Clippinger, Allen, Jarabek, et al., 2018).

The breathing mode is one of the most obvious and significant physiological differences between rodents and humans. Humans are oronasal breathers while rodents breathe mandatory via nose. . This difference causes a less adequate filtration of particles and gases in the humans due to oral breathing compared to nasal breathing, with a consequent greater delivery of material to the peripheral airways (Clippinger, Allen, Jarabek, et al., 2018).

Other aspects that differ among species are the chemotactic attraction of macrophages implicated in clearance and biochemical mechanisms of airway activation and detoxification (Bogdanffy & Keller, 1999; Csanády et al., 1993).

An essential requirement for a non-animal method is the relevance and comparability with the anatomical characteristics that it should represent being modeled. Based on these considerations, animal models can only reproduce some aspects of complex human diseases such as lung fibrosis, emphysema (Moore & Hogaboam, 2008) and COPD (Wright et al., 2008). Because of significant differences in lung physiology they are not able to recapitulate the full spectrum of human patho-physiology and this can explain why over 80% of drugs that pass preclinical phases in rodents fail to demonstrate efficacy in patients during clinical trials (Miller & Spence, 2017).

The ideal model would enable to reproduce not only the different phenotypic lesions such as emphysema, small airway remodeling (including goblet cell metaplasia), chronic bronchitis, and pulmonary hypertension, but also the molecular mechanisms leading to them in humans. For example, several different approaches have been used in the effort to represent COPD in animals, but there are some more general principles that will affect any COPD model such as considerable differences among species in lung development and maturation; in lung anatomy and responsiveness to toxic agents (Wright et al., 2008).

2.4 *In vitro* cell-models

Cell-based models are crucial in the drug discovery and development process. To be suitable for *in vitro* studies (toxicology studies, permeability evaluation and compound efficacy assessment) the cell culture models should simulate the

functions and the defense mechanism of the lung epithelium in the best possible manner.

Well-known *in vitro* models are being routinely used to assess the air pollution-mediated respiratory toxicity and lung diseases to enhance knowledge on molecular and pathophysiological mechanisms. For example, if a compound is known to be metabolized (or if it is unknown if the compound is subjected to a toxification or detoxification mediated by the metabolism), an *in vitro* cell culture model must be metabolically competent. Similarly, if the transport of a compound has to be evaluated, the model should express the physiological barrier functionalities and transporters.

Many pulmonary models have been developed with several level of complexity. *In vitro* cell culture can be set up by using primary cultures or continuously growing cell lines. The *in vitro* lung models extend from simple cell-free biochemical assays, to submerged monoculture models to the most new and sophisticated multi-cell type cultures grown at air-liquid interface

The simplest option is the standard submerged two-dimensional cell culture characterized by low cost and high-throughput. However, these standard submerged cell cultures do not represent the lung physiology such as the cells exposure to air. The complexity of *in vitro* models can then be enhanced with the addition of characteristics that progressively correspond with the human condition. Examples of such models include co-cultures, consisting of two or more cell types in one well, and three-dimensional (3D) cultures. By increasing the complexity of models, the physiological relevance generally increases and this entails that also the quality and the reliability of data that can be obtained from these more complex models can be significantly improved. In line with the complexity of models and the physiological relevance also the costs increase (*Figure 4*).

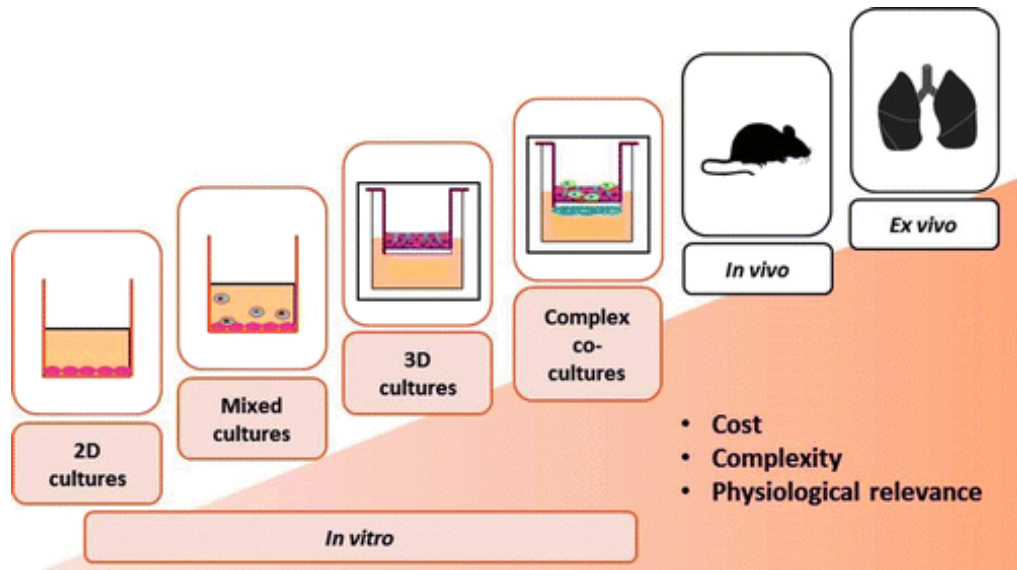


Figure 4. Respiratory models available from simple to complex (taken from Lacroix G., 2018)

Cell lines: cell lines are usually obtained by transforming primary cultures of epithelial cells, using viral vectors (e.g. the large T-antigen of the SV40 or human papillomavirus) (Mathias et al., 1996). Usually, the continuous cell cultures are more reproducible and simpler to use than primary cell cultures: they are easier to handle, do not display inter-donor variability and have a prolonged life span. However, they often do not have the differentiated morphology and the biochemical characteristics of the original tissue (Hiemstra et al., 2018).

The differentiation, such as the formation of cilia, the production of surfactants and mucus, the expression of transporters and proteins may be affected or reduced under submerged culture conditions, the passage number of the cells, cell seeding density, composition of the culture medium and the time in culture (Forbes & Ehrhardt, 2005).

For this reason, it is important to qualify cell cultures by assessing the extent of correlation with the *in vivo* situation in humans. Many cell lines from different part of the respiratory system are available.

A549 Cell line. The A549 together with NCI-H441 are human pulmonary epithelial cell lines widely used as models for the alveolar epithelium for biopharmaceutical research (Ehrhardt et al., 2008; Salomon et al., 2014).

A549 is probably the most frequently used alveolar epithelial cell line. It is derived from human lung adenocarcinoma and when they are grown on filter inserts they have a morphology similar to alveolar type II cells. A549 cells contain multilamellar cytoplasmic inclusion bodies, like those typically found in human lung ATII cells, although these hallmarks disappear as culture time increases. The cells synthesize lecithin with a high percentage of desaturated fatty acids via the cytidine diphosphocholine pathway and therefore they have been used to study the regulation of pulmonary surfactants synthesis (Lieber et al., 1976). These cells do not form tight monolayers of polarised cells, due to the lack of capacity to form functional tight junctions (Foster et al., 1998).

A549 cells might be a useful model in other areas of biopharmaceutical research, including metabolism studies or cytotoxicity studies for various substances. This cell lines possess P450 IA1 and P450 IIB6. These isozymes are significant due to their possible role in bioactivation of pro-carcinogens which may lead to lung cancer

NCI-H441 human bronchiolar epithelial cells. NCI-H441 is a human epithelial cell line, isolated from a papillary adenocarcinoma of the lung. They are capable of forming a polarised monolayer with tight junctions, showing characteristic of both AT-II and bronchiolar Clara cells (Shlyonsky et al., 2005). This cell line functionally expresses P-glycoprotein and several members of the organic cation transporter family (Salomon et al., 2014). Therefore, the NCI-H441 cells cultured at an air-liquid interface could replicate the phenotypic and functional ion transport characteristics of primary cultures of human type II alveolar epithelial cells, but the culture conditions strongly influence the morphological, phenotypic and functional characteristics of the model (Ren et al., 2016).

The Calu-3 and 16HBE14o cell lines, two immortalized human bronchial epithelial cell lines, have been suggested as suitable models to investigate the airway epithelial barrier function (i.e., tight junction properties) (Wan et al., 2000; Winton et al., 1998).

Calu-3 cell line. The Calu-3 is an adenocarcinoma cell line of sub-mucosal glandular epithelial origin, comprising a mixed phenotype of ciliated and secretory

cells (Mathias et al., 2002). The Calu-3 cells form *in vitro* polarized and well differentiated monolayers, with tight junctions, and they can be cultured at the air-liquid interface with a morphology similar to *in vivo* bronchial epithelial cells. It has been reported that the use of submerged culture conditions may reduce the level of differentiated morphology expressed by Calu-3 cells (Florea et al., 2003; Foster et al., 2000).

16HBE14o. The 16HBE14o cell line, originally developed by SV40 large T antigen transformation of normal bronchial epithelial cells, are non-ciliated, but in culture they are able to form functional tight junctions and to express a wide range of transporters. Even if this cell line is not capable of generating the desired phenotype at the air-interface, it has been used for drug absorption and drug/epithelial interaction studies (Manford et al., 2005).

BEAS-2B. The BEAS-2B cell line was originally developed by immortalization of normal human bronchial epithelial cells using AD12-SV40 virus. Another cell line frequently used to study epithelial cell structure and function, metabolism, cytokine regulation and interaction of xenobiotics is the Bronchial epithelial cell line (BEAS-2B), but since BEAS-2B cells do not generate tight junctions, the use of this cell line in drug permeability/transport studies is limited (Noah et al., 1995).

Primary cell cultures: The cultures of primary cells presents characteristics closer to the *in vivo* situation, and therefore they can represent a good model for the drug transport and toxicity studies. However, primary cells from animals or humans have a limited lifespan in culture; in addition, scarce tissue availability and time-consuming isolation procedures are hurdles that need to be considered (Haghi et al., 2014). Primary airway epithelial cells may be isolated from bronchial biopsies during bronchoscopy and cultured on porous supports at an air-liquid interface (ALI) resulting in a polarized muco-ciliary differentiated airway epithelial cells (Fulcher & Randell, 2013).

Although methods for isolating and culturing adult rat, murine type II cells and fetal human type II cells have been available for years, only limited success has been

achieved in maintaining the differentiated functions of adult human alveolar epithelial cells in primary cultures (J. Wang et al., 2007). For example, alveolar epithelium is composed of structural type I and surfactant producing type II cells (Fehrenbach, 2001). Isolation and culture of type II human alveolar cells from healthy human lungs are able to generate confluent monolayers of cells expressing tight junctional proteins (Elbert et al., 1999). However, over time these type II cells change their morphology and develop a type I-like phenotype (S. Wang & Hubmayr, 2011). Despite the disadvantages that primary cultures possess, an advantage of using primary cultures is that they provide the closest *in vitro* representation of the native epithelium.

Models of tracheobronchial epithelium from primary human airway epithelia have not been widely used so far to assess transport, because primary cultures represent a heterogeneous population of different cell types and therefore development of the model results to be time consuming and shows great variability (Forbes & Ehrhardt, 2005).

For over a century, traditional 2D cell cultures have been used in drug discovery. There is increasing evidence that the cell cultures as thin monolayers on plastic surfaces under submerged condition (the traditional 2D model) do not adequately enable human-relevant studies of cell behavior. These traditional models do not take into consideration the contributions of different cell types within the airway microenvironment, such as fibroblasts, endothelial cells, and immune cells that can be responsible of exposure outcomes. Thus, to achieve greater physiological relevance, other relevant airway cell types must be incorporated into 3D and organotypic *in vitro* models (Faber & McCullough, 2018).

This comprehension has accelerated the development of more complex 3D models, where cells grow in multiple layers, better reflecting the normal cell interactions that occur in their natural environment.

In these models, multiple epithelial and non-epithelial cell types, plus an extracellular matrix that contributes regulate cell behavior, are represented.

Examples of such 3D models are organoid or spheroid cultures, as well as various dynamic air-liquid interface (ALI) models (e.g., lung on a chip).

The most recent bronchial ALI models represent a fully differentiated epithelium with more than one cell type (ciliated cells, goblet cells, and basal cells) that are often combined with immunocompetent cells (dendritic cells, macrophages, neutrophils) (Upadhyay & Palmberg, 2018). ALI systems therefore have the potential to conceptually provide relevant data since it is possible to construct them from human-derived cells and create modeling scenarios that are close to the *in vivo* situation. Recently, ready-to-use cultures of primary epithelial cells have been made commercially available (e.g. EpiAirway™ or MucilAir™, Mattek Corporation© and Epithelix, respectively). However, these models are still in their infancy and they have not yet undergone a proper qualification process; for this reason, not many data are currently available in the public domain.

Briefly, to produce the cell cultures, airway cells are obtained from healthy patients undergoing surgical lung lobectomy. The epithelial cells are isolated by enzymatic digestion, amplified and cultured directly on the microporous membrane of Transwell inserts. The cultures are grown in a commercially available defined airway culture medium. Once confluent, the cultures are switched to ALI. After 3–4 weeks of culture, the epithelium becomes fully differentiated (Lacroix et al., 2018).

The complexity of the *in vitro* models of human airways is due to the presence of different cell types. In this regard, SmallAir™, with 17% Club cells and 2% goblet cells, replicates better the morphology and function of the human small airways *in vitro*. (S. Huang et al., 2017). Furthermore, SmallAir™ contains basal cells and ciliated cells, showing cilia beating and muco-ciliary clearance. Therefore, these features make the SmallAir™ a unique and powerful tool for studying the physiology and function of small airways and it should provide new approach for lung diseases assessment and drug development (Lacroix et al., 2018).

Lung-on-a-chip

Most *in vitro* models are two-dimensional (2D) and therefore do not mimic the inherently complex nature of tissues. For example, intracellular signaling pathways are affected by the loss polarity when grown in 2D culture. These model do not recreate the active tissue-tissue interface between the micro-vascular endothelium

and parenchymale tissues where transport of fluids, nutrient and regulatory factors take place. Moreover, they do not allow the application of dynamic mechanical forces that are critical for the development and function of specific tissues (Huh et al., 2010). Recently, the integration of microfluidic with advanced biological approaches such as organoids, referred as organ-on-a-chip models, have been developed and extensively investigated.

Lung-on-a-chip is a micro-engineered cell culture model that replicates the microarchitecture, breathing movements and primary physiological functions of the human lung (Huh et al., 2010). This model is representing a new approach with strong potential to study the complex pathophysiology of lung diseases and improve the drug development (Shrestha et al., 2020). Typically, they are created in microfabricated polymeric devices consisting of multiple layers of cell culture chambers to mimic three-dimensional micro-architecture of the tracheobronchial airways and alveoli. (Clippinger, Allen, Jarabek, et al., 2018). A typical lung-on-a-chip is represented in *Figure 5*. The device structure allows co-cultures of human alveolar epithelial cells and pulmonary microvascular endothelial cells on the opposite sides of a membrane. A computer-controlled cyclic vacuum system can mimic physiological breathing motions and concomitant tissue deformation (Huh et al., 2010).

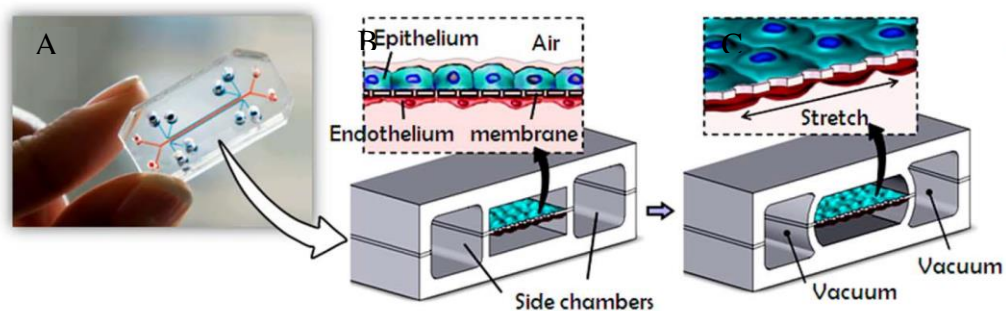


Figure 5. Representation of a lung-on-a-chip structure. A. Image of a polymeric device. B. Structure of a lung-on-a-chip: human alveolar epithelial cells and pulmonary microvascular endothelial cells are co-cultures on the opposite sides of a membrane. C. A computer-controlled cyclic vacuum system can mimic physiological breathing motions and concomitant tissue deformation (modified from Clippinger et al., 2018).

2.5 Lung Toxicity

As previously mentioned, the unacceptable toxicity associated with inhaled therapies represents the major obstacle in the development of inhaled drug (Cook et al., 2014). Respiratory toxicities are typically identified at a relatively late stage in preclinical testing. Therefore, during the development of new molecules, an early identification and prediction of potential lung toxicity would help in reducing the attrition in drug research and development, with a possible impact on the 3Rs too. The pathophysiological mechanisms associated with pulmonary tissue damage by the use of xenobiotics are diverse, probably due to the heterogeneity of the lung composition with many different cell types, each one with different sensibility to toxic agents (Castell et al., 2005). Pulmonary drug toxicity may result from a direct or indirect drug effect. To date, more than 380 medications are known to cause drug-induced respiratory diseases (Fröhlich, 2017).

Drugs with high potential to cause severe lung toxicity belong to very different chemical classes and therapeutic categories, including but not limited to: i) chemostatic (i.e. bleomycin, busulfan, and cyclophosphamide), ii) cardiovascular drugs (i.e. amiodarone and hydroxymethylglutaryl-CoA reductase inhibitors), iii) anti-inflammatory drugs (i.e. aspirin, methotrexate, gold, penicillamine, azathioprine, sulfasalazine), and antimicrobials (e.g. nitrofurantoin, amphotericin B, and sulphonamides).

The accumulation in the lung and the lung-specific bioactivation may play a crucial role in the toxic effect. Due to its high incidence and high mortality of 40–50%, amiodarone-induced lung disease is one of the best-studied (Fröhlich, 2017).

Various respiratory cells can be used to screen the cytotoxicity of a specific drug to lung cells. In general, A549 cells is a suitable cell line because their cytochromes (CYPs) enzyme expression pattern is more similar to the *in vivo* situation (Castell et al., 2005).

Furthermore, a more relevant exposure systems, such as air-liquid interface culture with exposure to the formulation as aerosol or small treatment volume, may improve the predictive value for reaction *in vivo* (Lacroix et al., 2018).

2.6 Factors affecting drug delivery to the lungs

The evaluation of *in vivo* events post-deposition of the compound such as the lung distribution and pulmonary pharmacokinetics needs to consider that the lung has several efficient defence mechanisms that have the function to eliminate the exogenous substances, including inhaled therapeutic agents. The drug disposition in the lung is the result of the kinetics of absorption and non-absorptive clearance mechanisms. As shown in *Figure 6*, different events can occur after the inhalation of a compound. Most of the lung absorption takes place in the alveolar region, where a thin (approximately 1 μm) and large (approximately 140 m^2) epithelium is present, to the pulmonary blood circulation. Part of the absorption can occur in the thicker (10-60 μm) and smaller (1-2 m^2) tracheobronchial airways (Sakagami, 2006).

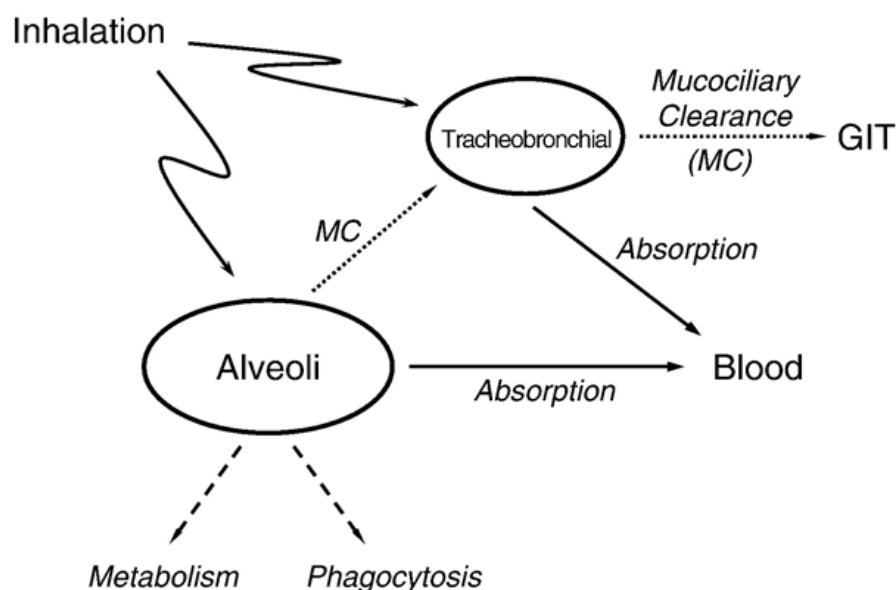


Figure 6. Mechanism following inhalation and lung deposition (MC= Muco-ciliary Clearance; GIT= Gastrointestinal tract) (taken from Sakagami M., 2006)

An inhaled substance may be eliminated from the lung by different non-absorptive mechanisms such as the muco-ciliary or cough clearance into the gastrointestinal tract, by phagocytosis and/or metabolism in the mucus or lung tissue, reducing the bioavailability for inhaled therapeutics.

2.6.1 *The Muco-ciliary Clearance (MCC)*

The airways, from the nose to the alveoli are continuously exposed to pathogenic agents, particulates and gaseous material with potentially harmful effect. Therefore, a series of defence mechanisms are in place to protect the respiratory tract from these insults. The upper airways protect the lung with the anatomical barriers. Factors such as the mucus layer, macrophages, alveolar epithelium and the basal membrane can inhibit drug permeation into the circulation, associated with the cough reflex and muco-ciliary clearance with enzymes and immunoglobulin A. Furthermore, drug availability can be affected by the cellular uptake pathways, proteolytic degradation and surfactant interaction (Nicod, 2005). The inhaled drugs have to overcome these defence systems to ensure efficient drug deposition as well as retention in and absorption from the lung.

The MCC is the primary innate defence mechanism of the lung. This is the process of physically eliminating the particles from the lung into the gastrointestinal tract by the coordinate interaction of the air surface liquid (ASL) and cilia beating.

The functional components are the protective mucous layer, the airway surface liquid layer, and the cilia on the surface of ciliated cells.

The cilia are specialized organelles that beat in metachronal waves to propel pathogens and inhaled particles trapped in the mucous layer out of the airways. The cilia beating is regulated by multiple physiological factors.

The adult lung is estimated to contain $\sim 3 \times 10^{12}$ total motile cilia, 6.5 to 7 μm long with a diameter of 0.1 μm . The core structure is the highly conserved axoneme that is extended from the basal body in the apical region of ciliated cells into the periciliary liquid. The ciliary axoneme (*Figure 7*) consists of nine outer doublet microtubules surrounding two central single microtubules.

The cilia of the airways beat in a coordinated fashion that results in metachronal waves. The basal CBF ranges between 10 and 20 Hz (Satir & Christensen, 2007), yielding a muco-ciliary clearance velocity of ~ 5.5 mm/min (Hofmann & Asgharian, 2003). The cilia beating frequency (CBF) is stimulated by β -adrenergic agonists, intracellular increase cAMP and cGMP and intracellular increase in Ca^{2+}

(Bustamante-Marin & Ostrowski, 2017). The CBF can also be affected by pH changes and temperature because there is an optimal temperature for the enzymatic hydrolysis of ATP, with low temperatures decreasing the CBF.

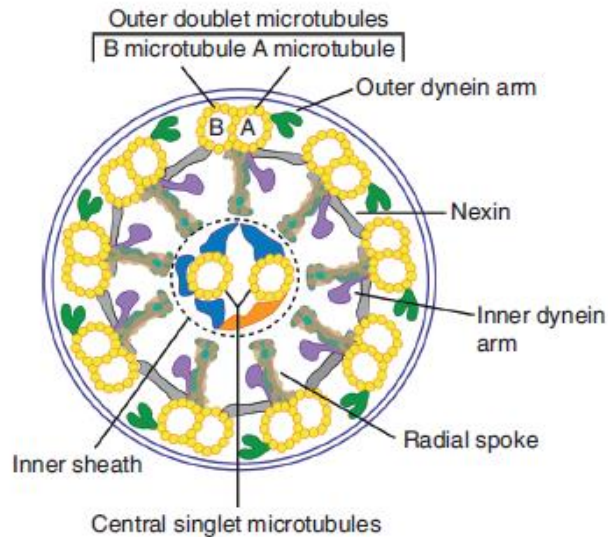


Figure 7. Cilia Axonema structure. The core structure is the axonemal with the characteristic 9+2 pattern consisting of nine peripheral doublets microtubules surrounding a central pair of single microtubules (taken from Bustamante-Marin X.M., 2017).

The standard measurement of MCC rates in humans requires the inhalation of a non-permeating radiolabelled marker. This method is not suitable for routine experimental studies, therefore, various methods have been used to study MCC in many different animal or *ex-vivo* models (Bustamante-Marin & Ostrowski, 2017). The recent models of differentiated human airways cultures, such as ALI 3D models, have shown to be able to maintaining the coordinated activity, providing a valid tool to monitor the MCC. Impaired MCC is a feature of many airway diseases, including both genetic and acquired disorders. For example, in cystic fibrosis, mutations in the cystic fibrosis transmembrane conductance regulator protein result in a viscous, thick mucus that cannot be easily cleared, leading to repeated infections, bronchiectasis, and, eventually, respiratory failure. More in detail, the cystic fibrosis is caused by mutations in CFTR, a gene encoding an ion channel [cystic fibrosis transmembrane conductance regulator (CFTR)] that transports chloride and bicarbonate across epithelial cell membranes. Lung disease is

considered the cause of most mortality in people with CF and it is provoked by a host defense impairment which leads to bacterial infections (Hoegger et al., 2015). Ballard and colleagues pioneered the use of ex vivo pig tracheas for studies of MCC and Joo N.S.(Ballard et al., 2002; Joo et al., 2016) and colleagues extended this approach to the ex vivo ferret trachea.

Muco-ciliary dysfunction is also a major component of other diseases, including COPD and asthma.

Therefore, there is a high interest in better understanding the MCC for the development of therapeutic approaches to improve ciliary clearance in patients.

The MCC and therefore the permanence time of an inhaled drug in the lungs is a factor that affect the drug absorption.

2.6.2 Phagocytosis by Alveolar Macrophages

In the alveoli region, the alveolar macrophages (AM) form the major defence to the transport of macromolecules from the lungs into the bloodstream, particularly for medium to large-sized proteins (Lombry et al., 2004). Macrophages are a key component of the primary innate immune response and are present in almost all tissues of the body. In the lung, they are the most abundant immune cell type present under homoeostatic conditions (Byrne et al., 2015).

They phagocyte insoluble particles that are deposited in the alveolar region and then they are removed by the lymphatic system or moved into the ciliated airways and eliminated via the muco-ciliary clearance (Labiris & Dolovich, 2003).

2.6.3 Lung metabolism

Although the lungs have the primary function of gas exchangers, they also perform several important non-respiratory functions. During the breathing, the respiratory tract is frequently exposed to environmental toxicants and carcinogens and it plays an important role in their detoxification. The same enzymes involved in the detoxification process may also contribute to the metabolism and elimination of inhaled, orally and intravenously administered drugs (Yilmaz et al., 2018). Some inhaled drugs such as theophylline, salmeterol, isoprenaline, budesonide, and

ciclesonide have been found to undergo significant metabolism in the lung (Joseph et al., 2013). Every compound administered intravenously, intramuscularly, subcutaneously or topically circulates through the lung before reaching the liver and therefore it may be subject to the lung metabolism (Yilmaz et al., 2018).

All metabolic enzymes found in the liver are also present in the lung, although at a lower level. For example, cytochrome P450 is 5–20 times lower in the lung compared to the liver. Phase I cytochrome P450 (CYP450) enzymes, flavin-containing monooxygenases (FMO), monoamine oxidase (MAO), aldehyde dehydrogenase, NADPH-CYP450 reductase, for example, are all present in the lung (Labiris & Dolovich, 2003). The enzyme involved in the drug metabolism are shown in the *Figure 8*.

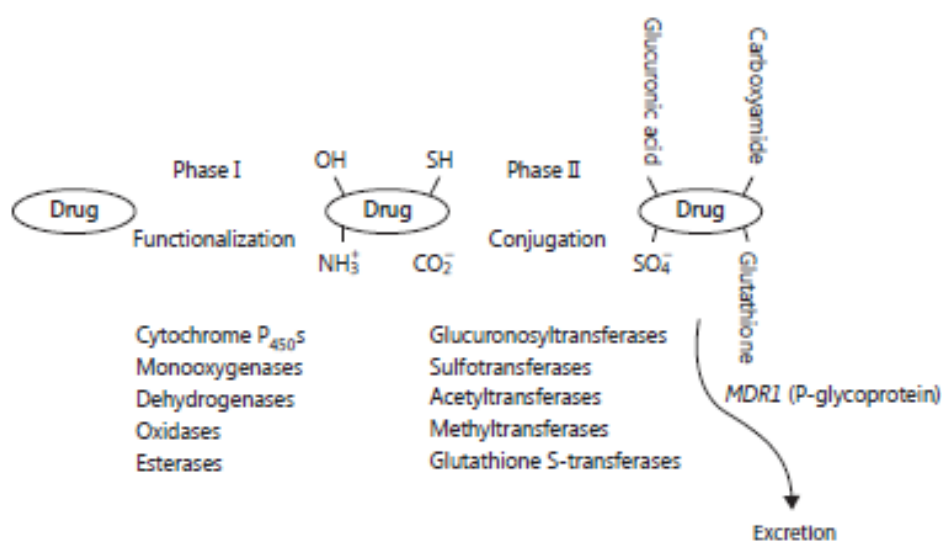


Figure 8. Metabolic pathways and the role of efflux transporters (taken from Mortens N.P., 2014.

The human lung, however, appears to be a poor site for sulphation.

Proteins and peptides undergo hydrolysis by the proteases present in the lung. Sources for the proteases are the alveolar macrophages and other inflammatory cells, such as neutrophils. Therefore, the combined administration of proteins and peptides with protease inhibitors, such as bacitracin and sodium glycolate, can reduce the metabolism and increase the lung absorption (Labiris & Dolovich, 2003). Certain cells in the airways are known to have a high metabolic activity, such as Clara cells.

Type II alveolar epithelial cells express enzymes required for metabolism, such as cytochrome P 450, but type I cells are thought to have little capacity for metabolism (Mortensen & Hickey, 2014).

Bio- transformation occurring in the lungs can be exploited in order to improve airway selectivity and minimize systemic side-effects of some inhaled drugs, designed as prodrug.

For example, the prodrug beclomethasone dipropionate is metabolized to the more active 17-beclomethasone monopropionate by esterases in the lungs, reducing the side-effects in the oropharyngeal tract.

Metabolism of inhaled chemicals is not always beneficial. For example, some innocuous chemicals in cigarette smoke are metabolized into potential carcinogens by the lung (Joseph et al., 2013).

Regarding the expression of metabolising enzymes *in vitro* cell line, the principal phase I metabolising enzyme, cytochrome P450 (CYP) has been studied in A549 (Foster et al., 1998), Calu-3 (Foster et al., 2000), BEAS-2B (Garcia-Canton et al., 2013), but published data are still limited in this area. A recent review observes that in the several substructures and within them the various cell types possess a different pattern of xenobiotic-metabolizing enzymes (Oesch et al., 2019).

2.7 Mechanisms of drug transport across the lung barrier

The pulmonary epithelium is the most significant barrier to absorption. It separates the air-filled compartment of the respiratory system from the aqueous interstitial compartment and at the same time, it regulates the exchange of solutes and water between these compartments.

The two cell types in the alveolar epithelium form a narrow band formed by tight junctions (TJ) between the adjacent squamous alveolar type I (AT-I) cells and much broader TJ complexes between adjacent AT-I and the cuboidal alveolar type II (AT-II) cells. This reflects the heterogeneity of claudin (cldn) expression in alveolar epithelial cells. Both alveolar epithelial cell types express cldn3, cldn4 and the splice variant cldn18-1 with different patterns as shown in *Figure 9* (Wittekindt, 2017).

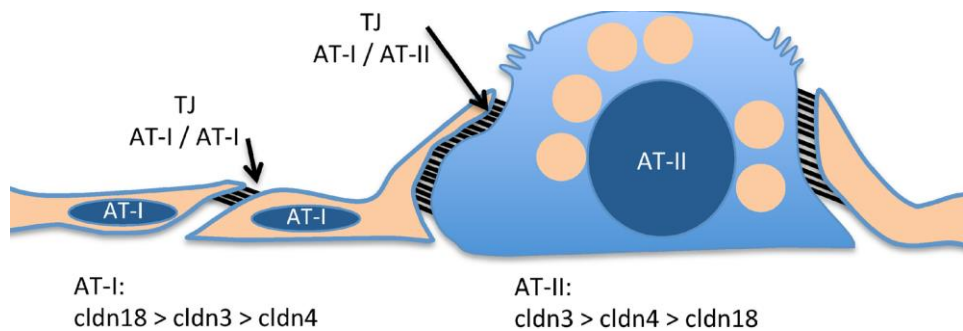


Figure 9. Structure of alveolar epithelium. The tight junctions between adjacent AT-I cells are narrower than those between AT-I and AT-II cells (taken from Wittekindt., 2017).

The process of absorption is described in Figure 10 and it can occur via passive diffusion or carrier-mediated active transport via paracellular or transcellular pathway depending on the drug and site of absorption (Liu et al., 2013)

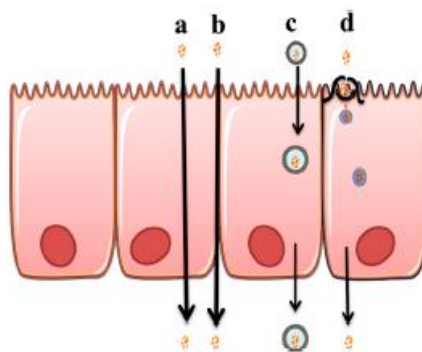


Figure 10. Epithelium drug transport mechanisms: a. Transcellular diffusion, b. Paracellular transport, c. Vesicle mediated transport, and d. Carrier mediated transport (taken from (Ghadiri et al., 2019)).

Passive transport: Most exogenous macromolecules are thought to be absorbed from the airspaces non-specifically through tight junctions and via endocytic vesicles (Patton et al., 2004).

Small, lipophilic molecules and compounds are generally absorbed via transcellular diffusion, in which they pass from the apical to the basolateral side by traveling through the cellular membrane. The hydrophilic molecules may cross the epithelium via the paracellular route, which they pass through aqueous pores in the intercellular junction. For small hydrophilic molecules, molecular weight and

degree of ionization seem to affect the absorption rate, due to the interaction with the proteins and lipids forming the pore. Because a solute tends to pass from a point of higher concentration to a point of lower concentration by passive diffusion, the flux through the membrane can be calculated as the net number of passing moles per unit area in unit time perpendicular to unit area and it is represented by the following formula (Eq. 1)

$$Flux = \frac{dm}{A \cdot dt} = \frac{V dc}{A dt}$$

Eq. 1. dm = moles of substance, A = unit area, dt = unit time, V = volume, dc = concentration of substance (Baldan, 2017).

Some interspecies differences are noted for water-soluble drugs, whereas the rate of absorption of lipophilic compounds is about the same (Schanker et al., 1986). This can be due to inter-species differences in alveolar pore number and pore size (Manford et al., 2005).

The existence of membrane vesicles within the alveolar endothelial and epithelial type I cells has long been recognized. In particular, the majority of the vesicles are non-coated and morphologically classified as caveolae (Gumbleton, 2001). The general view is that alveolar vesicle-mediated trafficking across the air-blood barrier works as a minor pathway in protein absorption (Gumbleton, 2001; Patton, 1996).

Active absorption: A number of compounds undergo active or carrier-mediated transport. This transport moves molecules against the concentration gradient; as such, it is energy-dependent and it can be inhibited by competitor compounds with similar structural characteristics (Patton J.S., 1996). The absorption rates of molecules transported by this way are saturable, such that the absorbed percentage decreases by increasing concentration. The active absorption depends on the lung regional expression of receptors or transporters (Liu et al., 2013).

The lungs express a broad range of both uptake and efflux transporters (Bosquillon, 2010), whose role on the disposition of inhaled drugs has received little attention

so far. Active transport may affect the permanence time of a drug on the epithelium and therefore it affects the absorption kinetic. Lung transporters might be involved in the uptake of drugs from systemic circulation, and their possible accumulation in the lung, causing pulmonary toxicity or affecting the drug pharmacodynamics. (Haghi, 2014).

The most notable among the transporters is the efflux transporter P-gp. Other transporters include the breast cancer resistance protein (BCRP), the multidrug resistance-related protein (MRP), the OCT/Ns organic anion transporters (OAT), organic anion transporting polypeptide (OATP) and oligopeptide transporters (PEPT1/PEPT2).

- **P-gp**

P-glycoprotein is an efflux transporter encoded by the MDR1 (multi drug resistance) gene. P-gp substrates cover a broad range of drug classes, although many are lipophilic or large amphiphilic molecules containing electronegative groups that can form hydrogen bonds. The functionality of P-gp is usually assessed by measuring the bidirectional efflux ratio (i.e. basal-to-apical:apical-to-basal) of a substrate such as rhodamin 123 or digoxin. Digoxin is not entirely selective for P-gp as it is also a substrate for organic anion transporting polypeptide transporters (Madlova M., 2009)

The P-gp is found in bronchial cell lines (e.g. Calu-3) and NHBE cells on the apical surface, similarly to human alveolar epithelial cells (Haghi M.,2014), as well as in Caco-2 cell line.

- **MRP**

Multidrug resistance-related proteins belong to the adenosine triphosphate binding cassette superfamily of membrane transporters ABC superfamily that obtain the energy by ATP hydrolysis (Scheffer et al., 2002).

MRPs are responsible for efflux of amphipathic anions, glutathione S-conjugated drugs and MRP1 expression showed regional difference and

its high expression in bronchi and alveoli may play a role as defense mechanism (Haghi et al., 2014).

MRP expression has been demonstrated in the whole lung, in the apical or basal surface of primary epithelial cells isolated and cultured from human lung samples and in immortalized cell lines such as Calu-3 (Haghi et al., 2014).

- **BCRP**

Breast cancer resistant proteins act as an efflux transporter with a broad range of substrates. It is the third most abundant transporter expressed in the human lung and it has been showed to be involved in the transport of beclomethasone, ciclesonide, mometasone and ciprofloxacin. Moderate expression levels of BCRP have been observed in primary bronchial epithelial cells, whereas slightly lower level were observed in Calu-3 cells (Haghi, 2014).

- **OCT, OCTN**

Organic cation transporters (OCT) are encoded by members of the solute carrier (SLC). The study of OCT transporters has been mainly focused on liver, kidneys, intestine and blood–brain barrier, but several common inhaled drugs positively charged at physiological pH, have been reported to interact with OCT (Salomon J.J. 2012)

Differences have been observed in the OCT expression among different airway cell lines (Ingoglia et al., 2015).

- **OAT and OATP**

Organic anion transporters (OAT) and Organic anion transporting polypeptides (OATP) mediate adsorption and elimination of organic ions. Little or no expression of OATs in cultured bronchial epithelial and A549 cells was observed and the isoform OAT4 was the only transporter expressed exclusively in Calu-3 and 16HBE14o, suggesting a very

limited role of this transporter in the distribution of drugs in the lung (Haghi M., 2014).

The OATPs transport (uptake and efflux) cationic, neutral, zwitterionic and anionic compounds. The OATPs share some substrates with P-gp, BCRP and MRP efflux transporters, therefore, the net disposition of a substrate molecule results from the combined contribution of all these transporters. In cultured bronchial epithelial cells, significant variation in the expression profiles of OATPs has been observed (Haghi M., 2014).

- **PEPT**

Oligopeptide transporters (PEPT1, PEPT2) transport a wide range of peptide and non-peptide drugs. In whole human lungs, only the expression of PEPT1 was reported. High expression of PEPT2 has been observed in all bronchial cell lines and primary bronchial and alveolar cells, while PEPT1 has been only expressed in Calu-3, 16HBE14o-, BEAS-2B and primary bronchial cells (Haghi M., 2014).

Due to these different expression of transporters among the lung cell lines, it is necessary to take into consideration the possibility for many compounds to be delivered via multiple transporters. Therefore, the knowledge of transporters involved in the delivery of the drug of interest is important in the selection of immortalized lung cell lines for the better evaluation of compound transport (understanding and/or prediction in transport studies (Sakamoto A., 2015).

2.8 Exposure System

The purpose of delivery of inhaled substances to ALI cultures is to mimic the physiological processes happening in the lung. Aerosol effects on lung cells are often addressed in environmental toxicology (Aufderheide & Mohr, 2000; Bitterle et al., 2006). These investigations are mainly focused in evaluating long-term effects of low-dose exposed materials like dust or particulate matter and pollution (Hein et al., 2011)

In contrast, pharmaceutical aerosols are aimed to deliver a specific dose of a given drug with a single administration. Drugs can be applied directly pipetting liquid formulation onto the ALI surface. Different methods have been used to expose cells cultured at ALI to aerosolized compounds either in dry powder form or by nebulization of solutions. Drugs can be delivered through the air using drug delivery systems that mimic methods of deposition in different regions of the lung that can be integrated with the inhalers device for human administration.

The Inertial impaction devices represent the basis on which many currently devices operate. It works on the principle of inertia; devices use a series of perpendicular nozzles, stages and collection plates to separate particles based upon the magnitude of their inertia (Karra et al., 2019) (*Figure 11*).

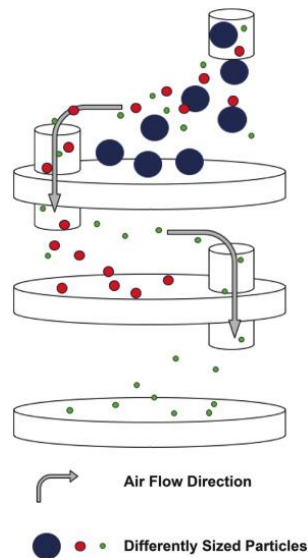


Figure 11 Schematic representation of an inertial impaction. Arrows indicating airflow direction and particle separation based on inertial force, smaller particles are able to follow the airflow and therefore to continue to the next stage, whereas larger particles cannot due to the impact onto the surface (taken from Karra et al., 2019)

This method is used in devices such as impingers (twin stage impinger and multi-stage liquid impinger) (*Figure 12*) and impactors (Marple-Miller, Anderson cascade and next generation).

An example of the use of this device for the ALI treatment is showed in *Figure 12* where a transwell containing cell monolayer is added at a specific stage (Karra et al., 2019).

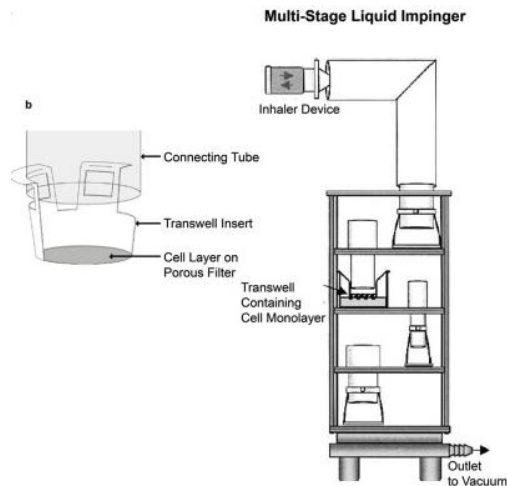


Figure 12. Schematic representation of a Multi-Stage Liquid Impinger (modified from Karra et al., 2019).

In electrostatic impaction devices, aerosolised particles are charged and flow through a humidifier. The deposition onto cells grown at ALI, is allowed by an electrode below the membrane which attract the charged particles (Figure 13).

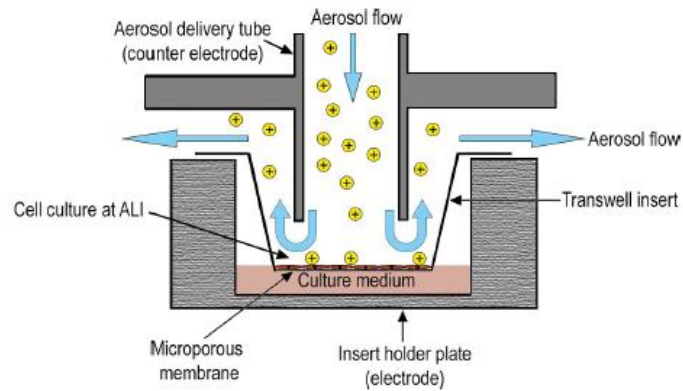


Figure 13. Schematic representation of the aerosol flow and particle deposition on the cell culture by electrostatic precipitation (modified from Geiser et al., 2017)

Sedimentation and diffusion devices are based on pressure differences to gently deposit compounds onto cells Figure 14. Particles are flowed through a tube at high pressure, and with low pressure outlets above wells housing insert with cell cultures. Air will naturally flow from an area of high to low pressure allowing sedimentation and diffusion (Karra et al., 2019)

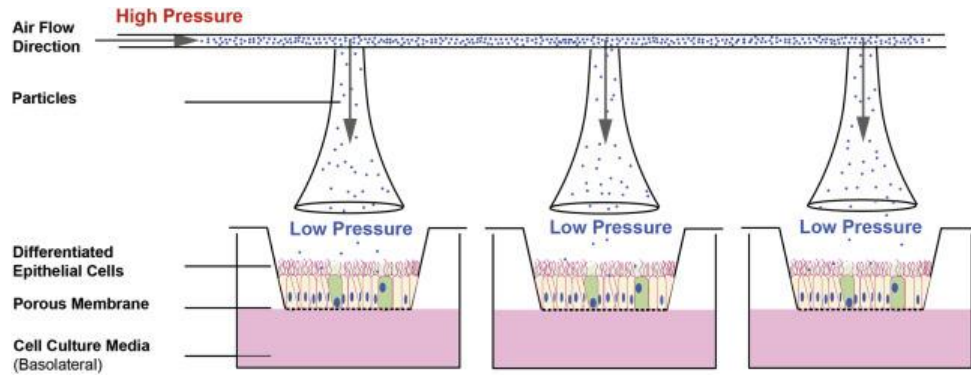


Figure 14 Schematic representation of Pressure Derived Sedimentation and Diffusion devices
(Taken from Karra et al., 2019).

Commercial devices using pressure difference to deposit particles with airflow include CULTEX® (Figure 15) (Aufderheide et al., 2017), VITROCELL® (Mülhopt et al., 2016) (Figure 16 and Figure 17) and the PreciseInhale Xpose ALI (Figure 18) (Ji et al., 2017).



Figure 15 CULTEX® RFS module (Taken from Cultex® website)



Figure 16. Vitrocell® exposure system for liquid aerosols with single droplet sedimentation (Taken from Vitrocell® Systems website).



Figure 17. Vitrocell® exposure system for dry powder can be applied from all commercially available inhalers or via direct dosing (Taken from Vitrocell® Systems website).

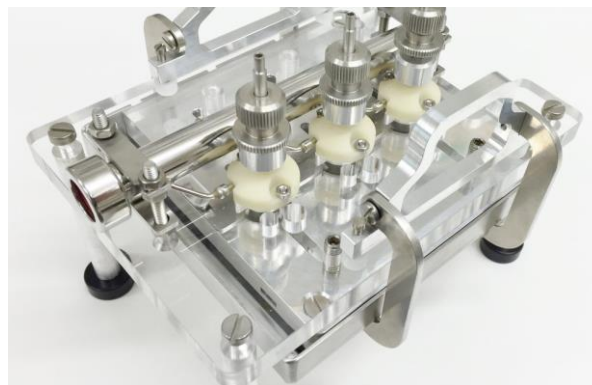


Figure 18. XposeALI® 3D cell exposure module (Taken from Inhalation Sciences).

3 AIM OF THE PROJECT

The aim of this project was to evaluate the implementation of an Integrated Strategy (IS) to be applied to the drug development process of new and generic inhaled drugs. The idea was to integrate a preliminary screening method for the toxic potential evaluation with multidisciplinary approach applied to a unique 3D human lung model to evaluate different parameters such as toxicity, permeability through the tissue and inflammatory end points. These data should be integrated with *in silico* models, in order to obtain more predictive data for the selection of the best candidate to be progressed in pre-clinical investigations and in clinical trials. This approach is expected to reduce the rate of failure in clinical trials. Furthermore, this approach is expected to have an impact on the number of animals to be used in *in vivo* studies for the regulatory submission. In this project the research has been focused on the following main aspects:

- 1) Characterization of SmallAir™ cell model as potential *in vitro* model:
 - for respiratory acute toxicity test
 - for transport assessment of drug compounds and nicotine contained in the aerosol produced by e-cigarette
 - for inflammatory mediators and end-points evaluation
 - for the muco-ciliary clearance assessment
- 2) Evaluation of a possible integrated approach consisting in the use of different parameters including toxicity, permeability data collection and MCC obtained in the *in vitro* SmallAir™ cell model together with *in silico* methods, such as multiple path particle dosimetry model (MPPD).

4 MATERIALS AND METHODS

4.1 Materials

SmallAir™ tissues and the specific SmallAir™ culture medium were obtained from Epithelix Sàrl (Switzerland). Each batch was supplied with a Certificate of Analysis reporting donor information (sex and age), cell information (cell type, data of seeding and data of air/liquid interface) and quality control results (sterility, Micoplasma, Trans-epithelial electrical resistance (TEER), cilia beating frequency, morphology, mucus and virus testing). The tissues were supplied cultured in Transwells, transferred in 24-well Falcon® plates (Corning Incorporated, Tewksbury, Massachusetts, USA).

A549 cells, adenocarcinomic human alveolar basal epithelial cells (ATCC® CCL-185™) were obtained from ATCC, Manassas, Virginia, USA. The cells were cultured on cell culture Corning™ T75 flasks (Corning Incorporated, Tewksbury, Massachusetts, USA) in RPMI Medium con GlutaMAX™ (Gibco®, Thermo Fisher Scientific, Waltham, Massachusetts, USA). For the toxicity test cell were cultured in 96-well Falcon® plates (Corning Incorporated, Tewksbury, Massachusetts, USA).

The permeability test substances Salbutamol (Lot. SC/48032), Budesonide (Certified Reference Material European Pharmacopoeia Reference Standard Council of Europe EDQMCS30026, Code: B1157300, Batch: 5.0), Fluticasone Propionate (Lot. ACR/2933), Propranolol Hydrochloride (Lot. BCBD8251V), Tiotropium Bromide Monohydrate (Lot. TIMHN0R802) and Theophylline (Lot. 091M0214V), were purchased from Sigma-Aldrich (Merck KGaA, Darmstadt, Germany). Digoxin (ID D6003, Lot. BCBT0180). GF120918 (ID SRP010305e, Lot. FE650161550) was purchased from Sequoia Research Products Ltd (Pangbourne, UK). Dimethyl sulfoxide (DMSO) was purchased from Sigma-Aldrich (Merck KGaA, Darmstadt, Germany).

For the permeability nicotine test e-cigarettes and e-liquid were provided by a Client and details are not reported due to a disclosure agreement, Lucifer Yellow

(ID L0144, Lot. MKBB2552) was purchased from Sigma-Aldrich (Merck KGaA, Darmstadt, Germany).

For the toxicity test, Dimethylamine (CAS 124-40-3), Glycidol (CAS 556-52-5), Dimethylamine (CAS 124-40-3), Hydrogen Peroxyde (CAS 7722-84-1) were purchased from Sigma-Aldrich Corporation (St. Louis, Missouri, USA).

Recombinant human TGF- β (240-B) was purchased from R&D System, Inc., Minneapolis, USA. LPS (from *P. aeruginosa* Serotype 10) and Bleomycin were purchased from Sigma-Aldrich (Merck KGaA, Darmstadt, Germany).

Hank's Balanced Salt Solution (HBSS) was purchased from Sigma-Aldrich (Merck KGaA, Darmstadt, Germany). HBSSH was obtained by adding 10 and 12.5 mM HEPES (Gibco®, Thermo Fisher Scientific, Waltham, Massachusetts, USA) for toxicity test and permeability respectively.

Resazurin for the toxicity was purchased from Sigma-Aldrich (Corporation, St. Louis, Missouri, USA).

LDH-Glo™ Cytotoxicity Assay Kit (Promega Corporation. Madison, USA)

For the cytokines analysis the MILLIPLEX MAP Human Cytokine/Chemokine Magnetic Bead Panel - Immunology Multiplex Assay (HCYTOMAG-60K-08) purchased from Merck KGaA, Darmstadt, Germany was used. For the SMAD2 analysis used the L45MA-5 MULTI-ARRAY® 96 Sm Spot GAM Plate, purchased from Mesoscale Discovery, Maryland, USA was.

For the evaluation of muco-ciliary clearance of ciliary movement, Micro particles based on polystyrene (BEADS) 30 μ M, Forskolin (FRSK) and CFTRInh-172 were all purchased from Sigma-Aldrich Corporation (St. Louis, Missouri, USA).

4.2 Test System

4.2.1 *SmallAir™ 3D Model*

The SmallAir™ tissues arrived in agar and they were transferred in a 24-well plate and cultured by ALI method (Air Liquid Interface) with 500 μ L of SmallAir™

culture medium added with penicillin-streptomycin, in the basolateral compartment. Tissues were incubated at 37 °C in humidified air atmosphere containing 5% CO₂ and 100 % humidity. The medium was changed every 2-3 days. The SmallAir™ presented native tissue properties such as a pseudostratified morphology, the presence of multiple cell types (mucus producing, goblet cells, ciliated cells with actively beating cilia, basal cells and club cells), functional tight junctions and mucus (*Figure 19*). Each batch of tissues showed a TEER values above 200 Ω·cm² and cilia beating frequency between 5 and 12 Hz. The experiments were conducted at least one week and 5 weeks after the arrival of the tissues.

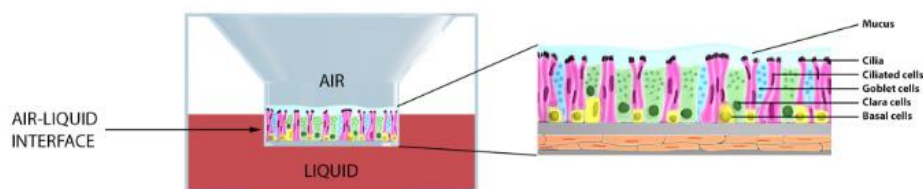


Figure 19. Schematic representation of SmallAir™. Taken from the Epithelix web site.

4.2.2 A549 Cell Model

The cells were cultured in adherent and submerged condition in RPMI Medium with GlutaMAX™ at 37 °C in humidified air atmosphere containing 5% CO₂ and 100 % humidity in cell culture flasks. Cell culture passages < 20 were used for the experiment. The day before the treatment 5000 cells/well of a 96-well plate were incubated at 37°C for approximately 24 hours.

This model was used as further respiratory model in acute toxicity test.

4.3 Methods

4.3.1 Acute Toxicity Assay Protocol

To avoid to generate and characterize an aerosol, the substances solutions were applied directly to the surface of SmallAir™ inserts and A549 cultures. Stock

solution were diluted in HBSSH (Hank's Balanced Salt Solution with CaCl₂ and HEPES 10mM).

Approximately 24 hours before the treatment the inserts of SmallAir™ were visually inspected to insure the quality of the epithelia and rinsed apically with 200 µL HBSSH. The washing step allows removing accumulated mucus and therefore minimizes the risks of interference with the test.

Treatment Protocol for single dose Acute Toxicity Assay (Test 1 and Test 2) in SmallAir™: before the treatment the TEER of each SmallAir™ tissue was measured. Two different study design were evaluated as follow: Test 1 with a treatment period of 6 hours and Test 2 with a treatment period of 72 hours. A volume of 100 µL of Dimethylamine 0.73 mg/mL (Test 1) and of LPS 100 ng/mL, CdCl₂ 100 µM and TGF-β 10 ng/mL (Test 2) was applied onto the surface of transwells (in triplicate) and then incubated for 6 hours or 72 hours respectively at 37 °C in humidified air atmosphere containing 5% CO₂. After the incubation period, transwells and cell cultures were washed with HBSSH added with CaCl₂ and a cytotoxicity assay was performed The TEER was measured after 24 hour and at the end of the treatment period and compared with TEER pre-treatment values. One tissue for each treatment of Test 2 was then processed for the histological observation.

Treatment Protocol for Dose-related Acute Toxicity Assay (Test 3) in SmallAir™ and A549 cell model: Chemicals tested in the evaluation of acute toxicity after a single treatment of a range of concentration were selected from substances previously tested and published (Jackson et al., 2018), for which *in vivo* human or animal inhalation toxicity are available. In particular compounds chosen with the respective toxicity classification are reported in *Table 1*.

Table 1. Compounds tested in the acute toxicity test with the respective toxicity classification.

<i>Test chemical</i>	<i>GHS acute classification^a</i>	<i>EPA acute classification^b</i>	<i>Respiratory Tract irritation reported (SDS)</i>
Glycidol	3 (H331)	NA	Yes
Dimethylamine	4	IV	Yes
Diethylamine	4	IV	Yes
Hydrogen Peroxyde (H ₂ O ₂),	3 (H331)	NA	Yes

^a GHS = Globally Harmonized System Acute Inhalation Toxicity classifications (Category 1 and 2: Fatal if inhaled; Category 3: Toxic if inhaled; Category 4: Harmful if inhaled; Category 5: may be harmful if inhaled)

^b EPA = Environmental Protection Agency Acute Inhalation Toxicity classifications (Category I: Fatal if inhaled; Category II: may be fatal if inhaled; Category III: Harmful if inhaled; Category IV: caution)

NA = not available

The concentration range tested was selected on the basis of literature data (Jackson et al., 2018) and confirmed after preliminary test. In detail the concentrations were tested are reported in Table 2:

Table 2. Range of concentration test for each compound in the acute toxicity test both in the 3D SmallAir™ model and A549 cell model.

<i>Test chemical</i>	<i>Test chemical concentration</i>	<i>Test system</i>
Glycidol	1, 4 and 12 mg/mL	SmallAir™
		A549
Dimethylamine	0.5, 1 and 1.5 mg/mL	SmallAir™
		A549
Diethylamine	0.5, 1.5 and 3 mg/mL	SmallAir™
		A549
Hydrogen Peroxyde (H ₂ O ₂)	5, 15 and 30 mg/mL	SmallAir™
	0.1, 0.5 and 1 mg/mL	A549

For the test, a volume of 30 µL of test chemical solution was applied onto the surface of transwells (in duplicate) and in the wells with A549 cultures (in triplicate) and then incubated for 3 hours at 37 °C in humidified air atmosphere containing 5%

CO₂. After the incubation period, transwells and cell cultures were washed with HBSS added with CaCl₂ and HEPES (10mM) and a cytotoxicity assay was performed.

4.3.2 Viability Assay – Resazurin Test

Resazurin is a non-toxic, cell permeable redox indicator that undergoes colorimetric change in response to cellular metabolic reduction. The reduced form, resorufin, is pink and highly fluorescent, and the intensity of fluorescence produced is proportional to the number of living cells (*Figure 20*).

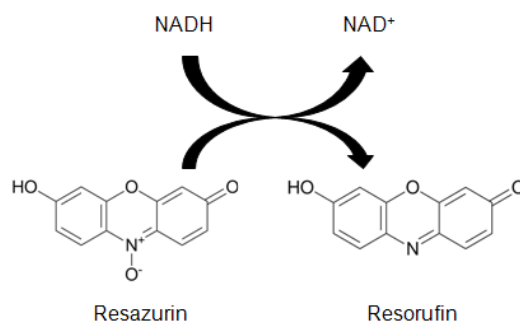


Figure 20. Structure of resazurin substrate and fluorescent resorufin product resulting from reduction in viable cells (taken from product sheet).

To measure the cell viability, the SmallAir™ transwells were transferred in a new 24 wells plate containing 500 μL of 6μM Resazurin in HBSS (1.25 mM CaCl₂ and 10 mM Hepes), a volume of 200 μL of the Resazurin solution was also applied onto the apical surface. For the A549 cultures, a volume of 200 μL of 6 μM Resazurin solution was applied into each well. The plates were then incubated for 1 h 37 °C in humidified air atmosphere containing 5% CO₂. After the incubation, 100 μL of the apical solution was transferred in a 96 wells plate and the fluorescence of the transformed product was measured (Fluorimeter Tecan Infinite F200, Tecan, Männedorf; excitation filter = 535 nm; emission filter = 590 nm). As baseline control a volume of 100 μL of non-transformed Resazurin solution was used in triplicate.

The transwells were then transferred in a new 24 wells plate containing 700 μ L of fresh medium and placed into the incubator (37 °C in humidified air atmosphere containing 5% CO₂).

Data handling: To determine the percentage of viability, the average absorbance values (A) of the replicate apical samples and baseline control were calculated using the following equation:

$$Viability (\%) = \frac{A (treated) - A (base line control)}{A (negative control) - A (base line control)} 100$$

where A(treated) is the absorbance of compound treated tissue, A (base line control) is the absorbance of the non-transformed Resazurin solution, A (negative control) is the absorbance of the tissues treated with vehicle (HBSSH).

Any possible effect on treatment group was assessed by the comparison with the negative control group. Statistical analysis was performed using the Student's unpaired t- test. Viability in percentage was graphically represented with the more appropriate plot and reported in tables with individual values and group means \pm standard error mean (SEM) for each test item tested.

P-values <0.05 was considered statistically significant. Statistical analysis was performed using SAS v.9.4. No statistical analysis was performed for the Test 1, given the low number of replicate (duplicates).

4.3.3 Trans-epithelial electrical resistance (TEER) measurement

Trans-epithelial electrical resistance (TEER) is a widely accepted quantitative technique to measure the integrity of tight junction dynamics in monolayers cell culture models.

TEER is the measurement of electrical resistance across a cellular monolayer and is a very sensitive and reliable method to confirm the integrity and permeability of the monolayer (Srinivasan et al., 2015). TEER measurements was performed using a Millipore Millicell-ERS cat. no. MERS 000 01 (Merck KGaA, Darmstadt) by placing electrodes on both sides of a cell layer grown on a semipermeable

membrane and measuring both current and voltage across the cell layer (*Figure 21*). TEER values were determined for all cultures before and after the experiments. In detail, for the TEER measurement of SmallAir™ a volume of 0.2 mL HBSSH and 0.5 mL HBSSH in the apical and basolateral compartments, respectively was added. The TEER values were calculated as follows: the resistance of the culture membrane will be subtracted (100 Ω for SmallAir™ Insert) from the measured values and then normalized with the surface of the insert (0.33 cm^2) and TEER was finally presented as $\text{Ohm}\cdot\text{cm}^2$ ($\Omega\cdot\text{cm}^2$).

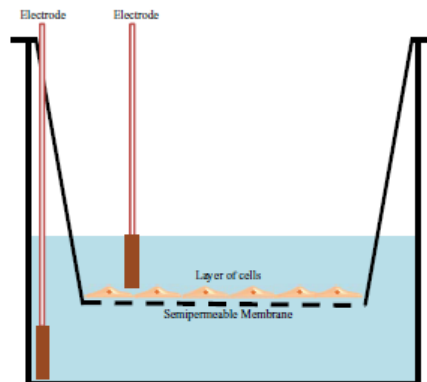


Figure 21. Transepithelial/ transendothelial electrical resistance (TEER) measurement with chopstick electrodes (taken from Srinivasan et al., 2015).

Statistical analysis was performed using the Student's unpaired t- test. TEER in $\Omega\cdot\text{cm}^2$ was graphically represented with the more appropriate plot and reported in tables with individual values and group means \pm SEM for each test item tested.

4.3.4 SmallAir™ Hystology

Histology observation was performed after Toxicity Test 2 only. Tissues were rinsed in PBS and fixed by immersion in 4% formaldehyde solution for 30 min and then washed with HBSS with $\text{Ca}^{2+}/\text{Mg}^{2+}$. For the dehydration process, tissues were placed in successive baths as follow:

Ethanol 30%, 15 min

Ethanol 50%, 15 min

Ethanol 70%, 15 min

Ethanol 90%, 15 min

Ethanol 100%, 30 min

Xylene-Ethanol (1:1), 30 min

Xylene 30 min

Paraffin at 60°C, 1 hr

Transwells were then embedded into paraffin, sectioned and processed for staining with Hematoxylin Eosin. Slides were evaluated by microscopical analysis.

4.3.5 Permeability Assay

4.3.5.1 Permeability studies in SmallAir™ - liquid treatment

The aim of this assay was to determine passive cellular permeability (Papp) and P-gp activity through the human SmallAir™ cells.

The permeability of the Salbutamol, Budesonide, Tiotropium Bromide, Theophylline and Digoxin on SmallAir™ tissues was assessed. Each compound was dissolved at 10 mM in DMSO and then diluted at 10 μM in HBSSH.

The apical and basolateral compartments were the donor and acceptor compartments, respectively in A to B permeability and oppositely in B to A permeability (*Figure 22*).

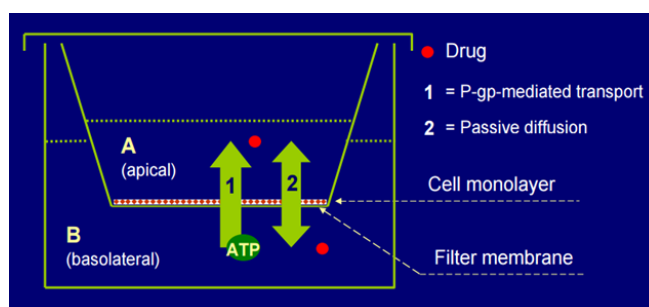


Figure 22. Schematic representation of permeability process (taken from Palumbo et al., 2008).

In details, for the A to B permeability, a volume of 200 μL of compound formulations at 10 μM in HBSSH buffer was applied onto the donor (apical) compartment and a volume of 500 μL HBSSH was added into the acceptor (basolateral) compartment. To assay the permeability a volume of 100 μL from the acceptor compartment and a volume of 10 μL from the donor compartment after 60

min was sampled. The samples were analyzed by HPLC–MS to measure the drug content.

For the B to A permeability, a volume of 500 µL of test compound formulation at 10 µM in HBSSH buffer was applied into the donor (basolateral) compartment and a volume of 200 µL HBSSH into the acceptor (apical) compartment. To assay the permeability a volume of 10 µL from the acceptor compartment and 100µL from the donor compartment after 60 min was sampled. The samples were analyzed by HPLC–MS/MS to measure the drug content.

Data Handling: For each treatment, the apparent permeability, Efflux Ratio and the Recovery was calculated.

The apparent permeability (P_{app}) index is defined as the initial flux of compound through the membrane (normalized by membrane surface area and donor concentration) (Palumbo et al., 2008). It represent how likely is a compound to pass through the test system.

The P_{app} values were calculated for direction [A to B] and [B to A], according to the following equation:

$$P_{app} = \left(\frac{dQ}{dt} \right) \times \left(\frac{1}{C_0} \right) \times \left(\frac{1}{A} \right)$$

Where dQ/dt is the steady-state flux across the cell layer (the amount of test item expressed as area ratio), C_0 is the initial concentration (mol/mL) in the donor chamber and A is the surface area of the filter (0.333 cm² for 24 well plates). The P_{app} was expressed as nm/sec and average \pm standard deviation (SD) for A to B and for B to A directions was calculated for each treatment. The P_{app} can be used to predict oral/intestinal bioavailability on the basis of a classification based on P_{app} of reference compounds as reported in *Table 3*.

Table 3. Permeability classification: correlation between *in vitro* Papp and predicted *in vivo* absorption.

<i>In vitro</i> Papp	Predicted <i>in vivo</i> absorption
Papp ≤ 10 nm/sec	0-20% (Low)
10 nm/sec ≤ Papp ≤ 100 nm/sec	20-70% (Medium)
Papp > 100 nm/sec	70-100% (High)

The Efflux Ratio (ER) is calculated according the following equation:

$$Efflux\ Ratio = \frac{A\ to\ B\ P_{app}}{B\ to\ A\ P_{app}}$$

When a drug diffuses only by passive diffusion both A to B and B to A permeability should be similar and therefore the ER should results about 1. While, when a drug is the substrate of specific transporters, the permeability will result increased in the direction A to B if an uptake transport is involved or in B to A direction when an efflux pump is engaged. With an ER greater than 2 the compound might be considered substrate of efflux transporters such as P-gp, whereas with a ER lower than 2 is generally not considered substrate for these king of transporters..

4.3.5.2 Permeability Assay – aerosol treatment

For the assessment of the permeability after aerosol treatment the CULTEX® RFS Compact (Cultex Laboratories GmbH, Hannover, Germany) has been evaluated as exposure device for nebulized formulation.

The CULTEX® RFS Compact consists of two main parts, the aerosol-guiding module and the sampling module where 6 cell culture inserts can be allocated. The device expose 3 insert positions to the aerosol treatment and the remaining 3 insert positions the clean air at the same time (*Figure 23*)

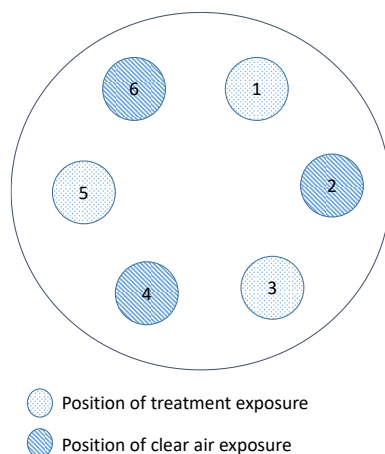


Figure 23. Schematic representation of exposure module of the CULTEX® Compact device Cultex Laboratories GmbH, Hannover, Germany.

For the application of a commercially available formulation for nebulizers, the CULTEX® device was connected to a simple nebulizer (Aerosol TurboBOY SX, Pari GmbH, Starnberg, Germany).

Briefly, Broncovaleas® (4 mL at 5 mg/ml suspension for nebulization) and Budesonide Aircort® (2 mL at 0.5 mg/ml suspension for nebulization) were nebulized and the aerosol was applied onto the SmallAir™ tissues with a flux of 1 ml/min. After the nebulization, samples of 100 µL of HBSSH from basolateral compartment and 10 µL (after the addition of 100 µL of HBSSH) from the apical compartment were collected. Samples were then analysed by a HPLC-MS/MS method for the quantification.

In addition, the CULTEX® RFS Compact, connected to a Borgwaldt smoking machine LM1E (Borgwaldt KC, Hamburg, Germany), was used to design a protocol for the assessment of nicotine permeability after e-smoke exposure. Two experiments have been conducted with two different commercial e-cigarettes containing the same e-liquid. Briefly, the e-cigarette was connected to the smoking machine (*Figure 24*) and the e-liquid aerosol (containing nicotine) and vehicle was distributed on the tissues following the CORESTA recommended puffing regime Method No.81 (CORESTA, 2015). A number of 16 puffs were taken with a puff volume of 55 mL in 3 seconds, with a puff interval of 27 s. For a better distribution,

the e-liquid aerosol was diluted with regular air (1 L/min) before being sucked into the CULTEX® RFS compact via a vacuum pump with a flow rate of 5 mL/min/insert. Two transwells with SmallAir™ tissues and an insert without cells were exposed for each test. In test 2 two runs were conducted. The insert without cells was used as reference to quantify the amount of nicotine that has actually reached the tissues. In each experiment vehicle and e-liquid containing nicotine have been applied. In addition a positive control (H₂O₂ 10%) was applied as liquid formulation.

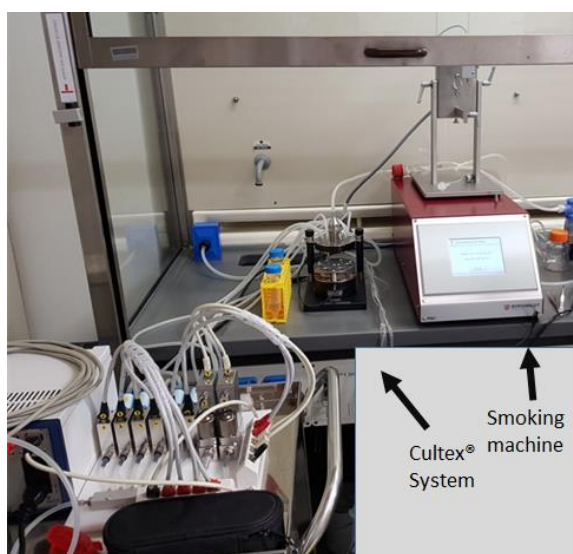


Figure 24. Image of the instrument set up for the assessment of nicotine permeability through the SmallAir™ tissues. CULTEX® RFS Compact, on the left, was connected to a Borgwaldt smoking machine LM1E

For each test TEER before and after e-smoke exposure was assessed. After the e-smoke exposure, cell viability by Resazurin test and the integrity of tissues by Yellow Luciferase Assay were assessed. At the end of the e-smoke exposure, one sample of 100 µL of medium from the sampling chamber was collected at different time points (2 and 5 minutes after the exposure). The concentration of nicotine was quantified by qualified method using liquid chromatography with tandem mass spectrometry detection (LC-MS/MS).

4.3.5.3 *Luciferase Yellow Assay*

This assay allows to assess the paracellular permeability as indicator of the integrity of the tissues using the yellow luciferase marker (LY) and therefore allows to determine if the permeability is due to a damaged tissue or to a physiological transport. When the tissue is constituted by selective barrier sealed by tight junction, no or really low paracellular flux is present and the transcellular pathway is the only way to cross the tissue. Molecules as LY that are unable to pass a cell monolayer grown on microporous membranes by transcellular pathway can be used to evaluate the barrier status.

LY permeability was measured in one direction, [A→B], at the end of incubation. Residual solutions in the apical compartment after the treatment was gently removed and 200 µL of donor working solution containing LY at 100 µM in culture medium were then added to the A compartment and 600 µL of receiver working solution (culture medium) to the B compartment. The cells were incubated at 37°C for 60 min.

A volume of 100 µL from receiver wells, 100 µL/well of donor solution containing 100 µM LY and 100 µL/well of Transport medium were transferred to 96-well clear bottom black plate (Nunc™ F96 MicroWell™ Black Polystyrene Plate, Thermo Fisher Scientific, Waltham, Massachusetts, USA). Fluorescence was measured by using a fluorescence plate reader (FLUOstar OPTIMA Microplate Reader, BMG LABTECH, Ortenberg, Germany), at Ex = 485 nm, Em = 535 nm.

Data handling: The percent permeability from the fluorescence values was calculated as follows:

$$\% LY \text{ rejection} = 100 * \frac{1-RFU \text{ basolateral}}{RFU \text{ apical}}$$

Where RFU are the relative fluorescence unit values (subtracted by the background mean values); RFU apical is the mean value of the donor solution LY 100 µM.

A % LY rejection >98% is considered acceptable, between 98% and 95% is considered acceptable with caution and < 95% is considered not acceptable.

4.3.5.4 Permeability Assay - NGI

The regional deposition in the lung is determined by the aerodynamic diameter of the particles. Impactors are the instruments of choice for the in vitro assessment of delivery efficiency of inhalation products. The Next Generation Impactor (NGI) is a high performance cascade impactor with seven stages (*Figure 25*) and it operated at any inlet flow rate between 30 and 100 L/min with the cut sizes spanning a particle size range nominally from 0.25- μm to 11- μm aerodynamic diameter which are collected in specific cup.



Figure 25. Next Generation Impactor in “open” position.

One NGI cup was modified by creating holes in the cup where transwells were allocated as showed in *Figure 26*. A Volume of 500 μL of medium was transferred in each well. Two wells were used to allocate the SmallAir™ tissue transwells, while one well was occupied with a transwell without tissues in order to measure the total compound applied. The transwell without tissue was equipped with plain filter to collect the dose deposited. The efficiency of modified cup was checked with a leak tester and found satisfactory.

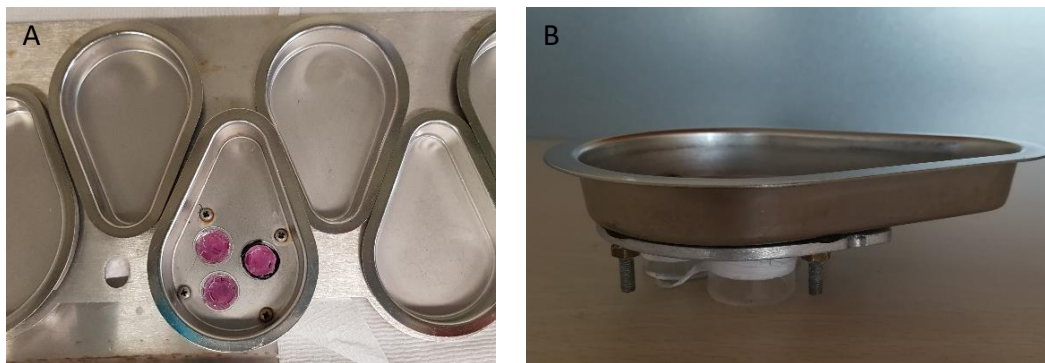


Figure 26. Images of Next Generation Impactor Cup modified, with tissue insert allocated. A. Top View B. Side view.

A preliminary test without tissues was performed to confirm that the same amount of compound was deposited in each well. This test was carried out as the final experiment except for adding filters in the empty transwells rather than the tissues. The modified cup was positioned at stage 3 place and three filters were inserted into the empty wells. Spiriva (Tiotropium Bromide) dry power inhaler (DPI) capsules and devices were used to test the modified cup. Prior to run the test, the Critical Flow Controller was adjusted to 39 L/min by using a calibration Dosage Unit Sampling Apparatus tube (DUSA tube) and then a Leak test was performed on the NGI impactor to verify eventual pressure leakage in the modified system. The NGI impactor was attached to the leak tester and a bung was placed into the throat to seal it. A pressure of 5 kPa was initially applied before adjusting it to 4 kPa and the pressure was recorded after 20 seconds. The resulting leak rate need to be lower than 100 Pa/s to pass and it was calculated as follows:

$$\text{Leak rate} = (4 - P \text{ recorded}) \times 1000/20.$$

After the Leak test, the flow rate of the NGI impactor was checked to be at 39 L/min and then 5 Tiotropium Bromide (18 μg) capsules were fired into the NGI impactor. The filters were collected after the firing and they were placed into three scintillation vials with the addition of 1ml of diluent (10 mM Ammonium dihydrogen phosphate buffer pH 2.9/ Methanol 70/30 % v/v). The samples were collected and they were then analysed by HPLC-UV at 237 nm, with a flow of

1.7 ml/min and a column temperature of 40°C. To confirm the data reproducibility, the test was performed twice.

The final test was performed at the same condition reported above with 2 SmallAir™ transwells and 1 insert without tissue. After the treatment the SmallAir™ transwells were incubated at 37 °C in humidified air atmosphere containing 5% CO₂ and 100 % humidity for 1 hour. After the incubation period, a sample of 100 µL of medium from each basolateral compartment was collected. A volume of 100 µL of medium was added to the apical compartment to dissolve and collect the possible compound deposited onto the surface.

4.3.6 Phospho-SMAD2 (p-SMAD2) measurement

SmallAir™ cultures were treated with recombinant TGF-β (final concentration 20 ng/ml) for 1 and 3 hours. At the end of the incubation period, the cells were lysed in complete TRIS lysis buffer and p-SMAD2 (at residues S465/S467) and total SMAD2 was measured with an MSD-based assay (L45MA-5 MULTI-ARRAY® 96 Sm Spot GAM Plate, Meso Scale Discovery's Assay). SMAD2 was analysed using two immune-assays in parallel: the capture antibody (against total SMAD2 form) was common to the two assays, whereas the detection antibody was either anti-total SMAD2 or anti-phospho-SMAD2 (Ser465/467)-specific. The use of appropriate MSD microplates (96 well-small spot Goat Anti Mouse –GAM- plate) with carbon electrodes integrated into the bottom of each well and a detection antibody conjugated with electrochemiluminescent labels (SULFO-TAG™) provided a specific electrochemiluminescent signal proportional to the target of interest measurable using a MSD reader.

Briefly, tissues were lysed in complete Tris lysis buffer and scraped after 1 hr incubation on ice. After a clearing step, protein concentration was assessed using BCA kit (Bicinchoninic Acid Assay protein determination kit) and the supernatant used immediately for SMAD2 analysis or stored at -80°C.

GAM plates were blocked with 3% Blocker A in Tris Buffer Saline with Tween 20 (TBST) for approximately 1 hour at RT, then the plate were coated with capture antibody [mouse anti-SMAD2/3 antibody (BD, 610843), 1:250 dilution] and incubated for 2hr. Tissue lysate (10µg) was transferred to MSD plates and incubated overnight at 4°C. Detection antibodies (rabbit anti-total SMAD2, Thermo Fisher,

51-1300, 1:500 dilution or rabbit anti-phospho-SMAD2 (Merck Millipore, 04-953, antibody 1:50 dilution) were added to the MSD plate. After 2hr incubation, MSD Sulfo-Tag labeled anti-rabbit diluted 1:500 were added and incubated for 1hr. 1X Read Buffer was added and plates were read immediately in a MSD reader (e.g. MSD Sector 6000).

Data handling: A semi-quantitative determination of phospho-SMAD2/SMAD2 level was used, normalizing phospho-SMAD2 (pSMAD2) levels to total SMAD2 levels (tSMAD2). Values are expressed as means \pm standard error.

Statistical analysis was performed using GraphPad Prism 8 or STATISTICA 10 by a One Way ANOVA followed by Post Hoc Fisher LSD test.

4.3.7 Cytokines and pro-inflammatory mediators measurement.

For the analysis of cytokines and pro-inflammatory mediators release, SmallAir™ cultures were treated in triplicate with a Bleomycin at concentration of 10, 30 and 100 μ M applied onto the surface (100 μ L).

Supernatant in the lower chamber was collected after 24 hours and 72 hours. The quantification of IL-6, RANTES, IP-10, ETXN, IL-4, MIP-1 β , IL-8, GRO was performed using a Luminex bead-based Multiplex Assay (MILLIPLEX MAP Human Cytokine/Chemokine Magnetic Bead Panel - Immunology Multiplex Assay) according to manufacturer instructions.

4.3.8 Lactate Dehydrogenase (LDH) assay

Lactate Dehydrogenase (LDH) assessment was performed in the samples obtained from the medium of SmallAir™ cultures treated in triplicate with a Bleomycin at concentration of 10, 30 and 100 μ M in the upper chamber for 24 hours and 72 hours. The LDH release was quantified using the LDH-Glo™ Cytotoxicity Assay.

The LDH-Glo™ Cytotoxicity Assay provides a simple bioluminescent method for quantifying LDH release. The bright luminescent signal provides the sensitivity to determine cytotoxicity in 3D microtissue spheroids, microfluidic cell culture chips, primary cells and stem cells. The method is based on a bioluminescence reaction. LDH catalyzes the oxidation of lactate with concomitant reduction of NAD⁺ to

NADH. Reductase uses NADH and reductase substrate to generate luciferin, which is converted to a bioluminescent signal by Ultra-Glo™ rLuciferase (Figure 27). The light signal generated is proportional to the amount of LDH present.

In the LDH-Glo™ Assay protocol, 25 µL LDH Detection Reagent (containing Lactate, NAD⁺, Reductase, Reductase Substrate and Ultra-Glo™ rLuciferase) was added to 25 µL sample of diluted cell culture media. After 1 hour of incubation at room temperature the luminescent signal generated was read by a luminometer (Victor³v, PerkinElmer, Waltham, Massachusetts, USA).

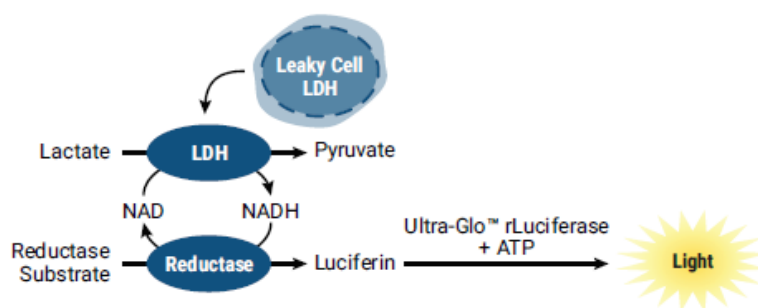


Figure 27. Schematic representation of LDH-Glo™ cytotoxicity assay mechanism..

Data handling: results were expressed as fold increase compared to the negative.

4.3.9 ROS measurement

For the measurement of reactive oxygen species (ROS) released in the medium by the SmallAir™ after treatment with Bleomycin at concentration of 10, 30 and 100 µM in for 24 hours and 72 hours, the ROS-Glo™ H₂O₂ Assay was used. This method is a homogeneous, rapid and sensitive luminescent assay that measures the level of the ROS hydrogen peroxide (H₂O₂).

ROS generated in cells can act as signalling molecules and, in excess, can lead to cell damage or death (Wittmann et al., 2012). Among the several ROS that are generated in cell cultures, the H₂O₂ is the most convenient to assay because it has the longest half-life of all ROS in cultured cells.

The ROS-Glo™ Assay mechanism for H₂O₂ measurement is shown in Figure 28. An H₂O₂ substrate reacts directly with H₂O₂ to generate a luciferin precursor. Upon

addition of ROS-Glo™ Detection Reagent containing Ultra-Glo™ Recombinant Luciferase and d-Cysteine, the precursor is converted to luciferin by the d-Cysteine, and the produced luciferin generates a luminescent signal that is proportional to H₂O₂ concentration.

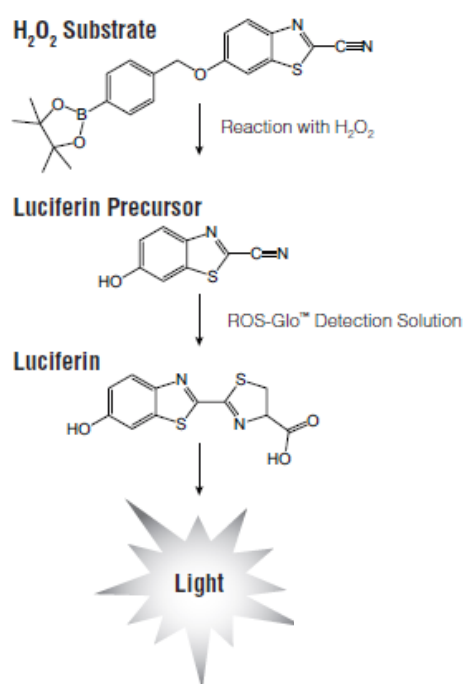


Figure 28. Schematic representation of ROS-Glo™ H₂O₂ Assay.

In the ROS-Glo™ Assay protocol, 10 mM H₂O₂ Substrate provided in the kit was diluted to 100 μM with the H₂O₂ Substrate Dilution Buffer and added to the tissues after Bleomycin treatment at concentration of 25 μM and incubated at 37 °C in humidified air atmosphere containing 5% CO₂ and 100 % humidity for 1 hour. Then, a volume of 10 μL of medium sample from each treatment condition was transferred into a 96-well plate in duplicate. A volume of 10 μL of ROS-Glo™ Detection Solution was added to each well. The plate was incubated for 20 minutes at room temperature and the relative luminescence was measured using a plate reader (CLARIOstar plate reader).

4.3.10 *Muco-ciliary Clearance Assay*

For the evaluation of the MCC the following compounds were tested: Forskolin 3 and 10 μM before and after treatment with CFTRInh-172 20 μM ; Carbachol 10 μM before the treatment with CFTRInh-172 20 μM ; Saline 3 %; LPS 100 ng/mL, 1 $\mu\text{g/mL}$ and 1 mg/mL; Salbutamol 10 μM ; Budesonide 10 μM ; Fluticasone Propionate (FP) 10 μM ; Theophylline 10 μM ; Tiotropium Bromide 10 μM .

The MCC was evaluated measuring the speed of the flow of the lining fluid on the surface of the SmallAir™ tissues after compound treatment. In particular, 30 μm polystyrene microbeads, diluted 1:25 in each test compound solution were added on the apical face of SmallAir™ at a volume of 30 μL and the movement of the microbeads was recorded with a 12 MPX f/1.7 Samsung S7 camera at 30 frames per second, on an inverted microscope (model Leica DML, Leica Microsystems S.r.l., Milan, Italy) with magnification 10X, at room temperature.

Agonist and Ion Transport Inhibitors. To test the effect of agonist, such as Forskolin (FRSK) and Carbachol (CCH) and ion transport inhibitors (CFTRInh172) different study design were applied:

- Test 1: Treatment with CFTRInh172 20 μM followed by the treatment with FRSK 3 μM and 10 μM ;
- Test 2: Treatment with agonist FRSK 3 μM and 10 μM followed by the treatment with CFTRInh172 20 μM ;
- Test 3: Treatment with agonist (CCH 10 μM) followed by the treatment with CFTRInh172 20 μM ;

For each tissues the baseline speed of the cilia was assessed with beads diluted in HBSSH in order to have a no-treated control to compare for the evaluation of the compound effect

The video were captured at the following time points after treatment: immediately after treatment (T0), after 10 minutes (T10) and after 20 minutes (T20).

Drug compound treatment. Test 4: Each compound was tested at the concentration of 10 μM and videos were captured at T0, T10, T20, T30 and T40. While LPS and Saline 0.9 % and 3 % have been tested at T0 only.

Data handling. Two different approaches were taken into consideration for the videos analysis, in order to individuate the more appropriate method of analysis: an automatic methods and a manual methods. Then all videos were analysed using the manual method.

4.3.10.1 Analysis method evaluation

The automatic and manual methods have been applied to Test 1 and Test 2 for a comparison. At first the automatic method was considered in order to capture a high number of trajectories. Videos are analysed using ImageJ Software (Mosaic-Particle Tracker 2D/3D plugins) (Figure 29) and 50 frames at time (for at least of 300 frames/video) were analysed.

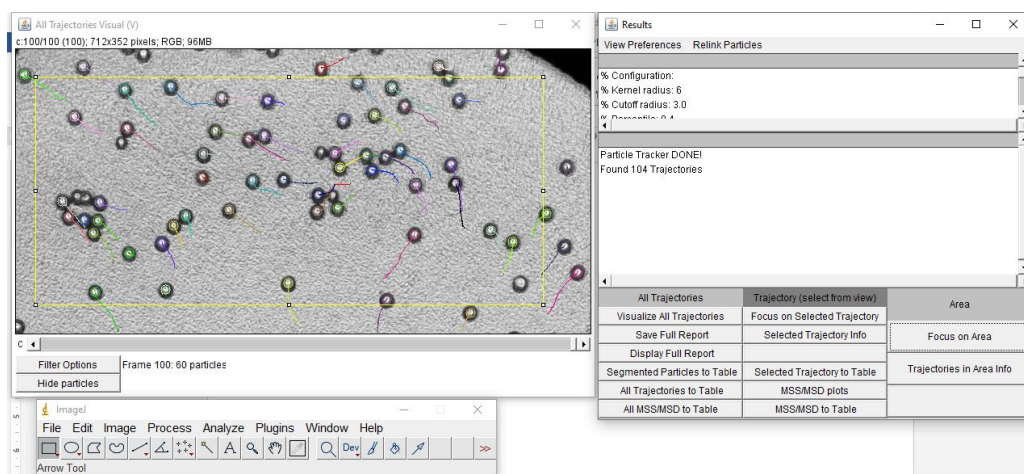


Figure 29. Example of trajectories selected by ImageJ (Mosaic-Particle Tracker 2D/3D Plugins).

In the manual approach, 50 frames at time (for at least of 300 frames/video) were analysed using ImageJ Software (MTrackJ plugins) (Figure 30), tracking at least 10 beads every 50 frames.

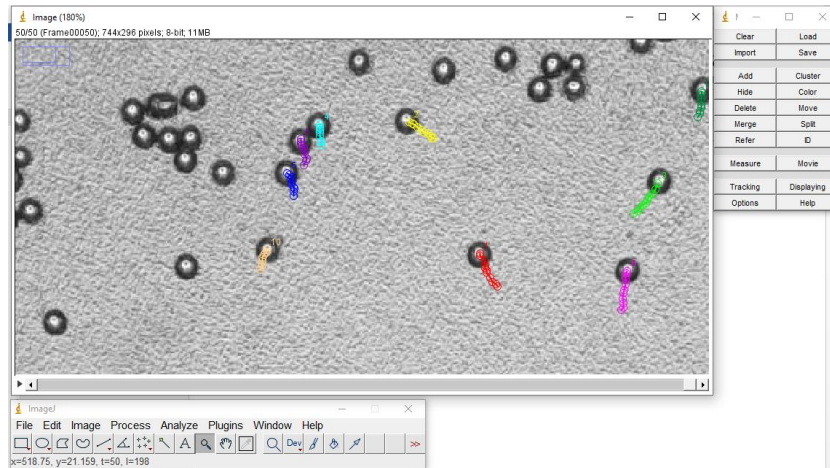


Figure 30. Example of trajectories selected by ImageJ (MTrackJ Plugins).

Data handling: the coordinates of beads were measured at each frame (in automatic approach) or every 5 frames (in manual approach) and used for the speed measurement. The beads speed in mm/sec was calculated using an Excel Sheet applying the Pythagorean Theorem to measure the distance travelled by the bead. A Bürker Chamber was used to measure the ratio mm to pixels (mm/pixels) applying the following step. The following equation was applied:

$$\text{Speed (mm/sec)} = \frac{r}{\frac{\text{frame } n}{\text{frames per sec}}} \frac{\text{mm}}{\text{pixels}}$$

where r = distance travelled by the bead in pixel; $\text{frame } n$ = (number of the frame); frames per sec = number of frames taken per second (30); mm = measure length on Bürker Chamber in mm (0.2 mm); pixels = number of pixel in 0.2 mm.

Statistical analysis was performed to evaluate the reliability of these approaches.

At first, an analysis of number of frames captured for each trajectories by automatic method was conducted and a higher number of trajectories compared to the number of beads was observed. This was because the software showed to lose the tracking of beads therefore trajectories with a number of frame lower than 45 were excluded from the analysis.

For each approach, averaged values of speed, for each trajectory, were analysed using an analysis of variance (ANOVA) followed by post-hoc Dunnett's test. The

speed measured for each treatment and time point was compared to negative control (base-line control). Furthermore speed of beads after FRSK treatment versus CFTRInh-172 at 20 minutes and CFTRInh-172 versus FRSK at 20 minutes for Test 1 and Test 2 respectively were compared. Bead speed was presented in graph and tables with group means \pm SEM for each negative control and treatment groups. P-values <0.05 was considered statistically significant. Statistical analysis was performed using SAS v.9.4.

Results obtained with automatic method was firstly compared with manual analysis and the manual approach was finally considered for the evaluation of MCC. For Test 1, Test 2 and Test 3 the statistical analysis describe above (ANOVA and post-hoc Dunnett's test) was conducted to compare each treatment versus the negative and the agonist versus inhibitor treatment for Test 1 and inhibitor versus agonist treatment for Test 2 and Test 3.

For Test 4 each time point was analysed versus the negative control only.

For the evaluation of the cilia beating synchronization the particle image velocimetry analysis of ImageJ Software (PIV plugins) was conducted.

4.3.11 MPPD prediction analysis

The multiple-path particle dosimetry model was used to integrate in vitro MCC result with the *in silico* method prediction. The parameters selected are reported in the *Table 4*. In addition to these parameters, additional parameters such as:

- Airway Morphometry: Functional Residual Capacity (FRC); Volume, Upper Respiratory Tract (URT);
- Inhalation properties: Density, Aspect Ratio;
- Exposure condition: Acceleration of Gravity, Body Orientation, Aerosol Concentration, Breathing Frequency, Tidal Volume, Inspiration Fraction, Pause Fraction;
- Deposition/Clearance: Fast Human Clearance Rate, Medium Human Clearance Rate, Slow Human Clearance Rate, Lymph Node Human

Clearance Rate, Rata Clearance Parameter (a, b, c, d), Lymph Node Rat Clearance Rate, Exposure Time Settings

were left as default.

Table 4. Parameters selected in the multiple-path particle dosimetry model

Airway Morphometry	
Species	Human
Model	Yeh / 5-lobe
Inhalation properties (Aerosol)	
Diameter	3 μM
Exposure condition	
Constant	Breathing Scenario Oral
Deposition/Clearance	
Deposition + Clearance	Tracheal Mucous Velocity 5.5 mm/sec for negative control (default); velocity expressed as mm/sec obtained in the MCC in vitro assay for the analysed compounds

The parameter “Tracheal Mucous Velocity” was considered 5.5 mm/sec as default for the not treated tissues. Average tracheal mucus velocities in healthy non-smokers, as measured by non-invasive radiological techniques, ranged from 4 to 6 mm/min; consequently, the value of 5.5 is considered as adopted by both International Commission on Radiological Protection (ICRP, 1994) and National Council on Radiation Protection and Measurements (NCRP, 1997) committees (Hofmann & Asgharian, 2003).

Data handling: the mucus velocity of 5.5 mm/min value was used to calculate a correction factor to be applied to the speed measured for the tissues compound treated. The following equations was used:

$$\text{Correction Factor} = \frac{5.5 \text{ mm/sec}}{\text{Speed not treated tissue (mm/sec)}}$$

Where 5.5 mm/sec is the default speed of the MPPD system and Speed not treated tissue is the speed measured by the analysis of the beads speed in the not treated tissue.

The “*Tracheal Mucous Velocity*” specific for the compound treated tissue was calculated using the following equation:

$$\text{Tracheal Mucous Velocity} = \text{Treated tissue MCC} \cdot \text{correction factor}$$

Where the treated tissue MCC measured by the analysis of the beads speed in the compound treated tissues.

After accepted the parameters setting and the run of the analysis, the results were plotted and reported in tracheal-bronco clearance (TB Clearance vs time).

5 RESULTS

5.1 Acute Toxicity Assessment

In this project a step-wise strategy is proposed in order to increase the rate of success in the drug candidate selection phase. Ideally, safety data should be integrated with early PK and efficacy indications in order to increase chances to select the candidate with the highest safety margin. With this ambitious objective in mind, two *in vitro* cell models were considered:

- A549 cell line was qualified and proposed as preliminary cell model for doses dependent toxicity of selected compound to be tested in the SmallAir™ model;
- SmallAir™ (Epithelix Sàrl) model was qualified and proposed as the final model to be used to generate physiological human-relevant data.

The 3D model SmallAir™ was evaluated as more physiological model for acute toxicity assessment both after single treatment of single concentrations and after a single dose of a range of concentrations.

In the single dose toxicity test three compounds known to be toxic for the lung were analysed in order to qualify the SmallAir™ model as possible *in vitro* model able to distinguish toxic and no toxic substances after a single dose exposure:

- 1) Dimethylamine Cadmium Chloride (CdCl₂)
- 2) lipopolysaccharides (LPS),
- 3) Transforming growth factor beta (TGF-β)

Cadmium Chloride is a well-known lung toxicant compound. It is a ubiquitous environmental pollutant, which can cause severe toxicity in various organs, mainly the lung, kidney, liver, bone and genitals. Lung tissue is one of the main targets of cadmium toxicity and the respiratory system is affected severely by the inhalation of cadmium-contaminated air (Oberdörster, 1992). Shortness of breath, lung edema and destruction of mucous membranes as part of cadmium-induced pneumonitis have been described (Seidal et al., 1993). Cadmium causes lung damage, pulmonary fibrosis, emphysema and inflammation in human and experimental animals. Cadmium may also adversely affect the lungs by decreasing the viability or modifying the function of individual lung cells (Låg et al., 2002). Epidemiological studies and *in vitro* studies demonstrated that CdCl₂ exposure causes the disruption of the ALI barrier (Forti et al., 2010).

LPS is widely employed as pro-inflammatory agent in the induced acute lung injury *in vivo* model (De Souza Xavier Costa et al., 2017).

The TGF-β plays an important role in normal pulmonary morphogenesis and function and in the pathogenesis of lung disease. The effect of TGF-β is regulated via a selective pathway of TGF-β synthesis and signaling that involves activation of latent TGF-β, specific TGF-β receptors, and intracellular signaling via SMAD molecules. TGF-β is involved in normal tissue repair following lung injury. However, in a variety of forms of pulmonary pathology, the expression of TGF-β is increased. These include chronic lung disease of prematurity as well as several forms of acute and chronic adult lung disease. The increase in TGF-β precedes abnormalities in lung function and detectable lung pathology, but correlates with the severity of the disease. TGF-β plays a key role in mediating fibrotic tissue

remodeling by increasing the production and decreasing the degradation of connective tissue via several mechanisms (Bartram & Speer, 2004).

For the dose-related toxicity test a range of concentration of known toxic substances have been tested, in order to estimate an EC75, considered as the effective concentration which results in 75% of viability of the tissue. These compounds were tested on the submerged A549 model, considered as possible model for a preliminary screening for the dose concentrations selection, and SmallAir™ as more physiological *in vitro* model.

Test 1 (single dose acute toxicity, 6 hours of treatment)

After 6 hours treatment with Dimethylamine 0.73 mg/mL a marked decrease of viability was observed up to 75.7% ± SD 11.2 of viability in comparison to negative control (Figure 31).

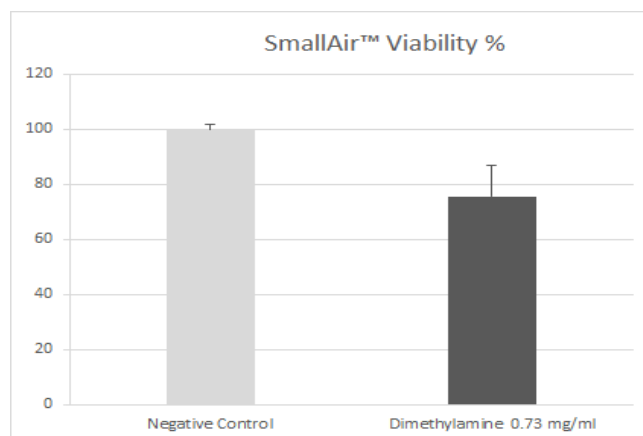


Figure 31. Test 1 Acute toxicity results: Viability assessed by the Resazurin test of the SmallAir™ after 6 hours treatment with Dimethylamine 0.73 mg/mL. The viability is expressed as % of mean viability of 2 tissues ± SD treated compared to negative control. The viability of tissues treated was 75.7% ± SD 11.2 compared to negative control.

A decrease in the TEER values, both for the negative control and for Dimethylamine treated tissues was observed after 6 hours treatment. No decrease

in TEER values was observed for the Dimethylamine treatment versus the negative after 6 hours of treatment (Figure 32).

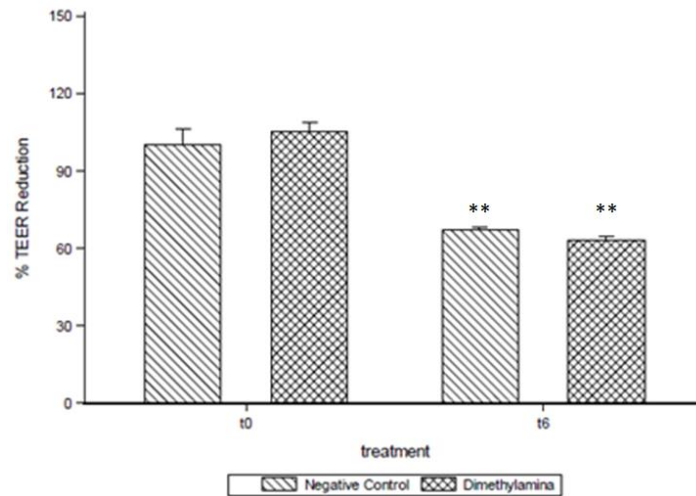


Figure 32. Test 1 TEER Reduction results: Graphical representation of TEER reduction of SmallAir™ tissues at T0 and after 6 hours of treatment with Dimethylamine 0.73 mg/mL. (mean of 3 tissues \pm SEM). A statistically significant decrease (**: $p \leq 0.01$) was observed after 6 hours both for negative control and treated tissues. No decrease was observed for the tissues treated compared to the negative control.

Test 2 (single dose acute toxicity, 72 hours of treatment)

Tissues treated with CdCl₂ showed a significant decrease in the viability (64.7% in comparison to negative control). Slight but no significant decrease in the viability was observed after the treatment with LPS while a significant slight decrease (92.5% in comparison to negative control) after treatment with TGF- β was observed (Figure 33).

Regarding the TEER values, a high variability was observed. However, a marked and significant decrease in TEER values was observed after 72 hours of treatment with CdCl₂, while a slight decrease was observed after TGF- β . No decrease was observed after LPS treatment (Figure 34).

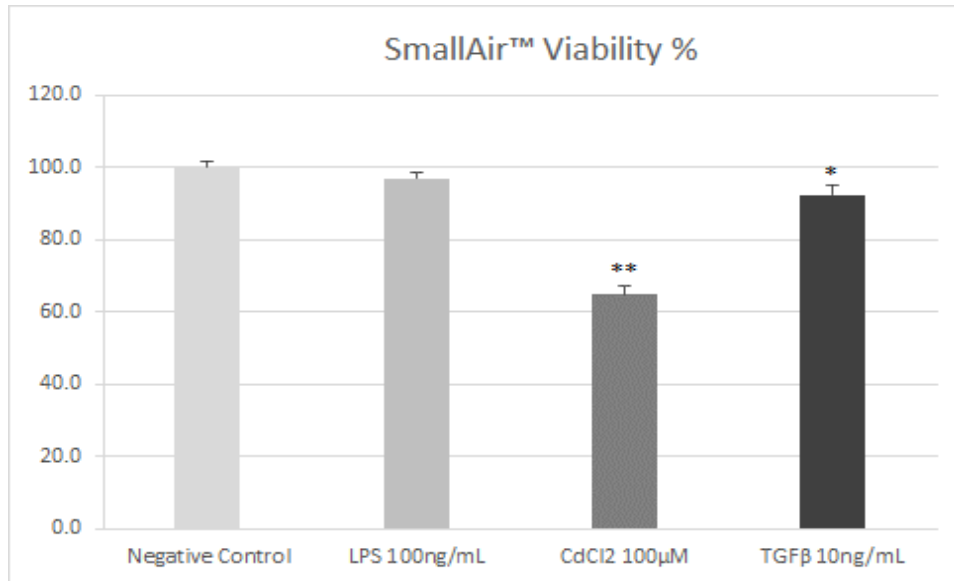


Figure 33. Test 2 Acute toxicity Results: Graphical representation of the viability assessed by the Resazurin test of the SmallAir™ treated with LPS 100 ng/mL, CdCl₂ 100 µM and TGF-β 10 ng/mL. The viability is expressed as % of mean viability of 3 tissues ± SEM treated compared to negative control. A statistically significant decrease of viability was observed for the tissues treated with CdCl₂ 100 µM and TGF-β 10 ng/mL (*: $p \leq 0.05$; **: $p \leq 0.01$).

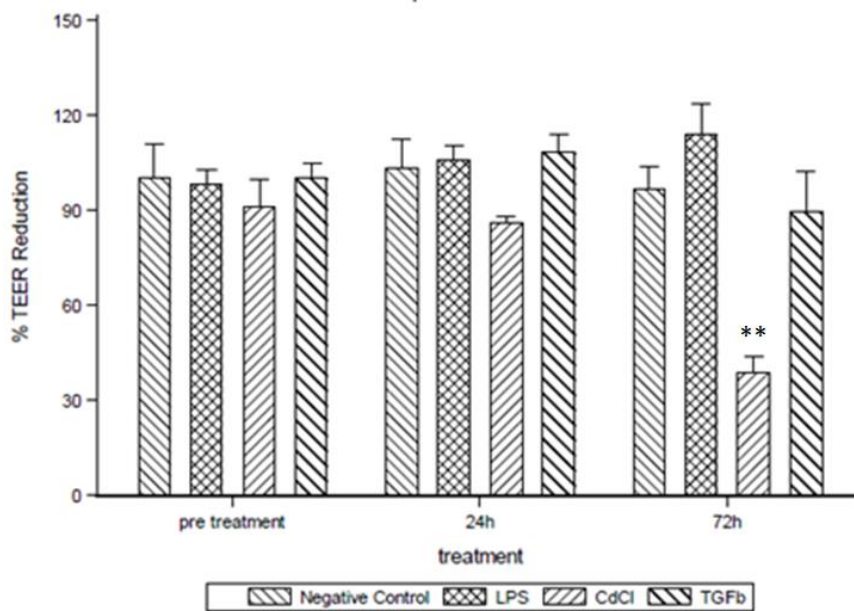


Figure 34. TEER Reduction Test 2 Results: A. Graphical representation and statistical analysis of TEER reduction of SmallAir™ tissues treated with LPS 100 ng/mL, CdCl₂ 100 µM and TGF-β 10 ng/mL. A significant decrease compared to negative control after 72 hours was observed for tissues treated with CdCl₂ 100 µM only. No decrease was observed in any other treatment condition (**: $p \leq 0.01$).

Test 3 (dose-related acute toxicity)

Data obtained in the Test 3 are reported for each test compound in *Figure 35* and *Figure 36* for SmallAir™ and A549 respectively.

In detail, a high variability intra experiments was observed, mainly for the negative control. Despite this variability, a dose related toxicity was observed for H₂O₂, Glycidol and Dimethylamine in both cell models and the EC75 was calculated for these compounds (*Table 5*). No dose related toxicity was observed for Diethylamine and no accurate EC75 was calculated

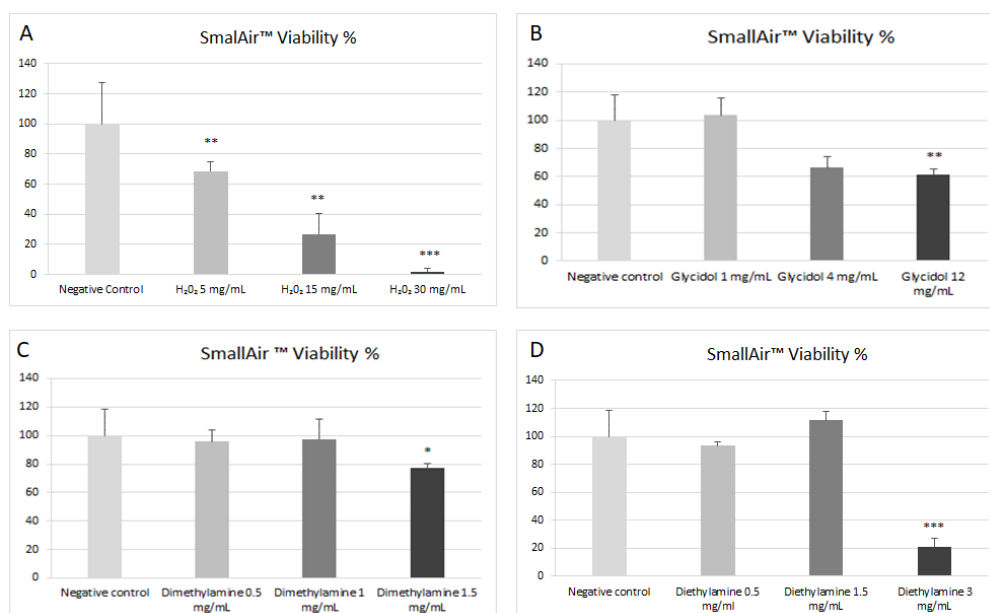


Figure 35. Acute toxicity Test 3 in SmallAir™ results: Viability of the SmallAir™ tissues assessed by the Resazurin test after 3 hour of treatment with a dose range concentration of H₂O₂ (A), Glycidol (B), Dimethylamine (C) and Diethylamine (D). A dose concentration related decrease of viability dose was observed for H₂O₂ and Glycidol. A decrease of viability at the highest concentration tested only was observed for Dimethylamine and Diethylamine treatment.

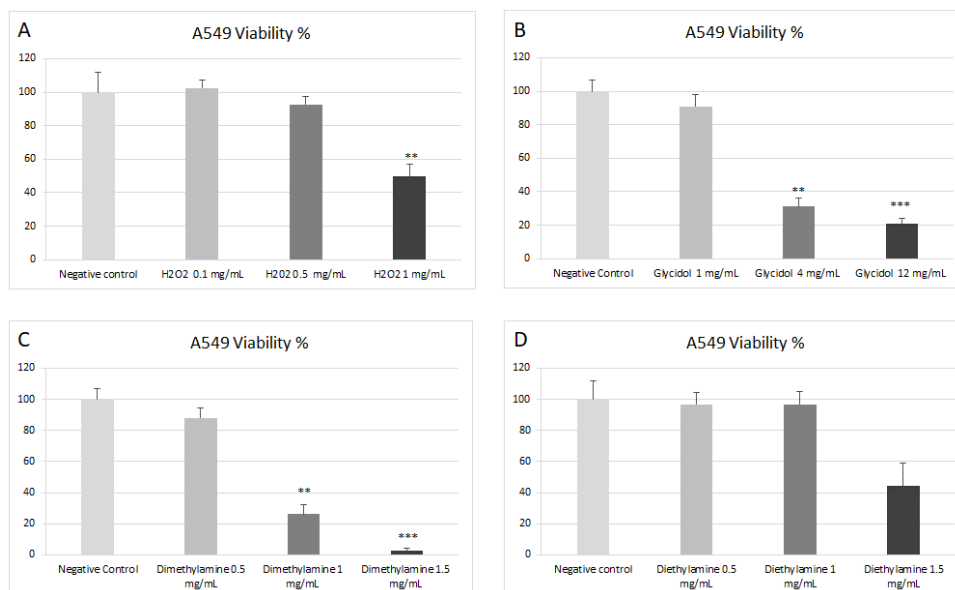


Figure 36 Acute toxicity Test 3 in A549 results: Viability of the A549 cultures assessed by the Resazurin test after 3 hour of treatment with a dose range concentration of H₂O₂ (A), Glycidol (B), Dimethylamine (C) and Diethylamine (D). A dose concentration related decrease of viability dose was observed for H₂O₂, Glycidol and Dimethylamine. A decrease of viability at the highest concentration tested only was observed for Diethylamine treatment.

Table 5. EC75 values calculated for Glycidol, Dimethylamine and H₂O₂, for SmallAir™ and A549. (GraphPad Prism 8)

Compound	SmallAir™ EC75 (mg/mL) ^a	A549 EC75 (mg/mL)
Glycidol	5.591	1.492
Dimethylamine	1.0575	0.62
H ₂ O ₂	4.338	0.741

a = mean of two experiments

The decrease in viability assessed by the Resazurin test was confirmed by the morphological observation. As shown in Figure 37, the tissue resulted damaged with the loosing of the integrity of the barrier and fluctuant cells. The extent of damage observed for each compound treatment correlated with the decrease of viability observed, ranging from slight loss of cells to the complete detachment of the tissue form the membrane. The image of tissues treated with Glycidol only is reported as example.

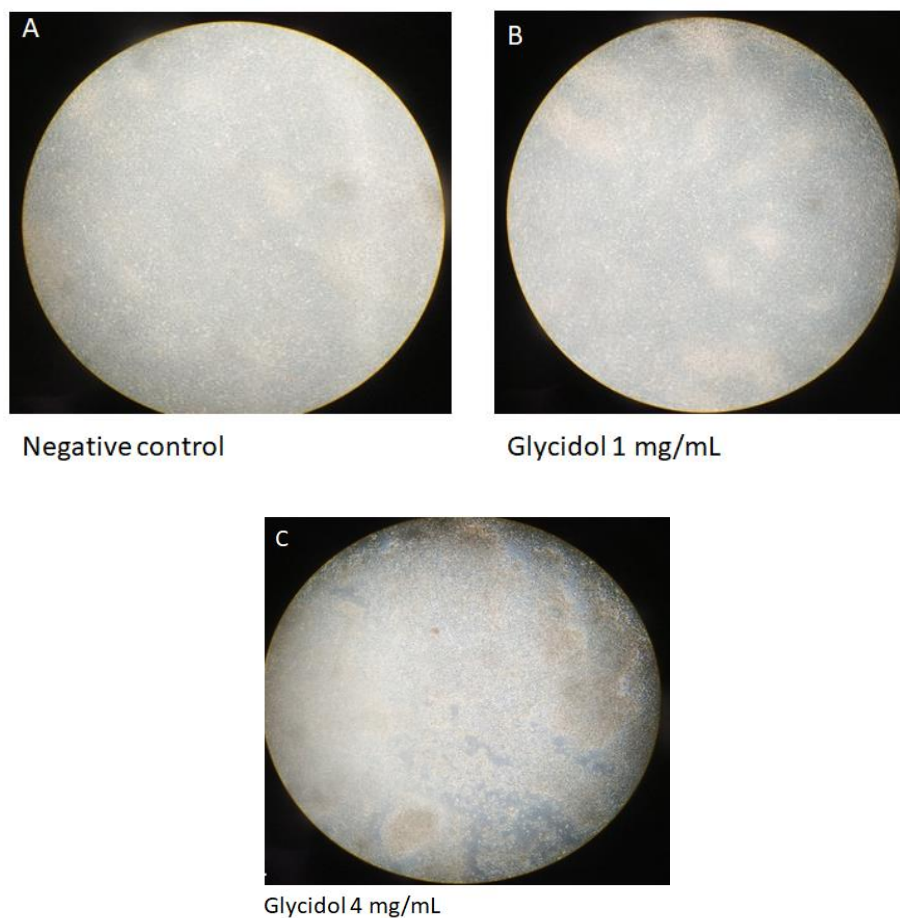


Figure 37. Morphology appearance of the tissues after 3 hours of treatment with negative control (A), Glycidol 1 mg/mL (B) and Glycidol 4 mg/mL (C). At the highest concentration a marked decrease of the integrity of the tissues was observed.(inverted microscope model Leica DML, 12 MPX f/1.7 Samsung S7 camera with magnification 10X).

The LDH released in the medium after treatment with H₂O₂, Glycidol, Dimethylamine and Diethylamine was assessed using LDH-Glo™ Cytotoxicity Assay and the fold increase in comparison to the negative control of each treatment is reported in *Table 6*. No clear dose related increase in the LDH was observed for all treatments and high variability was observed between tissues at the same treatment.

Table 6. LDH Release measured by LDH-Glo™ Cytotoxicity Assay in the medium after treatment with H₂O₂, Glycidol, Dimethylamine and Diethylamine. No dose related increase in LDH was observed. Furthermore, variability was observed between tissues at the same treatment.

Test Compound	Concentration (mg/mL)	Fold Increase \pm sem	
		Tissue 1	Tissue 2
Glycidol	1	1.372 \pm 0.059	0.959 \pm 0.032
	4	0.626 \pm 0.020	0.265 \pm 0.009
	12	1.485 \pm 0.068	0.081 \pm 0.002
Dimethylamine	0.5	0.996 \pm 0.034	0.536 \pm 0.015
	1	0.911 \pm 0.047	0.575 \pm 0.020
	1.5	1.744 \pm 0.073	1.028 \pm 0.014
Diethylamine	0.5	1.476 \pm 0.015	0.334 \pm 0.085
	1.5	1.686 \pm 0.050	0.736 \pm 0.004
	3	3.380 \pm 0.048	1.096 \pm 0.009
H ₂ O ₂	5	1.264 \pm 0.016	0.350 \pm 0.037
	15	4.061 \pm 0.049	-1.861 \pm 0.066
	30	1.903 \pm 0.004	1.300 \pm 0.007

The extent of the damage observed in the integrity of the tissues correlated with their ability to replicate and recover from the injury. As observed in a preliminary test, tissues presenting slight loss of cells were able to recuperate while, when the damage was more extensive, tissues showed not to be able to recover. As example, the images of tissues treated with Dimethylamine at 0.1, 0.5 and 2.5 mg/mL after 1 week of recovery period are reported in *Figure 38*. As can be seen, tissues treated with low concentrations showed to recover the loss of cells, appearing similar to the negative control, while in the tissue treated with the highest concentration the loss of cells was still evident with marked area without cells and fluctuant cells on the surface.

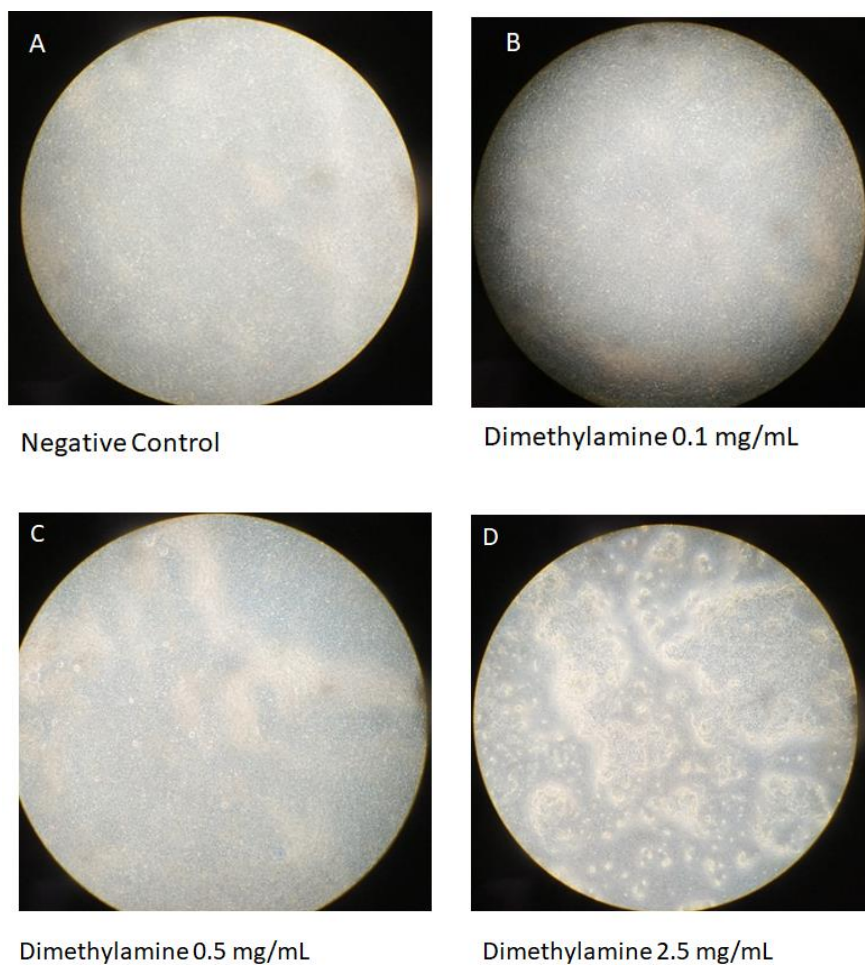


Figure 38. Images of tissue treated for 6 hours with Dimethylamine at 0.1, 0.5 and 2.5 mg/mL after 1 week of recovery. Dimethylamine 1.5 mg/mL. Tissues treated with the lower concentrations, show to recover the loss of cells and appearing similar to the negative control, while in the tissue treated with highest concentration the loss of cells is still evident with marked area without cells and fluctuant cells on the surface (inverted microscope model Leica DML, 12 MPX f/1.7 Samsung S7 camera with magnification 10X).

However, the similarity in the appearance with the negative control was not confirmed by the viability (< 75 % compared to negative control) measured by the Resazurin test (Figure 39). These results could be explained by the possible mechanism of action of the toxic compound tested not only as irritant and corrosive substances but also impairing the cell functionality.

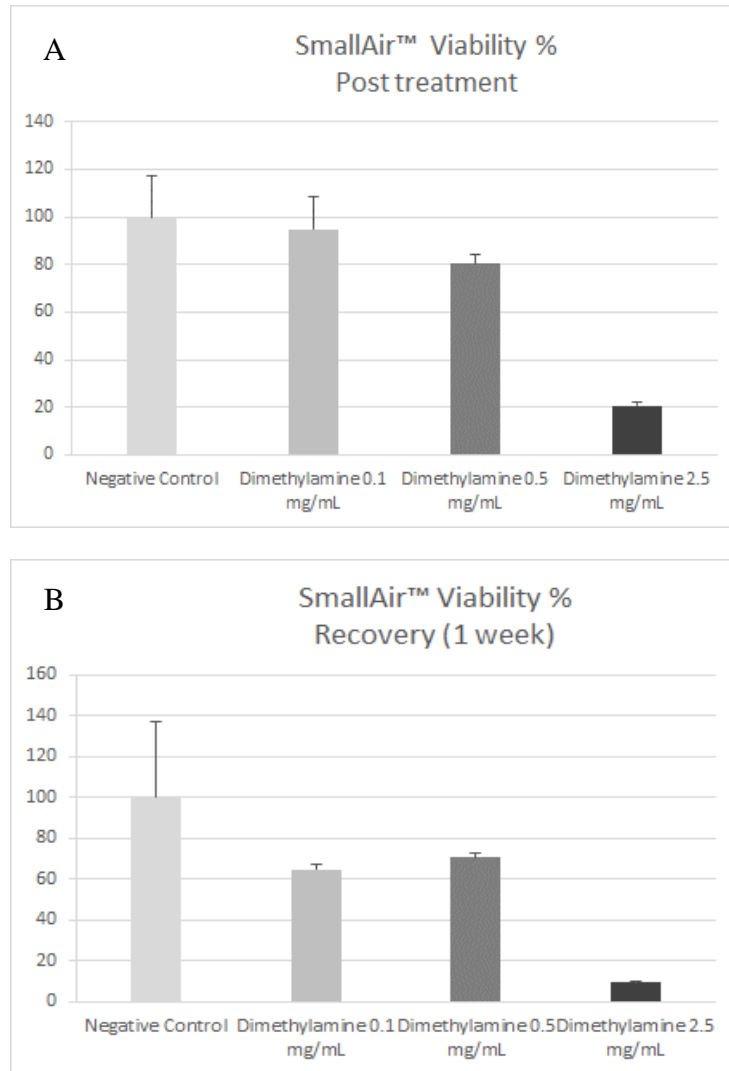


Figure 39. Graphical representation of the viability of SmallAir™ tissues assessed by the Resazurin test immediately after treatment with Dimethylamine 0.1, 0.2 and 2.5 mg/mL (A) and after 1 week of recovery period (B). After 1 week of recovery period all tissues showed a decrease in the viability compared to the values measured immediately after the treatment.

In order to confirm the ability of the tissue to recover the tissue integrity by its replicative capability, one tissue was damaged on purpose and left to recovery. After 24 hours cells replicated and were able to recover the damage and to reconstitute the integrity of the tissue as showed in *Figure 40*.

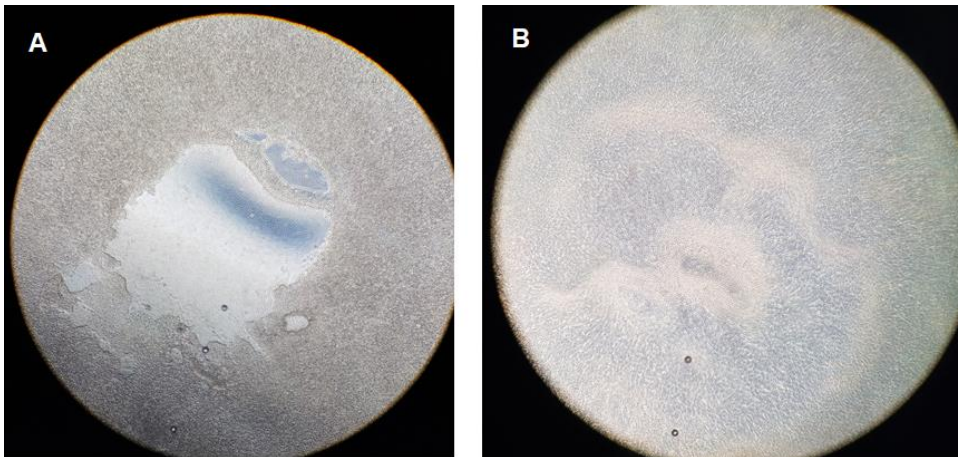


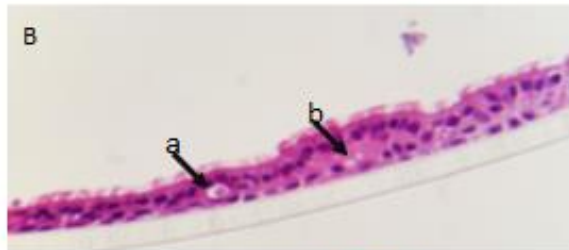
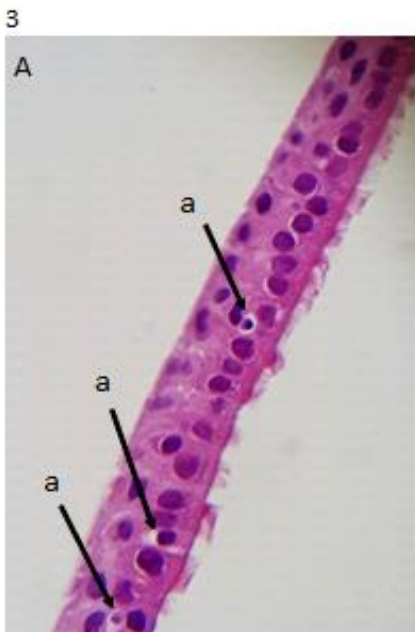
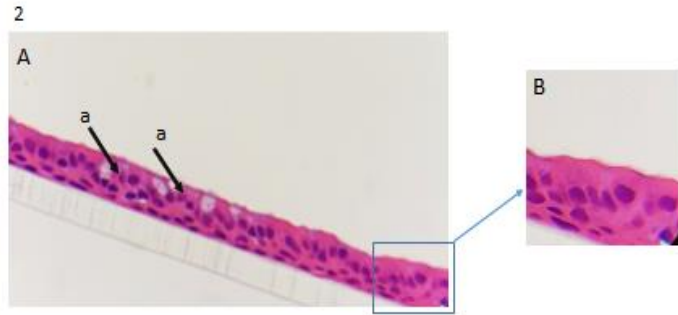
Figure 40. Image of tissue mechanically damaged (A) and the recovery of the integrity of the tissue after 24 hours (B) (inverted microscope model Leica DML, 12 MPX f/1.7 Samsung S7 camera with magnification 10X).

The results of the three test indicate that the Resaruin viability test was able to identify toxic and irritant compounds applied on SmallAir™ model. The TEER measurement, while the TEER measurement was considered not suitable as toxic end point.

5.1.1 Histology Observation

The tissue organization of SmallAir™ cells were evaluated by histological staining. The histoogical evaluation was conducted only in the single dose toxicity test after 72 hours of treatment with LPS, TGF- β and CdCl₂. In the not treated tissues a typical and well preserved respiratory epithelium characterized by AT-I and AT-II normally represented in number and shape was observed (**Error! Reference source ot found.**). In tissues treated with LPS minimal to slight increase in apoptotic cells was evident. Although in general tissue appeared well preserved and organized, focal areas of cellular disorganization were also present (**Error! Reference source ot found.**). In TGF- β treated tissue, a mild to moderate increase in apoptotic cells associated with necrotic cell characterized by nuclear shrinking and cellular debris. In addition an alteration of tissue architecture was evident (**Error! Reference ource not found.**). Finally, CdCl₂ treatment caused a severe tissue disorganization,

characterized by cellular hypertrophy and hyperplasia and associated with diffused necrotic areas. In addition, a detachment from the basal lamina was observed *Figure 41*.



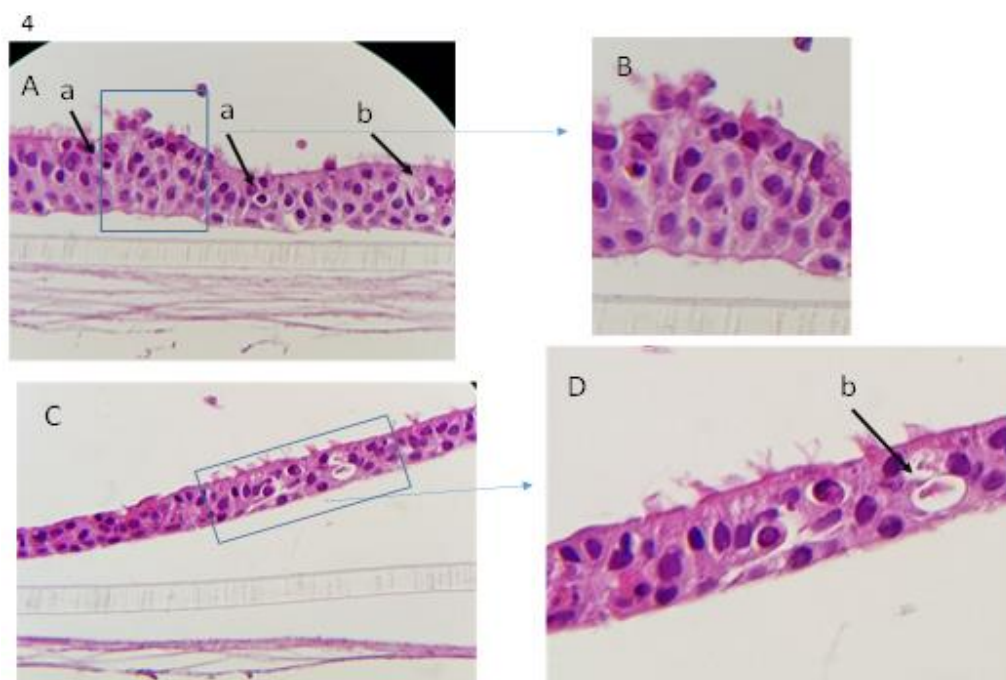


Figure 41. Histology examination of SmallAir™. 1. Not treated tissues with a typical and well preserved respiratory epithelium characterized by AT-I (a) and AT-II (b) normally represented in number and shape. 2. Tissue treated with LPS LPS 100 ng/mL for 72 hours. A. A slight increase in apoptotic cells was observed (a). B. Focal areas of cellular disorganization. 3. Tissue treated with TGF- β 10 ng/mL for 72 hours. A. A mild to moderate increase in apoptotic cells (a). B. Apoptotic cells associated with necrotic cell characterized by nuclear shrinking and cellular debris (b). C. Apoptotic and necrotic cells and alteration of tissues architecture. Focal areas of cellular disorganization. 4. Tissue treated with CdCl₂ 100 μ M for 72 hours. A. severe tissue disorganization, characterized by cellular hypertrophy and hyperplasia and associated with diffused apoptotic (a) and necrotic (b) cells. B. Detail of the tissue architecture disorganization. C. Necrotic area and detachment from the basal lamina was observed. D. Detail of necrotic area with necrotic cells characterized by nuclear shrinking and cellular debris (inverted microscope model Leica DML, 12 MPX f/1.7 Samsung S7 camera with magnification 20X).

These results confirm that irritant and toxic compound on SmallAir™ model induce a tissue disorganization and an increase in apoptotic and necrotic cells.

5.2 Transport Evaluation (Permeability)

The SmallAir™ 3D cell model was applied in order to evaluate the transport of selected compounds through lung tissues. Preliminary tests on transport of aerosol compounds produced by e-cigarette and transport of drug compound as powder formulation have been conducted.

Different cell lines are commonly used for *in vitro* permeability studies, but none of them is known to correctly represent the lung epithelium. The Caco-2 cells model

is considered the standard model and it is used for the Biopharmaceutics Classification System (BCS) by FDA (Food and Drug Administration)(Smetanová et al., 2011), but little is reported in literature about their translational contribution to the study of inhaled drugs.

The commercial 3D respiratory cells model SmallAir™ was evaluated as representative of a physiological model for permeability studies of new formulation of inhaled compounds. A set of commercially available inhaled compounds were tested as liquid formulation in SmallAir™ and permeability data obtained were compared with data obtained in the standard Caco2 cells model.

Compounds selected for the permeability assessment as liquid formulation were:

- Salbutamol: it is a β_2 -adenoreceptor agonist used in the treatment of asthma, COPD and bronchitis that acts relaxing the smooth muscles of all airways resulting in a bronchodilation (www.drugbank.ca). The Salbutamol was assessed as active pharmaceutical ingredient form (API) and as aerosol formulation (Broncovaleas®).
- Budesonide: they are corticosteroids used in the treatment of asthma and some kind of rhinitis (as well as some skin diseases) (www.drugbank.ca). Budesonide was used both as API and as suspension for nebulization (Budesonide Aircort®) while FP was used as API.
- Theophylline: it is a methylxanthine indicated for asthma, bronchospasm, and COPD treatment.
- Tiotropium bromide: it is an antimuscarinic bronchodilator used in the treatment of COPD and asthma commercially available as Spiriva Respimat (Boehringer Ingelheim Pharmaceuticals, Inc.) in the form of solution per inhalation with its inhaler (www.drugbank.ca).
- Digoxin: it is a well-known P-gp substrate and it was tested in order to assess the presence of the P-gp transporter in the SmallAir™ cells.

The commercial device CULTEX® RFS Compact (Cultex Laboratories GmbH, Hannover, Germany) has been evaluated as exposure device for nebulized drug formulation (L.Pomari 2019) and for e-smoke exposure.

Additionally, an experiment was performed to evaluate the permeability of a compound as powder formulation. For the treatment with the powder form of the compound tested, a modification of the Next Generation Impactor (NGI) was implemented. The permeability of the deposited powder was compared with data obtained after treatment with liquid formulation.

5.2.1 Permeability studies in SmallAir™ - liquid treatment

The permeability data obtained for each compound analyzed in SmallAir™ are showed in *Table 7*. The results are expressed as the mean of the permeability (Papp) values of each sample \pm SD, while the Efflux Ratio is expressed as mean of each experiment \pm SD.

Compound	A to B (nm/sec)	N	B to A (nm/sec)	N	Efflux Ratio	Net Flow direction
Salbutamol	2.92 \pm 2.12	12	5.70 \pm 4.63	9	2.47 \pm 1.98	Efflux
Budesonide	169 \pm 38	5	101 \pm 47	6	0.588 \pm 0.215	No net transport
Tiotropium Bromide	3.22 \pm 2.63	7	11.3 \pm 9.0	7	3.81 \pm 1.08	Efflux
Digoxin	37.0 \pm 4.9	4	45.2 \pm 6.2	4	1.22 \pm 0.13	No net transport

Table 7. Permeability results through SmallAir™. Permeability results of Salbutamol, Budesonide, Tiotropium Bromide and Digoxin in direction A to B and B to A in nm/sec and Efflux Ratio is expressed as mean values of replicate (N) \pm SD.

In detail, Salbutamol and Tiotropium bromide showed a higher B to A permeability, resulting to be low permeability compounds and therefore good candidates for efflux transporters' substrate. Budesonide did not show a net transport and therefore

showed to be a high permeability compound. Digoxine did not show a net transport but with a medium permeability in both directions.

Permeability observed in SmallAir™ cells showed to be comparable with data obtained in Caco2 (L. Pomari, 2019). However, a couple of differences were observed. First of all, B to A permeability of Tiotropium bromide and A to B permeability of Digoxin in SmallAir™ were statistical significant higher in comparison to Caco2 model (*Figure 42*).

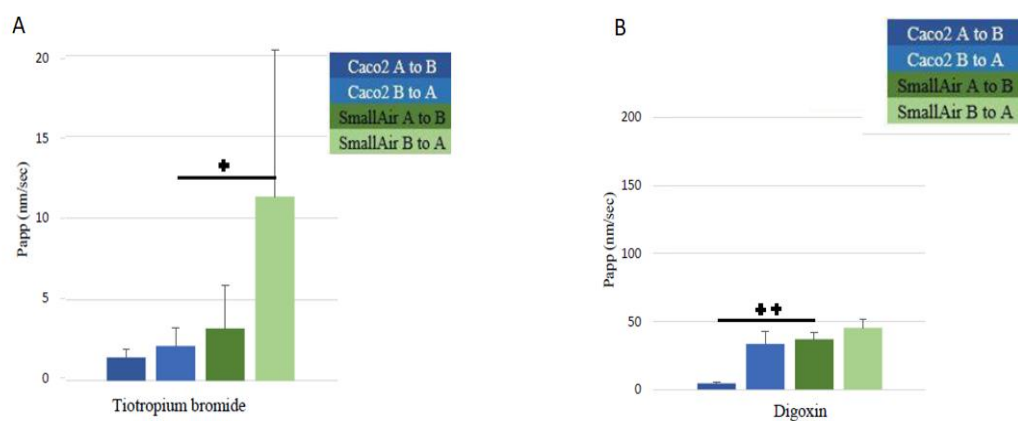


Figure 42. Permeability expressed as Papp (nm/sec) of Tiotropium (A) and Digoxin (B) in SmallAir™ and Caco2. A higher B to A permeability of Tiotropium bromide and A to B permeability of Digoxin was observed in SmallAir™ compared to Caco2 test system Data are expressed as Mean \pm SD with statistically significant increase (+: $p < 0.05$, ++: $p < 0.01$). Taken from L.Pomari, 2019.

Secondly, comparing the ER obtained in SmallAir™ and Caco2 cells, Salbutamol showed to diffuse passively in Caco2 while seems to have an efflux in SmallAir™ (even if the high variability observed in SmallAir™ did not allow to observe a statistically significant difference). Tiotropium bromide showed efflux only in SmallAir™. Budesonide did not show an efflux in both model. At last Digoxin, which is the reference compound as P-gp substrate for Caco-2 did not show any transport-mediated efflux in SmallAir™ (*Figure 43*).

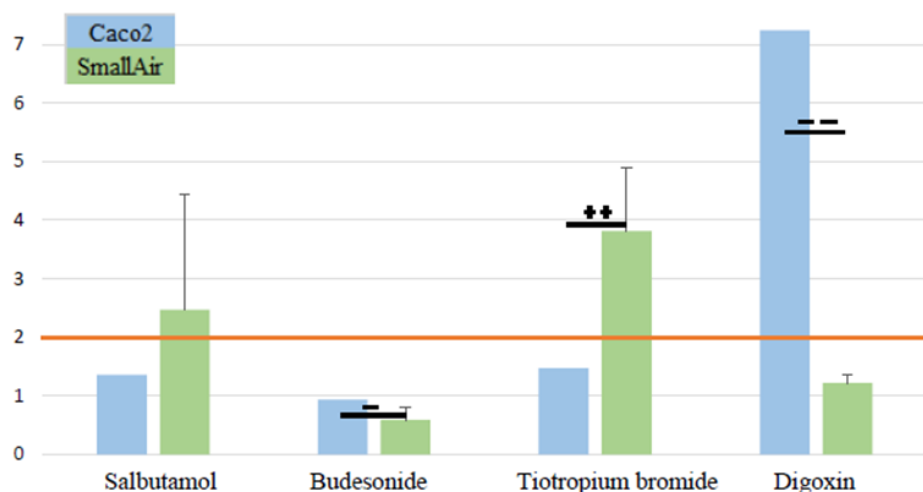


Figure 43. Efflux ratio in SmallAir™ vs Caco2, with limit for efflux consideration set at 2 for Salbutamol, Budesonide, Tiotropium bromide and Digoxin. Data are expressed as mean for Caco2 and as mean \pm SD with statistically significant increase/decrease (+/-: $p < 0.05$; ++/-: $p < 0.01$). Taken from L.Pomari, 2019.

Data showed a difference in Tiotropium bromide and Digoxin's efflux ratio. In particular, Digoxin, a well-known P-gp substrate, showed permeability values in the two directions A to B and B similar to each other. This observation should be due to a less abundant expression of P-gp in SmallAir™ or it might be expressed as different isoforme with different specificity for these compound.

These results indicate that SmallAir™ model should express specific lung transporter and better represent the *in vivo* situation.

5.2.2 Permeability studies in SmallAir™ - aerosol treatment

CULTEX® was used for the treatment of SmallAir™ tissues with Broncovaleas® and Budesonide Aircort®, but no reliable data were obtained. In particular, when the CULTEX® was connected to a mixing chamber to combine the aerosol with regular air, the aerosol condensation on the inner surfaces of the mixer chamber was observed and no aerosol was able to reach the tissues. For the following experiment, the nebulizer was then connected directly to the CULTEX® and in order to avoid tissues damage different time of exposure have been tested.

However, permeability results obtained were considered not reliable, showing an unreasonably high values probably due to the high fluid pressure that could facilitate the permeability of the drug through the monolayer.

In the permeability assessment of nicotine after e-smoke exposure, results of TEER measurement pre-treatment and post-treatment showed a high variability inter-tissues. However, all values were $>200\Omega\cdot\text{cm}^2$, indicating no loss in the membrane integrity (*Figure 44*).

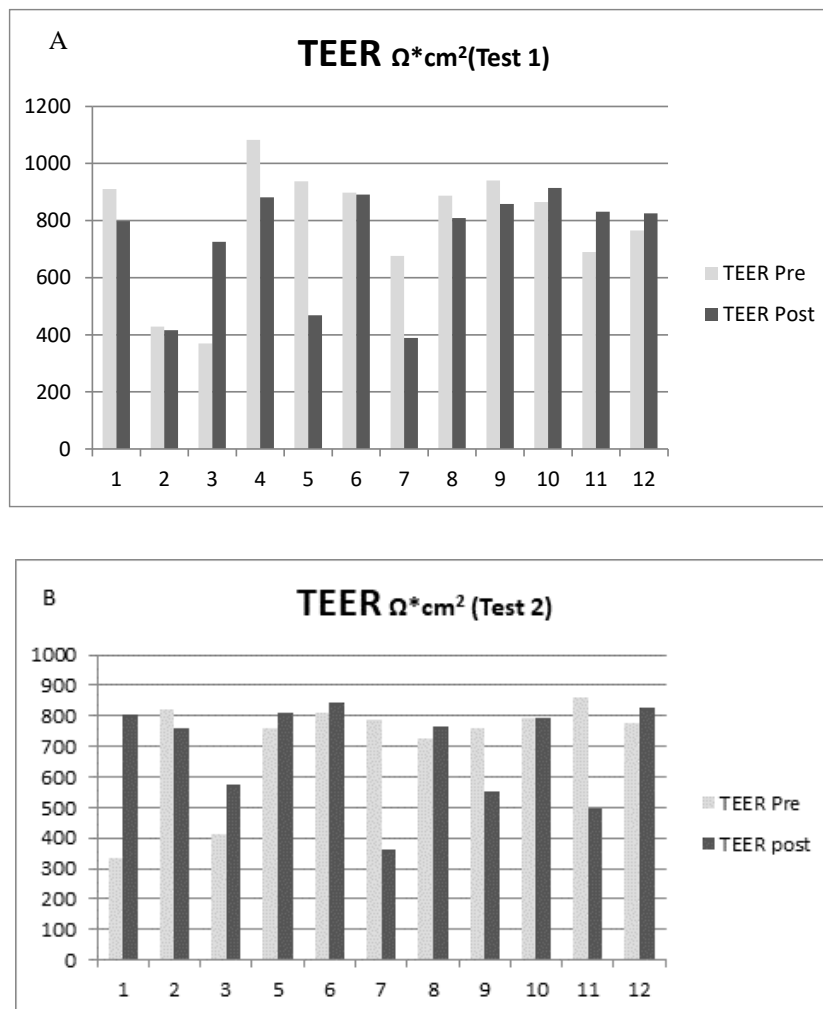


Figure 44. TEER values, expressed as $\Omega\cdot\text{cm}^2$, measured pre- and post-treatment with e-smoke produced by two different devices (A: Test 1 and B: Test 2).

The results obtained in the LY assay, also confirmed the integrity of the tissues. In particular in Test 1 % of rejection for all tissues were 100 % where in Test 2 tissue showed values of % of rejection ranging between 97.3 % and 98.4%.

The viability assessment of the tissues, in the Test 1 was 90.52% and 84.67% (average of two tissues) immediately after vehicle and e-liquid treatment respectively. In the Test 2, the viability of the tissues was 97.99% and 78.09% (average of two tissues) immediately after vehicle and e-liquid treatment respectively. Data are graphically showed in *Figure 45*.

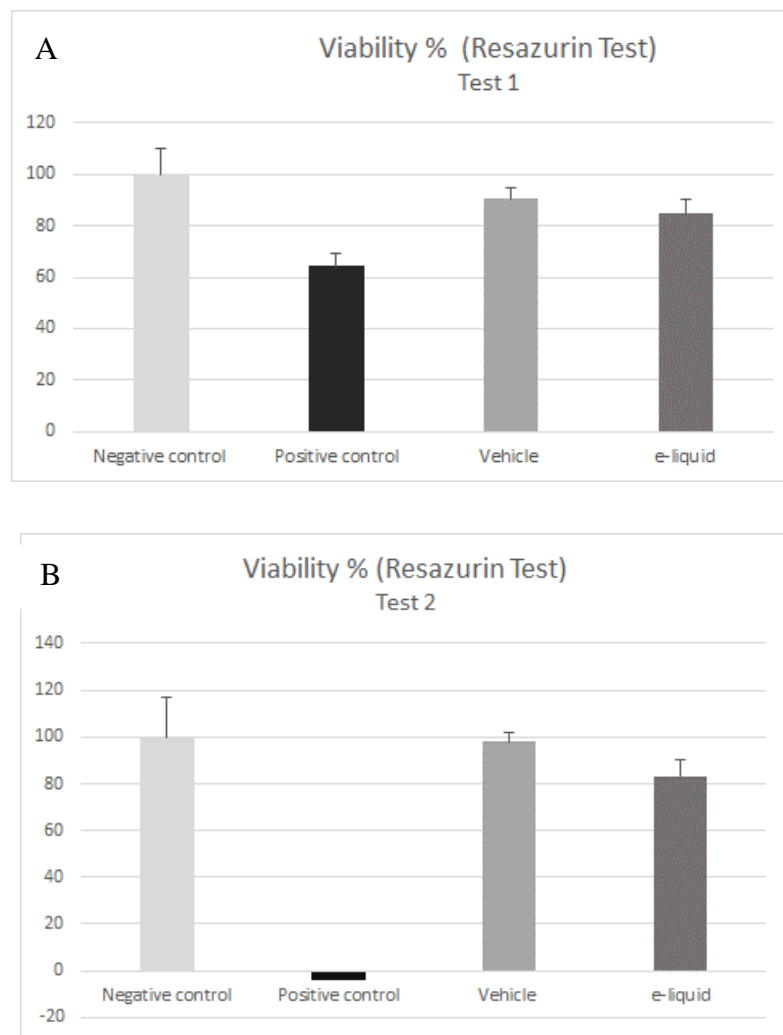


Figure 45. Graphical representation of viability of SmallAir™ measured after treatment with e-smoke produced by two different devices (A. Test 1 and B. Test 2). In both test, viability of tissues treated with vehicle and with e-liquid containing nicotine was above 80% indicating viability of the tissues. In test 2 the positive control showed a negative viability since due to technical problem the H₂O₂ remained in contact with the tissue for longer time compared to Test 1.

Nicotine concentration measured for each device is reported in *Table 8*. Similar nicotine concentrations were measured in the samples obtained from the well without tissue and in the samples from the well with tissues. These results, along with the integrity of the tissues confirmed by TEER and LY values, suggest that all the nicotine has been transported through the tissues. Differences observed between the two commercial e-cigarettes tested in Test 1 and Test 2 should be due to difference in the mechanism of action.

A

Nicotine Concentration ng/mL (Test 1)		
	Time point 2 min	Time point 5 min
No Tissue	3947.89	3943.75
Tissue 1	5523.31	5752.8
Tissue 2	2904.71	3129.06
Average	4125.30	4275.20
SD	1318.28	1342.91

B

Nicotine Concentration ng/mL (Test 2)			
		2 min	5 min
Run 1	No Tissue	1649.66	1383.02
	Tissue 1	1358.37	1470.72
	Tissue 2	NS	935.44
Run 2	No Tissue	378.43	367.75
	Tissue 1	368.23	397.34
	Tissue 2	213.26	212.86
Average		793.59	794.52
SD		659.91	548.02

NS = no sample due to technical issue

Table 8. Nicotine concentrations measured in the medium after e-liquid treatment produced by two different devices (A and B respectively). Similar nicotine concentrations were observed in samples collected from wells without tissue and with tissues indicating that all the nicotine applied passed through the tissues. Variability observed between the two tests should be due different mechanism of action of the two devices evaluated.

5.2.3 Permeability studies in SmallAir™ - powder treatment

The reliability of the use of the NGI modified as device to treat tissue transwells, was confirmed by the Leak Test that showed values below 100Pa/s.

Furthermore in the preliminary test conducted to confirm that the same amount of compound was deposited in each well comparable peak area (expressed as $\mu\text{V}\cdot\text{sec}$) were obtained, considering the analytical variability (*Table 9*).

TEST 1		TEST 2	
Sample 1	3396 $\mu\text{V}\cdot\text{sec}$	Sample 1	2848 $\mu\text{V}\cdot\text{sec}$
Sample 2	2591 $\mu\text{V}\cdot\text{sec}$	Sample 2	4102 $\mu\text{V}\cdot\text{sec}$
Sample 3	2239 $\mu\text{V}\cdot\text{sec}$,	Sample 3	6201 $\mu\text{V}\cdot\text{sec}$

Table 9. Area peak (expressed as $\mu\text{V}\cdot\text{sec}$) of Tiotropium Bromide dry powder results obtained in the preliminary test with NGI modified. Comparable peak area were obtained, considering the analytical variability.

In the final test, the TEER of the two tissues treated with Tiotropium Bromide dry power was measured pre and post treatment and no effect on TEER was observed indicating the integrity of the tissue. Value measured are showed in *Table 10*.

Sample	TEER $\Omega\cdot\text{cm}_2$	
	Pre-treatment	Post - Treatment
1	1125.3	1095.6
2	1141.8	1174.8

Table 10. TEER values ($\Omega\cdot\text{cm}^2$) measured pre and post treatment with aerosol of Tiotropium bromide, using the Next Generation Impactor.

Despite the TEER values, the microscopic observation (*Figure 46*) showed the presence of some air bubbles in one tissue that resulted in the detachment of tissue from the porous membrane and the consequent cell death.



Figure 46. Image of the tissues treated with aerosol of Tiotropium bromide by the Next Generation Impactor. Evident air bubbles have been observed, resulting in the final detachment and death of the tissues (inverted microscope model Leica DML, 12 MPX f/1.7 Samsung S7 camera with magnification 10X).

5.3 Inflammatory mediators assessment

The following inflammatory mediators were selected in the analyses:

- pSMAD2
- Cytokines and pro-inflammatory mediators: IL-6, RANTES, IP-10, ETXN, IL-4, MIP-1 β , IL-8 and GRO
- LDH
- ROS

5.3.1 pSMAD2 assessment

One of the major mediators of extracellular matrix (ECM) remodeling either in physiological (such as wound healing) or pathological conditions (as in pulmonary fibrosis) is the cytokine TGF- β 1. TGF- β 1 belongs to the TGF- β superfamily, and as the highly homologous isoforms TGF- β 2 and TGF- β 3, is usually present in the ECM in a latent form. Following TGF- β 1 activation (e.g. proteolytic cleavage, interaction with integrins or pH changes), active TGF- β 1 is free to bind its receptors at the cell surface. All the members of TGF- β superfamily signal via heteromeric complexes of two related transmembrane type I and type II serine/threonine kinase receptors, known as ALK5. The activation of ALK5 leads to the propagation of

signaling by the SMAD-dependent pathway, through ALK5-mediated phosphorylation of SMAD2 and SMAD3, which in turns regulate transcription of target genes (Zi et al., 2014).

TGF- β has been widely evaluated for its crucial role in the development of pulmonary fibrosis and airway remodeling during the late phases of chronic lung injury therefore in this project the SMAD2 phosphorylation was assessed in the SmallAir™, in order to evaluate the potential of this test system as more physiological in vitro pulmonary fibrosis model. Indeed, understanding the precise molecular mechanism that lead to ECM remodelling could help in the identification of novel therapeutic targets for fibrosis in the lung.

5.3.2 Cytokines release, ROS and LDH release

In vivo pulmonary toxicity is characterized by an initiating event such as bacterial or viral infection or chemical insult that leads to the activation of the inflammatory response. This initial activation induces the production of proinflammatory cytokines, such as interleukin 1-alpha (IL-1 α), interleukin 6 (IL-6), interleukin 8 (IL-8), tumor necrosis factor alpha (TNF- α), and TGF- β), that induce neutrophil activation and migration to the alveolar space. Activated neutrophils continue the immunological initiation process by induction of reactive oxygen species (ROS), cytokines and chemokines (Willoughby J.A., 2015). A preliminary experiment was conducted in order to evaluate the SmallAir™ model as possible in vitro model for inflammatory end points assessment such as cytokines secretion, lactate dehydrogenase (LDH) release and ROS. For this purpose, the effect of the bleomycin treatment was assessed.

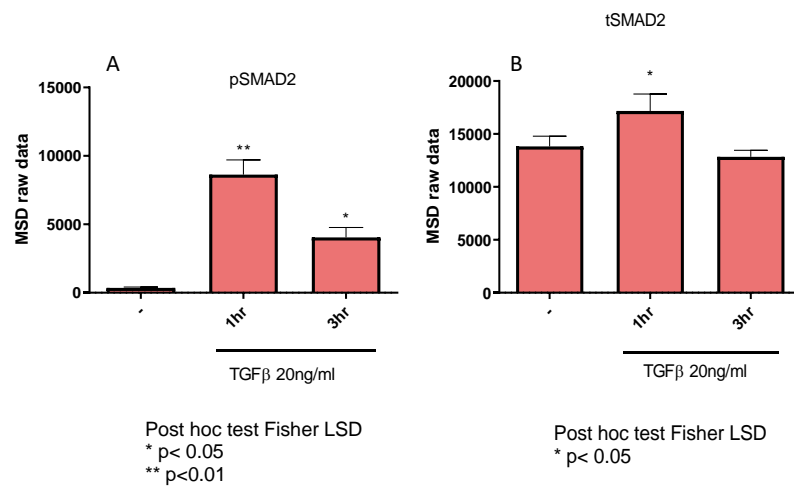
The most common animal model of pulmonary fibrosis is the bleomycin model in rodent. Over the years, numerous agents have been tested in this model. The translation of these results into clinical practice has not been accomplished yet, therefore the evaluation of alternative and/ or complementary models which better reflect human idiopathic pulmonary fibrosis (IPF) is desired (Moeller et al., 2008). Bleomycin is a chemotherapeutic antibiotic, produced by the bacterium “*Streptomyces verticillus*” and one of the major adverse drug effects of bleomycin in human cancer therapy is the pulmonary fibrosis (Hare, 1998; Karam et al., 1995).

The mechanism of bleomycin toxicity is unclear and likely multifactorial. Oxidative damage, release of inflammatory cytokines, a deficiency of the bleomycin hydroxylase enzyme in the lungs and genetic predisposition have been described (Ge et al., 2018). An overproduction of reactive oxygen species can lead to an inflammatory response causing pulmonary toxicity, activation of fibroblasts and subsequent fibrosis. The initial elevation of pro-inflammatory cytokines is followed by increased expression of pro-fibrotic markers (transforming growth factor- β 1, fibronectin, procollagen-1) (Moeller et al., 2008).

In order to evaluate the SmallAir™ cells as possible *in vitro* model for pulmonary fibrosis the effect of bleomycin treatment was assessed by the measurement of different end points such as cytokines and LDH, ROS production and viability.

5.3.3 pSMAD2 analysis

Results obtained for the pSMAD2 assessment are reported in the *Figure 47*. In detail, pSMAD2/tSMAD2 ratio was significantly increased by TGF- β treatment (20 ng/ml) both at 1 hour and 3 hour time-points.



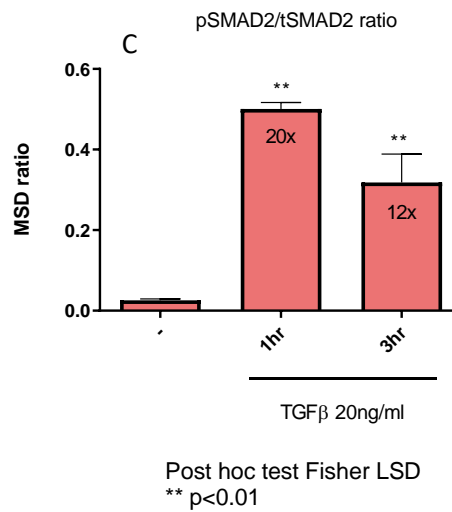


Figure 47. Results of pSMAD2 quantification in SmallAir™ after TGF-β treatment and statistical analysis (Meso Scale Discovery's Assay). A. pSMAD2 concentration (expressed as raw data) after 1 and 3 hours of treatment. B tSMAD2 concentration (expressed as raw data) after 1 and 3 hours of treatment. C. pSMAD2/tSMAD2 ratio after 1 and 3 hours of treatment.

5.3.4 Cytokines, LDH release and ROS evaluation

Cytokines release. Results obtained in the measurement of cytokines and pro-inflammatory mediatory release after Bleomycin treatment are presented in Figure 48.

Eight different cytokines and pro-inflammatory mediators were analysed: IL-6, RANTES, IP-10, ETXN, IL-4, MIP-1β, IL-8 and GRO.

IL-6 was not significantly modulated by Bleomycin treatment. RANTES and IP-10 showed a decreasing trend after Bleomycin treatment compared to negative control. Etxn, IL-4 and MIP-1β seems to be poorly secreted by the tissue, showing levels below the determination limit. While IL-8 and GRO levels showed to be out of range (for these parameters a sample dilutions should be recommended for further assay).

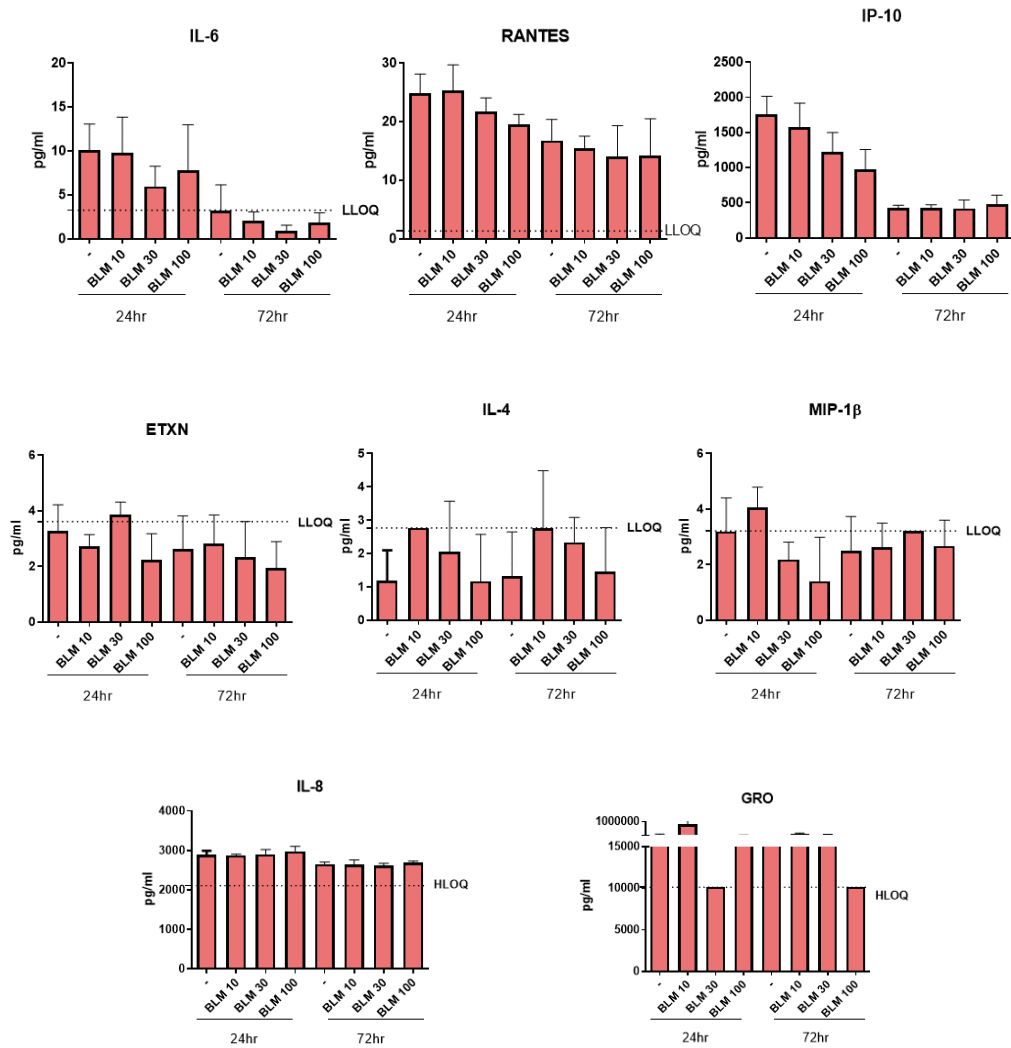


Figure 48. Cytokines measurement in the medium after Bleomycin treatment at 10, 30 and 100 μM for 24 and 72 hours (Luminex bead-based Multiplex Assay).

Viability of SmallAir™ tissues was measured in presence of increased amounts of Bleomycin. and results are presented in the Figure 49. No effect on viability was observed in SmallAir™ tissues after 48 hours of treatment with Bleomycin at 10, 30 and 100 μM .

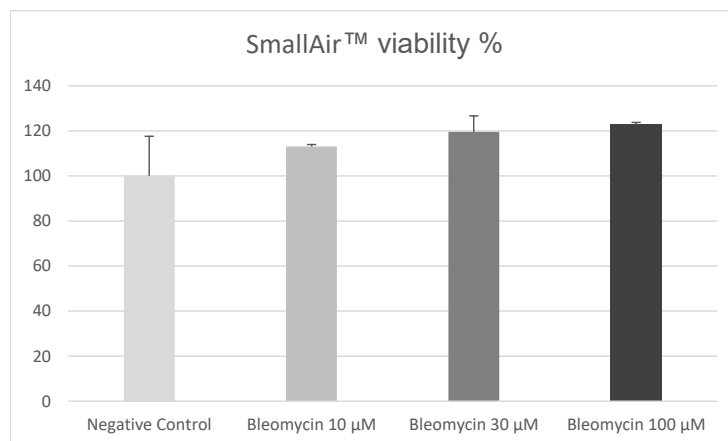


Figure 49. Viability of SmallAir™ tissues expressed as % versus negative control after 48 hours of treatment with Bleomycin at 10, 20 and 100 μM .

These results were confirmed by the microscopical observation. As showed in Figure 50 no damage to the integrity of tissues was observed.

LDH release. Samples obtained from the medium of SmallAir™ cultures treated with Bleomycin at concentration of 10, 30 and 100 μM were analyzed with a bioluminescence method (LDH-Glo™ Cytotoxicity Assay). Results are showed in Table 11. A high variability between the samples were observed. No increase was observed after 24 hours of treatment except for the Tissue 3 at 100 μM . A slight increase was observed after 48 hours for all condition tested, but no dose related trend was observed except for Tissue 3 at 100 μM . The LDH positive control was tested at different concentration (serial dilution) confirming the validity of the test.

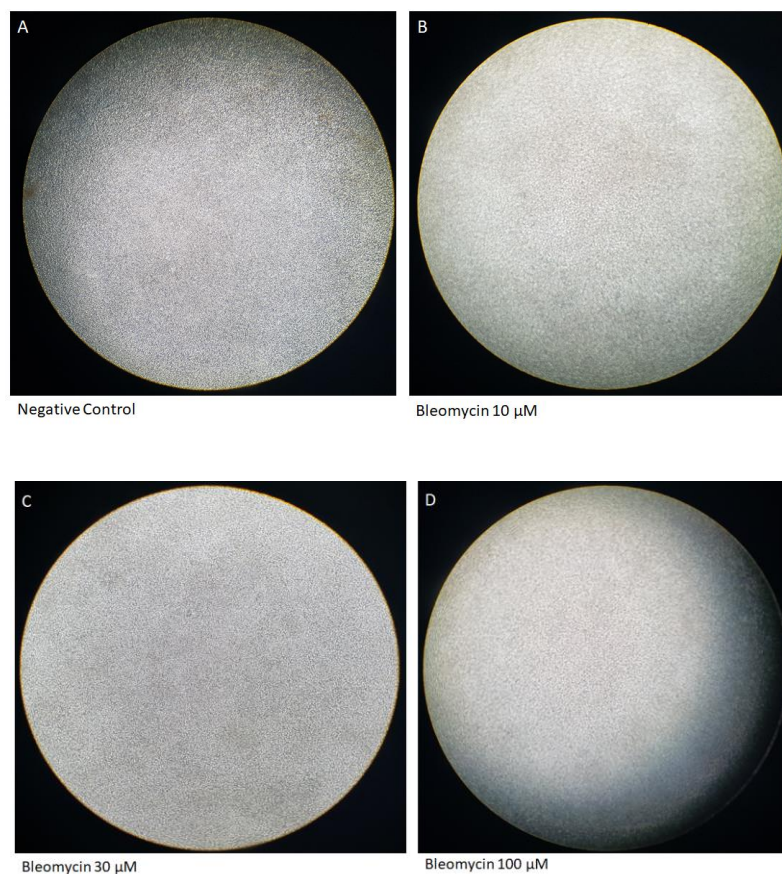


Figure 50. Images of SmallAir™ tissues after 48 hours of treatment with Belomycin at 10, 30 and 100 μM (inverted microscope model Leica DML, 12 MPX f/1.7 Samsung S7 camera with magnification 10X).

Table 11. LDH Release measured by LDH-Glo™ Cytotoxicity Assay in the medium following Bleomycin 10, 30 and 100 μM treatment after 24 and 48 hours. An increase in the LDH was observed in all samples after 48 hour of treatment. However no dose-elated effect was observed.

Bleomycin Concentration	Treatment	Fold Increase Tissue 1	Fold Increase Tissue 2	Fold Increase Tissue 3
10 μM	24 hr	0.71	1.21	1.22
30 μM		0.71	1.05	1.15
100 μM		0.65	0.91	1.76
10 μM	48 hr	2.58	1.24	1.04
30 μM		2.53	1.11	1.55
100 μM		0.86	1.48	3.19

ROS measurement. Samples obtained from the medium of SmallAir™ cultures treated with Bleomycin at concentration of 10, 30 and 100 µM were analysed with the luminiscence method ROS-Glo™ H₂O₂ Assay. The method was not able to measure any amount of ROS in the samples and all samples resulted to be under the detection limit indicating that the method used should be not suitable for the ROS measurement in SmallAir™ model.

5.4 Muco-ciliary Clearance Assessment

Different drugs can be administered in order to alleviate respiratory disorders, such as dyspnea and bronchospasm. Some of these drugs, however, are claimed to influence the (MCC). Since MCC plays an important role as defense mechanism, the influence on MCC of drugs administered to patients with respiratory disorders must be evaluated.

The role of airway clearance in inhaled drug therapy is complex. The knowledge of the influence of a specific drug on mucus clearance may lead to a better therapeutic use of such medication (Houtmeyers et al., 1999).

Furthermore, MCC is reported to be impaired in certain diseases, such as cystic fibrosis (CF), chronic obstructive pulmonary disease (COPD), primary ciliary dyskinesia (PCD), chronic rhinosinusitis (CRS), and asthma (Joo et al., 2016).

Optimal airway muco-ciliary clearance depends upon the speed and effectiveness of ciliary beating, the rheological properties of the mucus, and structurally intact airways.

In this project the SmallAir™ model was investigated as a possible in vitro model for the assessment of MCC in response to exposure to different compounds:

- agonists Forskolin and Carbachol
- ion transport inhibitors CFTRInh-172
- a set of commercially available inhaled compounds, ipertonic solution (NaCl 3%) and LPS

Forskolin is a member of the diterpene family and activates the Cystic fibrosis transmembrane conductance regulator (CFTR) chloride channel by raising the

amount of intracellular cyclic AMP, leading to fluid secretion. The CFTRInh-172 is an inhibitors of CFTR chloride channel and it is used as tools to investigate the role and function of CFTR conductance in cystic fibrosis research. (Melis et al., 2014). Joo N.S et al. observed in an ex vivo ferret trachea model that CFTR inhibitors modestly depressed MCCV stimulated by [cAMP]_i-elevating agents, but not basal MCCV nor that stimulated by [Ca²⁺]_i-elevating agents (Joo et al., 2016).

Carbachol, a synthetic choline, acts as nicotinic acetylcholine receptor agonist and it showed to increase the MCC by increasing [Ca²⁺]_i (Joo et al., 2016).

The effect of inhaled compound Budesonide, Salbutamol, Tiotropium bromide, Fluticasone and Theophylline on MCC in SmallAir™ was evaluated and results were used as input data for a in silico simulation with the MPPD model, in order to assess the impact of the MCC variation in the excretion of an inhaled compound.

Airways contaminants like lyposaccharide (LPS) activate a specific toll like receptors (TLR4) of the immune system that produce an inflammatory response associated to the production of cytokines by the airway epithelium. Test conducted on Primary cultures of mouse (Balbc) tracheal epithelium showed that LPS induces an increase in CBF in a dose response manner by increasing the release of ATP (D. V. Carreno et al., 2013).

The ipertonic solution (NaCl 3%) was assessed to confirm the block effect reported in literature (Schipper & Verhoef, J.C. & Merkus, 1991).

5.4.1 Results of Automatic and Manual methods evaluation.

The number of frames captured by the automatic analysis (Mosaic- Particle Tracker 2D/3D plugins), for both muco-ciliary Test 1 and Test 2 were analysed. Since reproducible results were obtained with both test, only one condition (negative control) is reported in *Figure 51*. In detail, the results showed that in each conditions analysed a high percentage of trajectories are constituted by few frames (lower than 10) or by the maximum of 50 frames. Observing the video of trajectories captured, the system showed to lose the tracking of many beads during the path making the analysis not reliable. Therefore for the following analysis of the speed of the beads, trajectories with less 45 frames were excluded from the analysis.

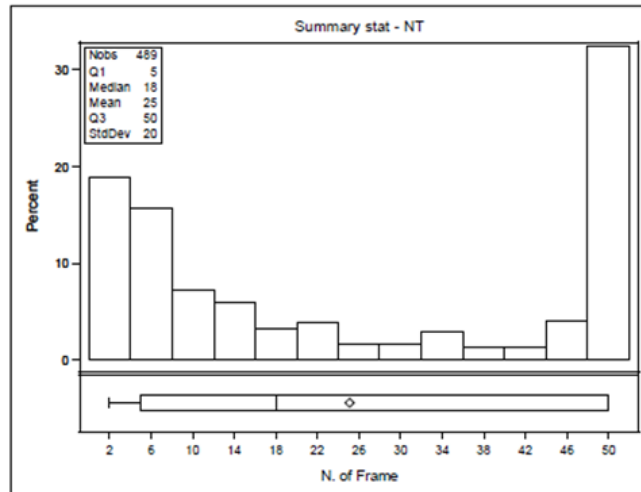


Figure 51. Analysis of the distribution of frames number for the trajectories captured by Mosaic-Particle Tracker 2D/3D plugins.

The effect on the MCC of the treatment with CFTRInh-172 20 μ M and FRSK 3 μ M evaluated by automatic and manual method are reported in *Figure 52* and *Figure 53* respectively. Both in automatic and in manual analysis the treatment with CFTR showed to decrease significantly the MCC in comparison to the not treated tissue. The FRSK treatment following the CFTR treatment showed to decrease the MCC in the automatic analysis while to increase the MCC in the manual analysis. Only the results obtained in the manual analysis confirmed the microscopical observation.

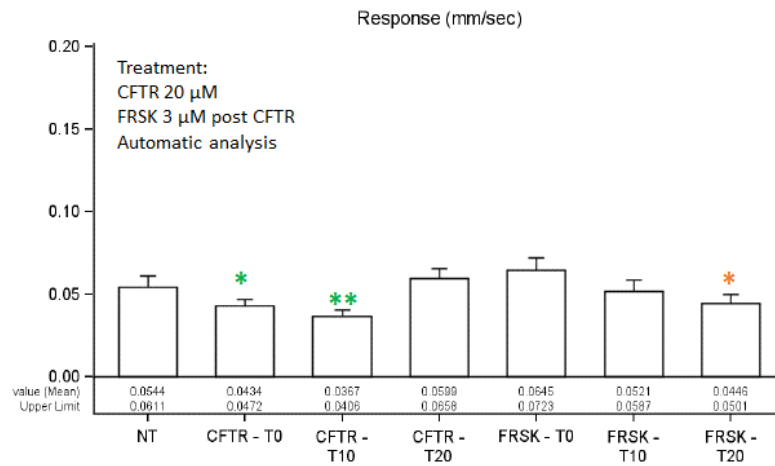


Figure 52. Muco-ciliary results expressed as beads speed (mm/sec) in SmallAir™ after treatment with CFTRInh172 at T0, T10 and T20 followed by treatment with FRSK 3 μM at T0, T10 and T20 obtained by automatic analysis. CFTR treatment showed to decrease the MCC compared to the not treated tissue at T0 and T10. A decrease of MCC after FRSK treatment following the CFTR treatment was observed at T20. Statistical significance difference of each treatment versus not treated tissues is represented by green * (*: $p < 0.05$; **: $P < 0.001$); the statistical significance difference of FRSK treatment versus the last time point of CFTR treatment is represented by red * (*: $p < 0.05$).

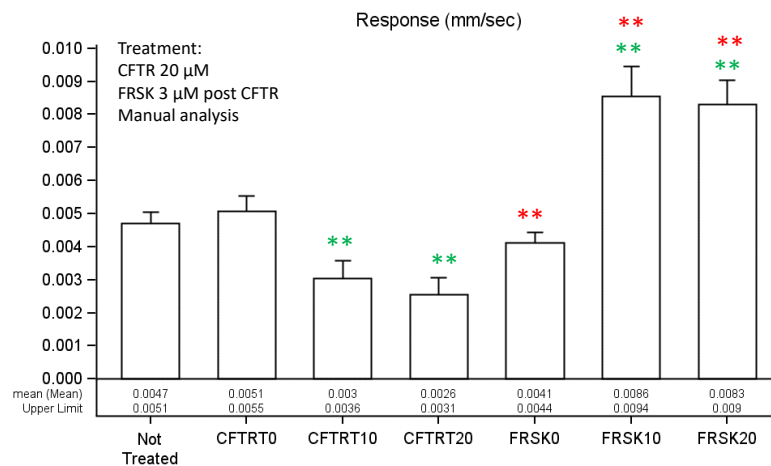
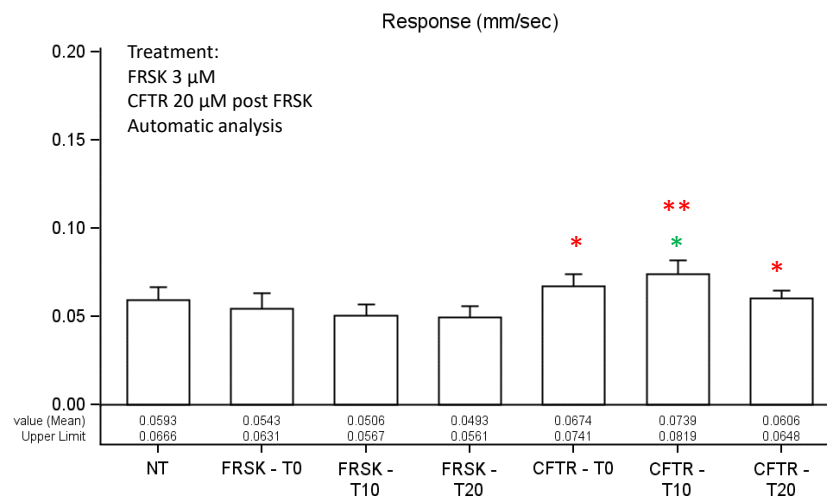


Figure 53. Muco-ciliary results expressed as beads speed (mm/sec) in SmallAir™ after treatment with CFTRInh172 20 μM at T0, T10 and T20 followed by treatment with FRSK 3 μM at T0, T10 and T20 obtained by manual analysis. CFTR treatment showed to decrease the MCC compared to the not treated tissue at T10 and T20. An increase of MCC after FRSK treatment was observed both in comparison to the not treated tissues at T10 and T20 and in comparison to the CFTR treatment at each time point. Statistical significance difference of each treatment versus not treated tissues is represented by green * (**: $P < 0.001$); the statistical significance of difference FRSK treatment versus the last time point of CFTR treatment is represented by red * (**: $P < 0.001$).

The comparison of the automatic and manual method in the analysis of the effect on the MCC of the treatment with FRSK 3 μM followed by CFTR is reported in *Figure 54* and *Figure 55* respectively. The CFTR seemed to increase the MCC in comparison to the not treated tissue in the automatic analysis while it showed to decrease the MCC in the manual analysis, confirming microscopical analysis. No increase in the in the MCC after FRSK treatment was observed both in automatic and in manual analysis.



*Figure 54. Muco-ciliary results expressed as beads speed (mm/sec) in SmallAir™ after treatment with FRSK 3 μM at T0, T10 and T20 followed by treatment with CFTRInh172 20 μM at T0, T10 and T20 obtained by automatic analysis. CFTR treatment showed to increase the MCC in comparison to the not treated tissue at T10 and at each time point in comparison to FRSK treatment. Statistical significance of difference of each treatment versus not treated tissues) is represented by green * (*: $p < 0.05$); the statistical significance difference of CFTR treatment versus the last time point of FRSK treatment is represented by red * (*: $p < 0.05$; **: $P < 0.001$).*

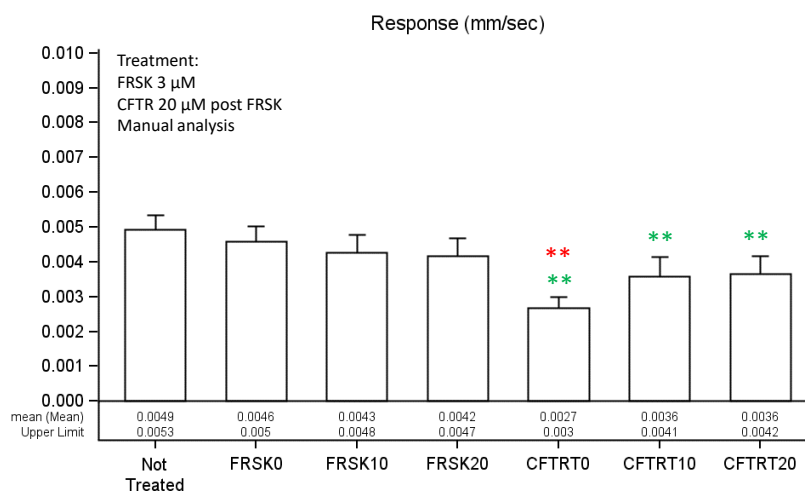


Figure 55. Muco-ciliary results expressed as beads speed (mm/sec) in SmallAir™ after treatment with FRSK 3 μ M at T0, T10 and T20 followed by treatment with CFTRInh172 20 μ M at T0, T10 and T20 obtained by manual analysis. CFTR treatment showed to decrease the MCC in comparison to the not treated tissue at each time point and at T10 only in comparison to FRSK treatment. Statistical significance of difference of each treatment versus not treated tissues (negative control) is represented by green * (**: $P < 0.001$); the statistical significance difference of CFTR treatment versus the last time point of FRSK treatment is represented by red * (**: $P < 0.001$).

In conclusion, the comparison between the automatic and manual method for the analysis of videos suggested that the manual method better represent the effect on beads speed observed by microscopical evaluation. Therefore, the manual method was choose as more appropriate method to be applied for the evaluation of the rest of videos.

5.4.2 Effect of agonists and inhibitor on MCC

Experiments to evaluate the effect of agonist Forskolin at 3 μ M and 10 μ M followed by inhibitor CFTR and of the inhibitor followed by Forskolin on MCC expressed as beads speed (mm/sec) were conducted. In all experiments treatment with Forskolin tested at 3 μ M and 10 μ M showed to increase the MCC both in comparison to the negative control and after CFTR inhibitor treatment as showed in Figure 56 and Figure 57 respectively. The CFTR showed to decrease the MCC both in comparison to the negative control and in comparison to FRSK treatment as showed in Figure 58 and Figure 59.

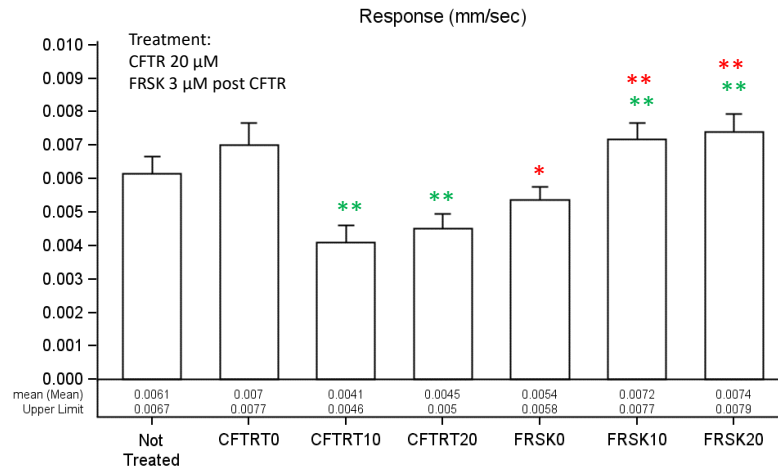


Figure 56. Muco-ciliary results expressed as beads speed (mm/sec) in SmallAir™ after treatment with CFTRInh172 20 μM at T0, T10 and T20 followed by treatment with FRSK 3 μM at T0, T10 and T20. CFTR treatment showed to decrease the MCC in comparison to the not treated tissue at T10 and T20. An increase in the MCC was observed after treatment with FRSK both in comparison to the not treated tissue at T10 and T20 and in comparison to CFTR treatment at each time point. Statistical significance of difference of each treatment versus not treated tissues is represented by green * (**: P<0.001); the statistical significance of difference of FRSK treatment versus the last time point of CFTR treatment is represented by red * (*: p< 0.05; **: P<0.001).

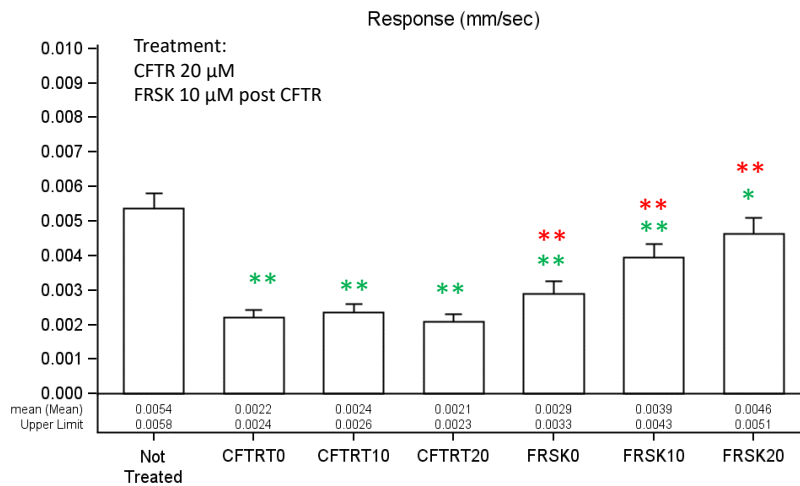


Figure 57. Muco-ciliary results expressed as beads speed (mm/sec) in SmallAir™ after the treatment with CFTRInh172 20 μM at T0, T10 and T20 followed by treatment with FRSK 10 μM at T0, T10 and T20. CFTR treatment showed to decrease the MCC in comparison to the not treated tissue at each time point. An increase in the MCC was observed after treatment with FRSK both in comparison to the not treated and in comparison to CFTR treatment at each time point. Statistical significance of difference of each treatment versus not treated tissues (negative control) is represented by green * (**: P<0.001); the statistical significance of difference of FRSK treatment versus the last time point of CFTR treatment is represented by red * (*: p< 0.05; **: P<0.001).

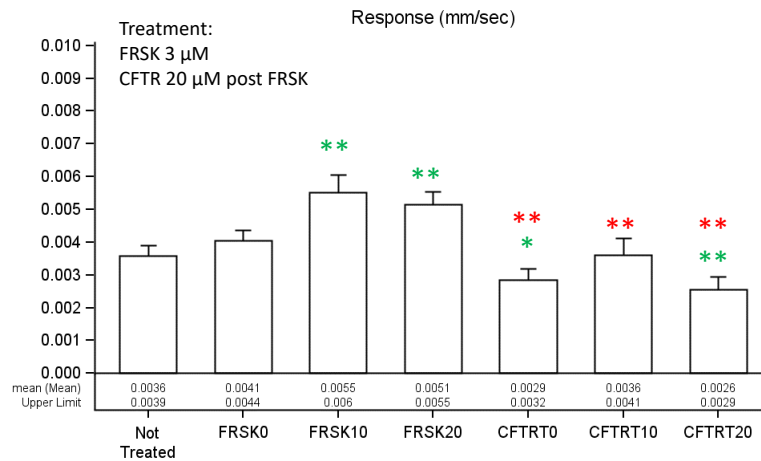


Figure 58. Muco-ciliary results expressed as beads speed (mm/sec) in SmallAir™ after treatment with FRSK 3μM at T0, T10 and T20 followed by treatment with CFTRInh172 20 μM at T0, T10 and T20. FRSK treatment increased the MCC at T10 and T20. CFTR showed to decrease the MCC in comparison to the not treated tissue at T0 and T20 and at each time point in comparison to FRSK treatment. Statistical significance of difference of each treatment versus not treated tissues (negative control) is represented by green * (*: $p < 0.05$ **: $P < 0.001$); the statistical significance difference of CFTR treatment versus the last time point of FRSK treatment is represented by red * (**: $P < 0.001$)

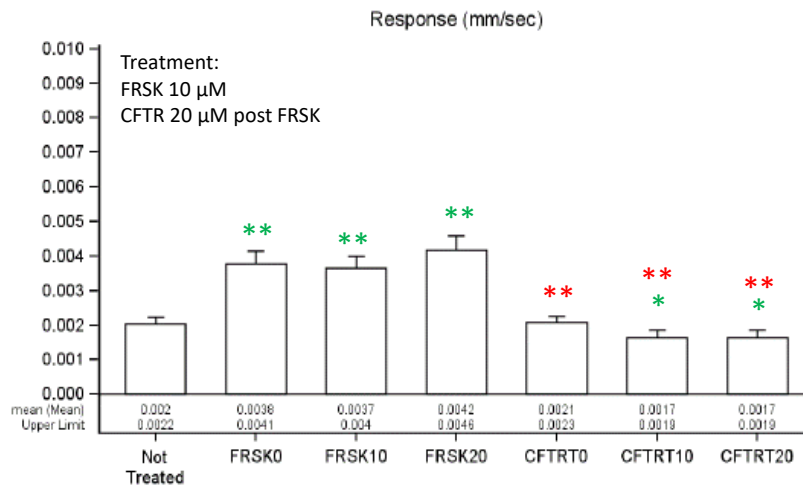


Figure 59. Muco-ciliary results expressed as beads speed (mm/sec) in SmallAir™ after the treatment with FRSK 10 μM at T0, T10 and T20 followed by treatment with CFTRInh172 20 μM at T0, T10 and T20. FRSK treatment increased the MCC in comparison to the negative control at each time point. CFTR treatment showed to decrease the MCC in comparison to the not treated tissue at T10 and T20 and at each time point in comparison to FRSK treatment. Statistical significance of difference of each treatment versus not treated tissues (negative control) is represented by green * (*: $p < 0.05$ **: $P < 0.001$); the statistical significance difference of CFTR treatment versus the last time point of FRSK treatment is represented by red * (**: $P < 0.001$).

Some differences were observed between the experiments in terms of the time point in which the beads speed was affected. This could be due to physiological difference between tissues derived from different donor and the maintaining time of tissues in culture.

No reproducible results were obtained in the evaluation of MCC after Carbachol treatment. In preliminary experiment, an increase in the beads speed was observed (*Figure 60*). While, when tested at different time point and followed by the inhibitor, the effect on beads speed was not confirmed (*Figure 61*).

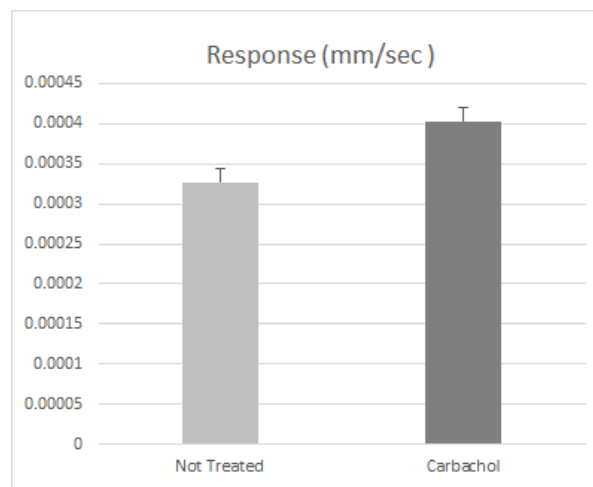


Figure 60. Muco-ciliary results expressed as beads speed (mm/sec) in SmallAir™ after the treatment with Carbachol 10 μ M at T0.

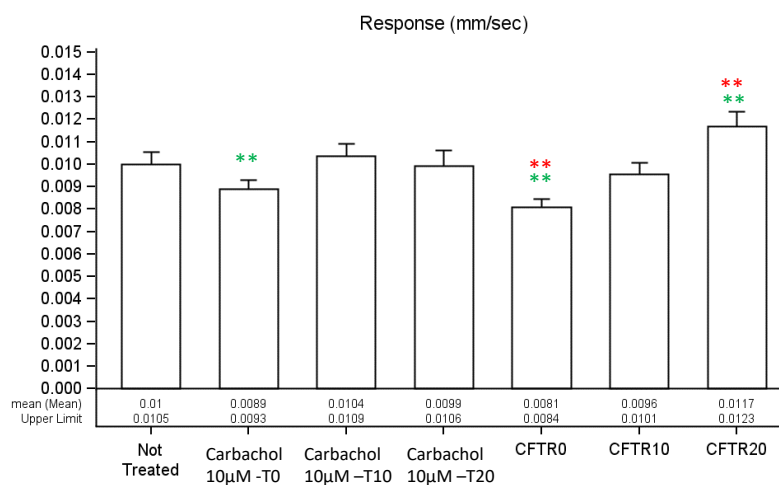


Figure 61. Muco-ciliary results expressed as beads speed (mm/sec) in SmallAir™ after the treatment with Carbacho 10 µM at T0, T10 and T20 followed by treatment with CFTRInh172 20 µM at T0, T10 and T20. No increase in MCC was observed after treatment with Carbachol as should be expected. Conflicting result were observed after CFTR treatment showing a decrease and then an increased the MCC at T0 and T20 respectively. Statistical significance of difference of each treatment versus not treated tissues (negative control) is represented by green * (**: P<0.001); the statistical significance difference of CFTR treatment versus the last time point of Carbachol treatment is represented by red * (**: P<0.001)

5.4.3 Effect of drug compounds on MCC

The MCC clearance in terms of beads speed was significantly increased by the treatment with Budesonide 10 µM at T20 and T40 (Figure 62), Salbutamol 10 µM at T0 and T40 (Figure 63) and Tiotropium bromide 10 µM at T20 and T40 (Figure 64). While, a significant decrease in the MCC was observed after Theophylline 10 µM treatment at T10 and T40 (Figure 65). A not significant effect after the treatment with Fluticasone 10 µM was observed (Figure 66).

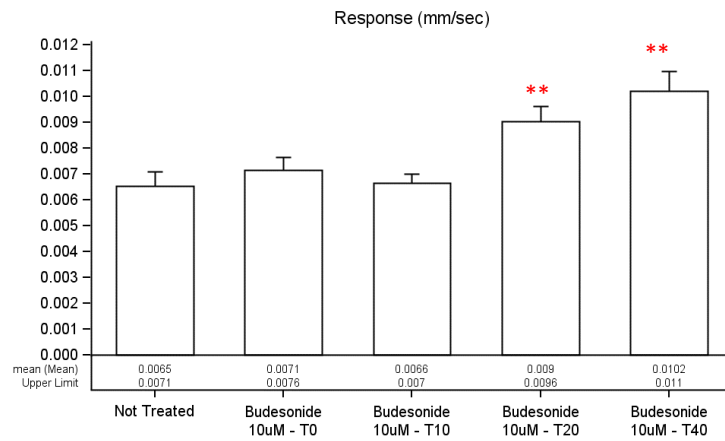


Figure 62. Muco-ciliary results expressed as beads speed (mm/sec) in SmallAir™ after treatment with Budesonide 10 μ M at T0, T10, T20 and T40. A significant increase in the MCC was observed at T20 and T40 in comparison to the negative control. Statistical significance is represented by red * (**: $P < 0.001$).

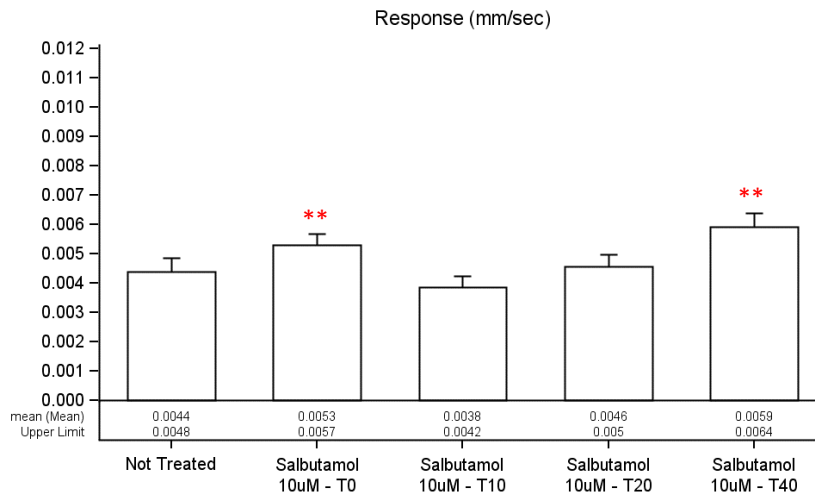


Figure 63. Muco-ciliary results expressed as beads speed (mm/sec) after SmallAir™ treatment with Salbutamol 10 μ M at T0, T10, T20 and T40. A significant increase in the MCC was observed at T0 and T40 in comparison to the negative control. Statistical significance is represented by red * (**: $P < 0.001$).

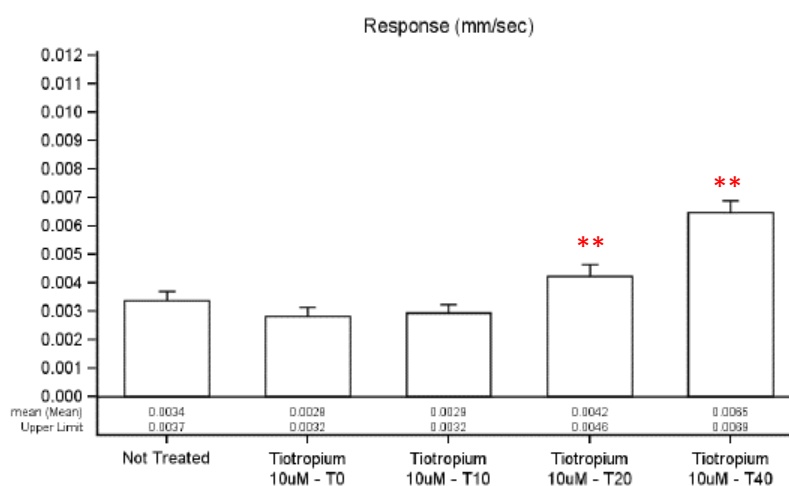


Figure 64. Muco-ciliary results expressed as beads speed (mm/sec) after SmallAir™ treatment with Tiotropium 10 µM at T0, T10, T20 and T40. A significant increase in the MCC was observed at T20 and T40 in comparison to the negative control. Statistical significance is represented by red * (**: $P < 0.001$).

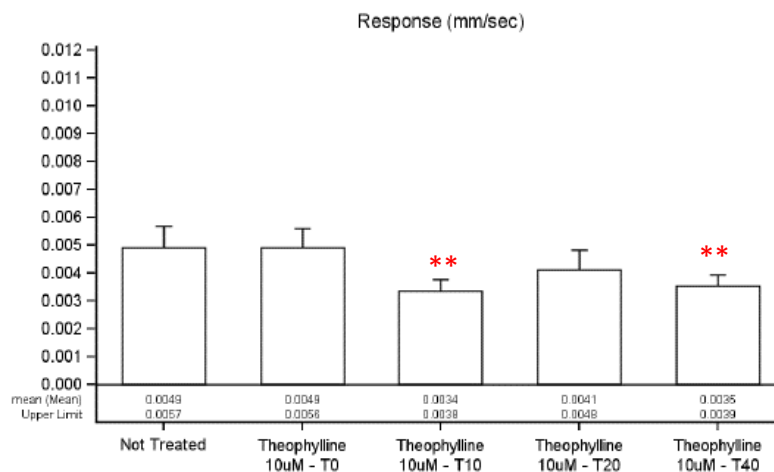


Figure 65. Muco-ciliary results expressed as beads speed (mm/sec) after SmallAir™ treatment with Theophylline 10 µM at T0, T10, T20 and T40. A significant decrease in the MCC was observed at T10 and T40 in comparison to the negative control. Statistical significance is represented by red * (**: $P < 0.001$).

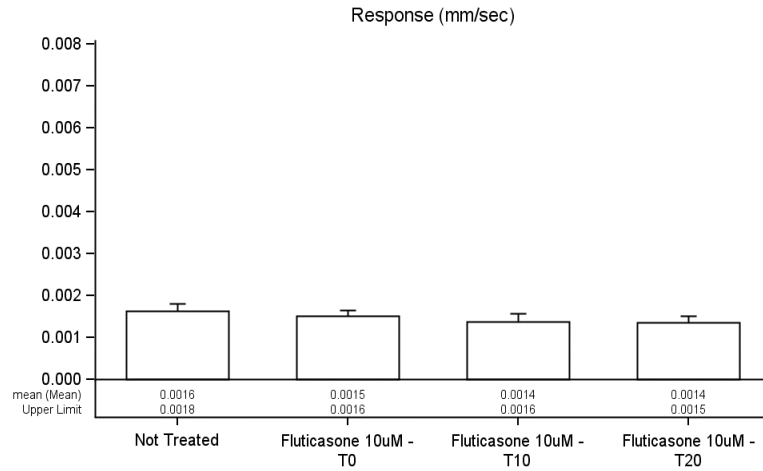


Figure 66. Muco-ciliary results expressed as beads speed (mm/sec) after treatment with Fluticasone 10 μ M at T0, T10 and T20. A slight but not significant decrease in the MCC was observed in comparison to the negative control..

A marked increase on MCC was observed after LPS 1 mg/mL treatment (Figure 67). Lower concentrations of LPS (100 ng/mL and 1 μ g/mL) were tested and they showed not to affect the MCC even after a longer time of exposure (Figure 68 and Figure 69).

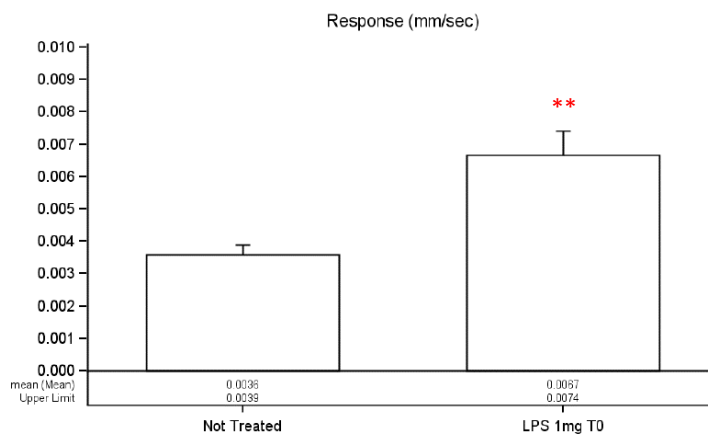


Figure 67 Muco-ciliary results expressed as beads speed (mm/sec) in SmallAir™ after treatment with LPS 1 mg at T0. A significant increase in the MCC was observed. Statistical significance is represented by red * (**: $P < 0.001$).

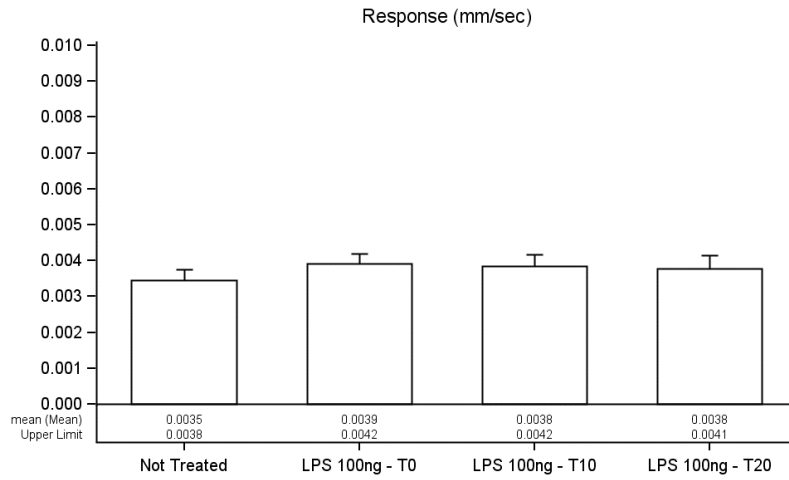


Figure 68. Muco-ciliary results expressed as beads speed (mm/sec) in SmallAir™ after treatment with LPS 100 ng at T0, T10 and T20. No effect was observed.

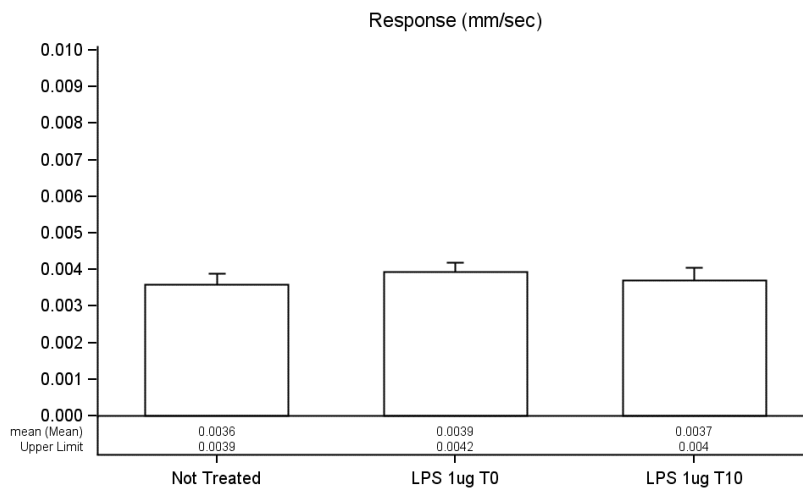


Figure 69. Muco-ciliary results expressed as beads speed (mm/sec) in SmallAir™ after treatment with LPS 1 µg at T0 and T10. No effect was observed.

Results obtained after Saline 3% (ipertonic solution) showed a marked decrease in MCC up to the complete stop of the beads movement, as showed in Figure 70.

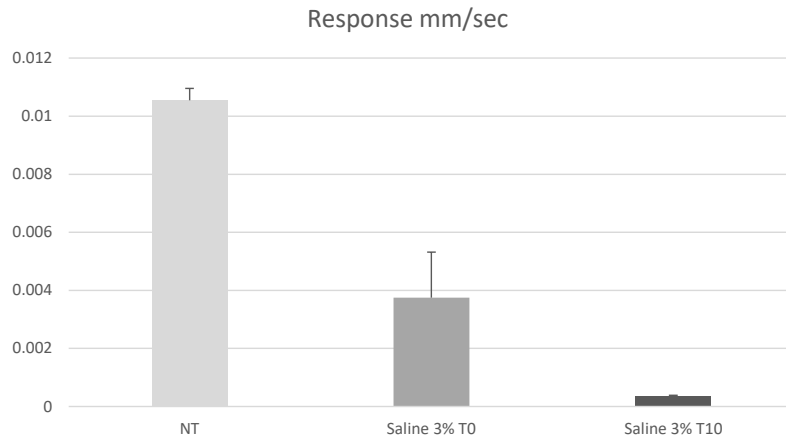
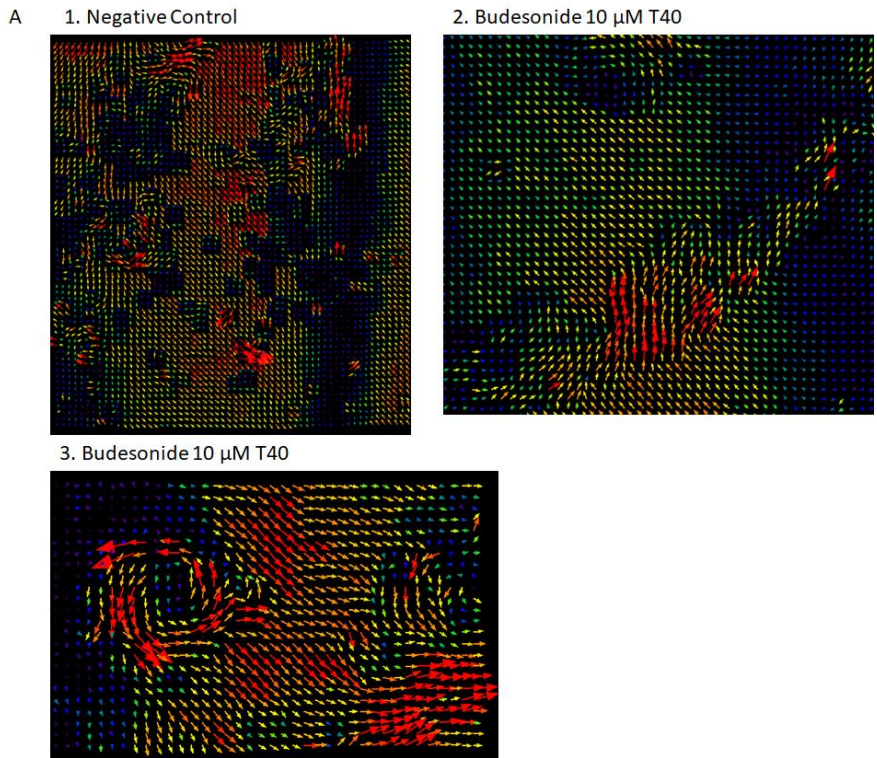


Figure 70. Muco-ciliary results expressed as beads speed (mm/sec) in SmallAir™ after treatment with Saline 3% at T0 and T10. After 10 minutes a complete stop in the beads movement was observed.

In addition Budesonide, Salbutamol and LPS treatment in SmallAir™ showed to synchronize the cilia beating moving all the beads in the same direction and showing a swirling movement. The vectors representing the beads paths are reported for Budesonide, Salbutamol and LPS treatment in Figure 71.



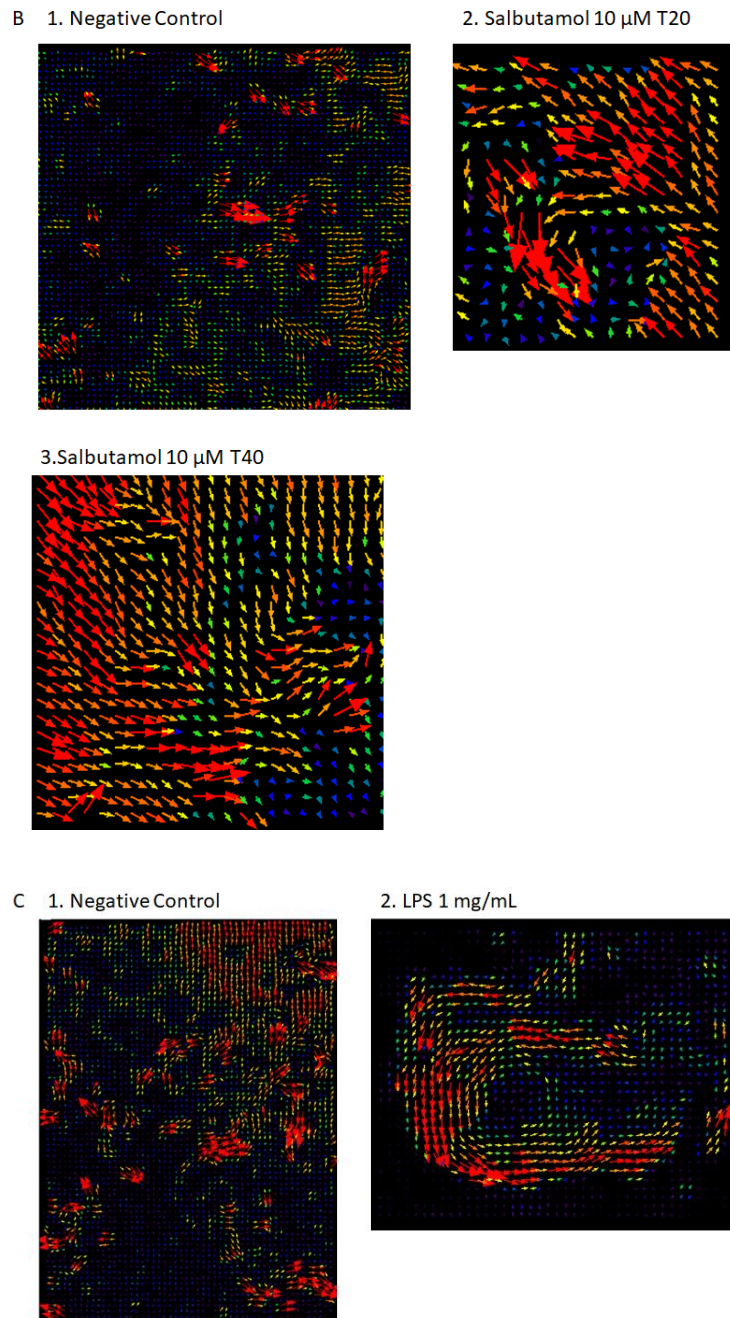


Figure 71. Direction of the beads represented by vectors (ImageJ- PIV Plugin).

A. Budesonide treatment: 1. No treated tissue. Casual directions of the beads trajectory was observed. 2. Tissue treated with Budesonide 10 μ M. A synchronization of the trajectories was observed with the most of beads moving in the same direction. 3. Tissue treated with Budesonide 10 μ M. Beads showed a swirling movement.

B. Salbutamol treatment: 1. No treated tissue. Casual directions of the beads trajectory was observed. 2. Tissue treated with Salbutamol 10 μ M. A synchronization of the trajectories was observed with the most of beads moving in the same direction. 3. Tissue treated with Budesonide 10 μ M. Beads showed a swirling movement.

C. LPS treatment: 1. No treated tissue. Casual directions of the beads trajectory was observed. 2. Tissue treated with LPS 1 mg/mL. A synchronization of the trajectories was observed with showing a swirling movement.

5.4.4 MPPD simulation

The Multiple Path Particle Dosimetry (MPPD) model was considered to evaluate the potential of integration of MCC information with *in silico* methods.

This model takes into account the lung asymmetry branching pattern and path variation resulting in more realistic determination of average deposition fractions (Fröhlich et al., 2016).

The MPPD model calculates the deposition and clearance of monodisperse and polydisperse aerosols in the respiratory tracts of laboratory animals and human for particles ranging in size from ultrafine (1 nm) to coarse (100 µm). The parameters used by MPPD to calculate deposition comprise the type of airway morphometry, the particle properties and the exposure, as well as the breathing pattern.

For the simulation of tracheobronchial clearance by the MPPD model, only the MCC values that significantly differed from the not treated value were used (time point at T20 and T40, *Table 12*)

In the graphs (*Figure 72*) the simulation of the tracheobronchial clearance of a compound assuming standard parameters of particle diameter (3 µm) and route of administration (oral route) applying the different MCC calculated *in vitro* is represented. As it can be observed, the amount of mass cleared is significantly affected by the MCC.

Interestingly, the tracheobronchial mass (TB mass) is significantly affected starting from the T0, indicating that the MCC can modify the amount of compound that deposit in the respiratory tract.

TREATMENT	Beads Speed (mm/min)	MCC (mm/min)
Not treated	0.39253	5.5
Budesonide T0	0.42790	6.00
Budesonide T10	0.39883	5.59
Budesonide T20	0.54076	7.58
Budesonide T40	0.61283	8.59
Correction Factor	14.01	

TREATMENT	Beads Speed (mm/min)	MCC (mm/min)
Not treated	0.09969	5.5
Fluticasone T0	0.09088	5.01
Fluticasone T10	0.08290	4.57
Fluticasone T20	0.08279	4.57
Correction Factor	55.17	

TREATMENT	Beads Speed (mm/min)	MCC (mm/min)
Not treated	0.26381	5.5
Salbutamol T0	0.31832	6.64
Salbutamol T10	0.23083	4.81
Salbutamol T20	0.27307	5.69
Salbutamol T40	0.35419	7.38
Correction factor	20.85	

TREATMENT	Beads Speed (mm/min)	MCC (mm/min)
Not treated	0.29431	5.5
Theophylline T0	0.29437	5.50
Theophylline T10	0.20174	3.77
Theophylline T20	0.24779	4.63
Theophylline T40	0.21277	3.98
Correction factor	18.69	

TREATMENT	Beads Speed (mm/min)	MCC (mm/min)
Not treated	0.20450	5.5
Tiotropium T0	0.16913	4.55
Tiotropium T10	0.17643	4.74
Tiotropium T20	0.25412	6.83
Tiotropium T40	0.38775	10.43
Correction factor	26.89	

Table 12. MCC expressed as mm/sec calculated for each treatment. Correction factor = beads Speed (mm/sec) Not treated / 5.5 mm/sec. MCC = Beads Speed (mm/sec) treatment * correction factor.

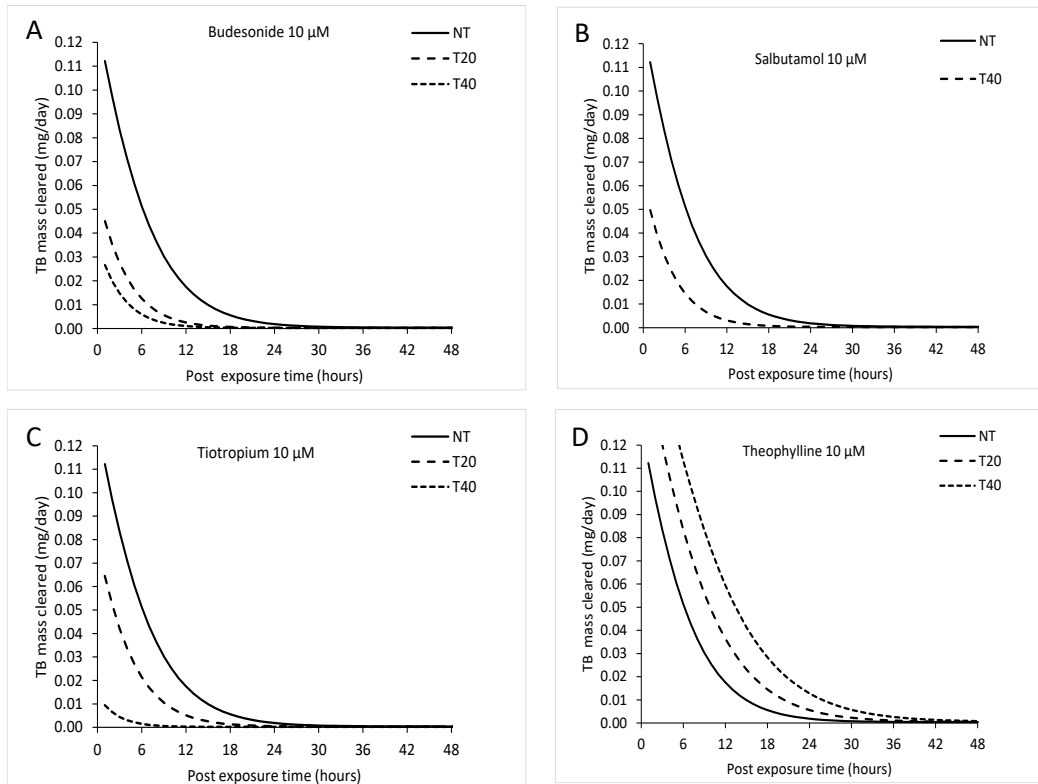


Figure 72. Graphical representation of tracheobronchial clearance (TB Mass Cleared) prediction of a generic compound (diameter 3 μM) via oral route on the basis of different MCC measured in vitro. A: Budesonide 10 μM; B: Salbutamol 10 μM; C: Tiotropium 10 μM; D: Theophylline 10 μM.

6 DISCUSSION

6.1 Acute toxicity Assessment.

The respiratory tract toxicity is a significant cause of failure of inhaled drug compound in clinical trials. Therefore, the early prediction of the respiratory toxicological effects potential is of interest for pharmaceutical industries.

In this project, the commercial SmallAir™ tissue model (Epithelix) was characterized as possible *in vitro* model to evaluate different parameters of interest in drug discovery and development.

Many studies describe application of *in vitro* model for the toxicity evaluation of nanomaterial (Loret et al., 2018; Mossman et al., 2007) or air pollution (Aufderheide et al., 2003; Upadhyay & Palmberg, 2018). Unfortunately, no toxic pharmaceutical compound was available to be tested in the model object of this study. Therefore a set of chemicals selected from the pre-validation study of a similar commercial respiratory *in vitro* model were assessed.

In the acute toxicity test the model was able to identify the toxicity of a single treatment of the well-known toxic compound Dimethylamine. In a further experiment, where the tissues were treated with a single dose of chemical toxic substances (CdCl₂ 100 µM) and irritant and inflammatory stimuli such as LPS and TGF-β respectively, a significant decrease of viability confirmed the toxicity of CdCl₂. The slight decrease observed for the tissues treated with TGF-β confirmed that the viability assessment by the Resazurin test allows to individuate toxic and irritant compound. These observations were confirmed also by the histological evaluation that showed a slight or moderate increase in apoptotic cells in LPS and TGF-β treated tissues and a severe tissue disorganization with necrotic areas in CdCl₂ treated.

The TEER measurement seems not to be a good parameter to assess tissue integrity for short time treatment (6 hours) since a decrease both for negative control and treated tissues was observed. While, for long time treatment the TEER measurement allows to assess the tissue damage after strong toxic compound. However, since TEER measurement is sensitive and many factors (such as temperature, medium formulation, cell culture period and shear stress) can affect

the TEER values, this parameters was considered not suitable as toxic end point (Srinivasan et al., 2015).

When the 3D SmallAir™ and the A549 cell culture were compared in the evaluation of a dose range concentration of a set of toxic compounds, the SmallAir™ seemed to be less sensitive than A549 showing higher EC75 values. This could be due to the different characteristics of the cell models. The SmallAir™ model is indeed a 3D tissue composed by different cell types in air-liquid interface maintaining physiological features such as cilia beating and mucus production that can protect the cells from the toxic effect, as already observed previously (Zavala, 2016). The LDH release resulted not to be a significant parameter for predicting lung toxicity, since no dose related increase was observed. This could be due to the mechanism of action of toxic compounds tested. Compounds tested are chemical substances with a mechanism of action not well characterized. These substances seemed to act mainly by corrosive mechanism with a consequent detachment of the cells that could be not resulting in an LDH release. Furthermore, the lack of LDH response could be due the presence of ciliated and mucus secreting cells and basal cells that likely could make this test system more resistant, as previous observed (Zavala, 2016).

6.2 Transport Evaluation (Permeability)

Permeability data obtained in SmallAir™ after liquid treatment showed to be comparable with permeability in Caco2. Differences observed between the two test systems seems to affect more low and medium permeability compounds. These observation should be due to the physiological differences between the two test systems. The Caco2 is the standard model used for the permeability study and it consists of immortalized cell line. The SmallAir™ is a pseudostratified epithelium derived from donor (different batch can show inter-batch variability) composed by different cell type expressing cilia and mucus production that can interfere with the permeability. Interestingly, the differences observed between the two models seems to be more evident for low and medium permeability compound. Furthermore, if different transporters are involved, the SmallAir™ values could be more representative of the in vivo situation. Therefore, Caco2 should be suggested as a

first model for preliminary screening and then the SmallAir™ can be used in following investigation as more physiological test systems. Indeed, if different transporter are present in lung tissue, the SmallAir™ could allow to obtain evaluation more representative of the *in vivo* situation. However, since the SmallAir™ model is still not well characterized for the permeability study of pharmaceutical compounds very few literature is published, therefore, more investigations are needed in order to identify and better characterize the membrane transporters expressed in this model.

Unfortunately, the tests conducted with the CULTEX® RFS Compact as device to apply aerosol drug onto the tissues did not allow to reach conclusive results requiring further improvement in the instrument set up.

Differently, the CULTEX® has been widely used for the assessment of traditional cigarette smoke, e-cigarette (Grellet et al., 2013; Scheffler et al., 2015) and pollutant effect on lung cell lines (Aufderheide & Mohr, 2000). In the early 2000s, electronic cigarettes were introduced as an aid for smoking cessation and replacement and in the last few years, the consumption has risen significantly. Even if, the regulation and control of e-cigarette liquids is not still standardized to ensure sufficient quality and safety for the user, the cytotoxic evaluation of e-cigarette aerosol is of great importance (Scheffler et al., 2015). *In vitro* e-cigarette aerosol testing are usually based on *in vitro* assays optimised for the assessment of cigarette smoke which is significantly different in terms of its chemical and physiological composition. Therefore, *in vitro* testing of e-cigarette aerosols still needs to be modified and adapted to the different characteristics of the aerosol produced. (Bishop et al., 2019). The aim of the test conducted and reported in this work, was to evaluate different concentrations of nicotine produced by two different devices and its permeability through lung tissues. Results obtained in the viability test, ensured that the tissue were viable immediately after the treatment, but nothing can be said regarding the cytotoxic effect of the e- smoke since only a short time treatment was applied. Interesting data for nicotine permeability were obtained, confirming that all nicotine that reach the tissues can pass through the SmallAir™ tissues.

In the preliminary experiment with NGI cup modified for the treatment of compounds formulated as powder, promising results were obtained regarding the powder distribution. Further experiments should be conducted to optimize the instrument set-up in order to avoid tissues damages and assess the permeability of powders, thus mimicking as much as possible the *in vivo* process of dissolution and permeation through the lung epithelium.

6.3 Inflammatory Mediators assessment

TGF- β is one of the major mediators of ECM remodelling and epithelial-mesenchymal transition (EMT) involved in carcinogenesis and fibrosis (Kolossova et al., 2011). The pathway is complex and involves different signalling pathways including Smads, mitogen-activated protein kinase (MAPK), and phosphatidylinositol 3-kinase (PI3K). Differential roles for Smad2 and Smad3 have been demonstrated in different cell types suggesting that this pathway activation may depend on the particular cellular context. The involvement of Smad2 in the lungs fibrosis was reported by Willis et al. (Willis & Borok, 2007). They found that TGF β 1 could cause alveolar epithelial cells to undergo EMT both *in vitro* and *in vivo* by activating smad2. Furthermore, TGF- β 1-induced Smad signalling in lung epithelial cells A549 was widely reported (Kunzmann et al., 2018; Tang et al., 2019). Results obtained in this study confirmed that the signalling via Smad2 is present in the 3D SmallAir™ tissues.

The bleomycin treatment of 3D SmallAir™ tissues did not reduce di viability, as already observed by previous author in a similar 3D lung tissues model (Willoughby, 2015). However the cytokines release did not correlate with what observed by Willoghby and colleagues. They showed that bleomycin induces expression of CYP1A1, Bcl2, TNF α , IL-1 α , IL-6, and IL-8 in EpiAirway 3D model confirming well known *in vivo* responses in humans and mice, as well as known responses of human cells in culture to bleomycin exposure (Cavarra et al., 2004; Willoughby, 2015). These difference in the results could be explain with the fact that in the present study the cytokine release in the medium and not the gene expression, was assessed. Therefore, low concentration in the medium could be not determined with the same sensibility as the gene expression analysis. While IL-8

and GRO levels showed to be out of range (for these parameters a sample dilutions should be recommended for further assay). Also, the LDH and ROS release measurement did not allow to assess the effect of bleomycin treatment on the SmallAir™. Since all evaluation were not consistent, some concerns about the bleomycin functionality have arisen. However, only one experiment was conducted, therefore further test are suggested to be performed in order to better characterize the cytokine release in the SmallAir™ model.

6.4 Muco-ciliary clearance

Results obtained in the evaluation of the effect Forskolin and CFTR confirmed the agonist and inhibitor effect on MCC respectively. Forskolin is a member of the diterpene family and it activates the Cystic fibrosis transmembrane conductance regulator (CFTR) chloride channel by raising the amount of intracellular cyclic AMP, leading to fluid secretion, while CFTRInh-172, an inhibitors of CFTR chloride channel, is used as tools to investigate the role and function of CFTR conductance in cystic fibrosis research. (Melis et al., 2014). Results obtained in SmallAir™ after FRSK and CFTR treatment correlated with observation by Joo N.S et al.. They reported in an ex vivo ferret trachea model that CFTR inhibitors modestly depressed MCCV stimulated by [cAMP]_i –elevating agents, but not basal MCCV nor that stimulated by [Ca²⁺]_i–elevating agents (Joo et al., 2016). The Carbachol a synthetic choline that acts a nicotinic acetylcholine receptor agonist, was used to induce [Ca²⁺]_i. However, conflicting results obtained after Carbachol treatment, did not allowed to confirm its effect on MCC (Joo et al., 2016).

The increase in MCC observed after Budesonide and Salbutamol confirmed the results already reported (Houtmeyers et al., 1999). Salbutamol is an adrenergic agents acting as bronchodilator. In addition to their relaxing effect on the bronchial smooth muscle, adrenergic agents are also reported to have an effect on MCC. In vivo data, showed that the single inhalation of adrenergic agonist is able to increase MCC significantly (Houtmeyers et al., 1999).

Budesonide and Fluticasone propionate are corticosteroids used in the treatment of chronic obstructive lung disease and asthma. Regarding the influence of corticosteroids on MCC, corticosteroids showed to increase the cilia beating

frequency significantly in isolated bronchial preparations in rats (Houtmeyers et al., 1999). Fluticasone results obtained in this study did not confirm this observation, therefore further experiments are needed to better elucidate its effect on SmallAir™ tissues.

Regarding the Tiotropium bromide effect, discordant results have been reported. Inhaled tiotropium bromide has been shown to improve lung function and reduce cough but muco-ciliary clearance was not improved in patients with COPD (Hasani et al., 2003). Other studies showed that tiotropium decreases symptoms in patients with COPD after tiotropium treatment. This effect may be derived from the inhibition of airway mucus hypersecretion and the improvement of airway mucociliary clearance (Tagaya et al., 2016).

Results obtained after Fluticasone treatment in SmallAir™ tissues confirmed the no effect on MCC as observed *in vivo* (Gizurason, 2015).

Discordant results was also observed in the Theophylline treatment. The methylxanthines, such as the Theophylline, are demonstrated to have a stimulative effect on lung MCC (Houtmeyers et al., 1999), while a decrease in the MCC was observed in the present study. The mechanism responsible for the observed improvement in MCC still remains a matter of debate. Administration of methylxanthines might increase the secretion of mucus, increasing the CBF as well as stimulate the secretion of fluid into the airway lumen, all factors involved in the final outcome of MCC. This particular mechanism of action could be not properly evaluated by the study design applied in this study, due to the washing step and time of exposure (Houtmeyers et al., 1999).

In conclusion, the *in vitro* SmallAir™ model, showed to be a promising model to assess the MCC *in vitro* after treatment with compound acting on ATP release and CFTR172inh. Further tests should be conducted to optimize the study design and confirm data obtained following inhaled compound treatment. For example, also the cilia beating frequency should be directly assessed in addition to the assessment of the MCC. Indeed, the suspension with beads applied as tracker, may be not able to detect correctly different mechanism of action.

6.5 In silico Prediction

In vitro and in vivo approaches are still costly and time-consuming. In experimental approaches comparison, computational methods have shown great advantages since they are fast, cheap, accurate, and most importantly they could be done before a compound is synthesized (Yang et al., 2018)

Several different *in silico* or non-testing approaches can help to predict the toxicity of substances after inhalation. These approaches are usually applied for chemicals and are considered to address further assessment such as hazard identification, quantitative risk assessment and national exposure standard setting (Clippinger, Allen, Behrsing, et al., 2018).

These approaches, to varying degrees, are based on the principle that similar substances are expected to exhibit similar biological activities.

Many in silico models are available and can be used individually or in an integrated fashion. Computational models developed for drug safety assessment can be generally divided into three categories: computational models based on SAR, Quantitative Structure-Activity Relationship modeling (QSAR), read-across extrapolations from measured data on analogous chemicals (Yang et al., 2018).

The availability of non-testing approaches to predict toxicity after acute inhalation exposures is limited and generally developed for chemical exposure.

The use of integrated approaches that combine existing data with *in vitro* and/or computational approaches to generate new data is fundamental to achieve global regulatory acceptance for non-animal testing approaches. Currently the biggest challenges are represented by the absence of centralized database of existing inhalation toxicity data and the identification and optimization of appropriate in silico models.

These topics require a global effort that were deeply discussed in 2016 at “Alternative Approaches for Acute Inhalation Toxicity Testing to Address Global Regulatory and Non-Regulatory Data Requirements”. Currently such models and databases are not yet available and this makes the use of animal models inevitable.

Poor pharmacokinetics along with toxicity of inhaled drug are important causes of costly late-stage failures in drug development (van de Waterbeemd & Gifford, 2003), therefore an early evaluation of these aspects has become important.

Pharmacokinetic studies support the studies of preclinical toxicology in animals (toxicokinetics) and allow to evaluate the correct use of drugs in therapy (choice of the best route of administration, choice of the best dose regimen, dose individualization, etc.) (Urso et al., 2002).

Compared with other routes of administration, a drug can be directly delivered to the target organ by the inhalation, conferring high local drug concentrations and, on the basis of its specific physico-chemical features, a low systemic drug concentrations. Therefore, drug inhalation is typically associated with high pulmonary efficacy and minimal systemic side effects.

However the lung is an organ with a complex structure and multiple pulmonary-specific properties that can affect the pharmacokinetic (Borghardt et al., 2018). Furthermore, local lung concentrations together with the systemic drug concentrations must be considered to assess the systemic safety profile of an inhaled drug. The systemic concentrations depend on a number of factors, including gastrointestinal absorption of the swallowed fraction of the drug, the rate and extent of absorption via pulmonary PK processes, and systemic disposition properties, such as distribution and elimination. Therefore characterizing the PK of inhaled drugs is highly complex because both the pulmonary and systemic PK have to be simultaneously evaluated. (Borghardt et al., 2018)

The systemic PK profiles of inhaled drugs in humans are still not fully interpretable and predictable in relation to the drug's molecular properties, inhaled aerosol delivery, and regional deposition, and various lung disposition mechanisms (such as muco-ciliary clearance, degradation, tissue binding/sequestration, and phagocytosis) (Raut et al., 2020). Several *in vivo* methods are applied to evaluate the drug deposition in the lung. Monitoring the pulmonary delivery is important to evaluate new delivery methods, new therapeutic drug formulations and for patients with impaired lung function that may require a confirmation of compound delivery (Tay et al., 2018). *In vivo* methods are technically demanding, require specific

tracers and are expensive. Therefore there is an arising interest for computational models (Fröhlich et al., 2016)

In recent years, several *in silico* methods have been developed in order to design specific molecule and predict their absorption, distribution, metabolism and excretion proprieties. Several software, can simulate the pharmacokinetic of drugs given by oral route using an integration of *in silico*, *in vitro* and *in vivo* data.

However, compared to oral application, prediction of plasma profiles of inhaled drugs is rarely reported (Fröhlich et al., 2016).

A PBPK (physiologically based pharmacokinetic) model is a mechanistic approach for predicting the pharmacokinetics of drugs with various degrees of accuracy based on pulmonary PK (e.g., dissolution, absorption) and systemic PK (e.g., distribution, excretion). The PBPK model incorporates anatomical and physiological aspects (e.g., organ perfusion rate, absorption surface area, etc.) and physico-chemical characteristics of the drug. Since the PBPK models is developed based on these predefined parameters it also called “bottom-up” approach, differently from “top-down” that predicts PK parameters from clinical data (Borghardt et al., 2015).

In preliminary evaluation, Salbutamol and Budesonide permeability results obtained in SmallAir™ were used to evaluate the potential integration of these *in vitro* data with PBPK predictions. The PBPK predictions provided very reasonable agreement between observed and simulated plasma concentration-time profiles. In particular, for the absorption process, values obtained in SmallAir™ seems to fit well the literature *in vivo* data, even if the access to reliable *in vivo* data for the validation of *in silico* models is still an issue (L. Pomari 2019).

The results obtained in the clearance simulation with MPPD, showed that the deposition and the time of elimination of an inhaled compound can be significantly affected by the variation on MCC that the compound itself can cause. Using a value of MCC measured in *in vitro* preliminary assessment can be really useful to evaluate the deposition of particles, which could affect the pharmacokinetic profile of the compound of interest.

7 CONCLUSION

The respiratory system is an important site for local and systemic drug delivery. Despite the popularity of inhalation as a drug delivery route, assessing the fate of inhaled compounds is difficult because of the complex nature of the lung.

Preclinical testing involves the use of primarily animal models to evaluate the deposition of a new drug in the appropriate tract of the respiratory system and to assess the correct therapeutic activity; and possible local and systemic toxicity.

This information are useful to improve formulations and delivery devices, or, if necessary, to decide to discard the drug prior to first-in-man studies.

However, major losses of new drug candidates can occur in first-in-man studies, for a variety of reasons such as failure in the deposition at the correct site; presence of effects in humans not observed in animals.

There is an urgent need to develop *in vitro* human based models, in order to better assess the possible toxicity effect and to evaluate the permeability of new inhaled medicines.

Indeed, a better *in vitro* characterization of new molecules in the early stage of the drug development should help in the selection of the best candidate for pre-clinical and clinical study, allowing to reduce *in vivo* study and reduce the risk of failure in first-in-man studies.

The *in vitro* studies conducted until now need to be carefully considered since at the moment a known reliable and validated test system has not been identified yet. However, this thesis wanted to be a first step in the direction of the development of an ethical and practical test system to improve the new inhaled drug selection and reduce the amount of animal tests conducted.

In this project, the 3D SmallAir™ model was characterized as possible more human relevant *in vitro* model to be used in the inhaled drug discovery sector. Different aspect has been investigated.

In particular, aspect such as the toxicity, the permeability and the effect on MCC were assessed. Furthermore, some *in vitro* data obtained have been used as input data for *in silico* evaluation, in order evaluate the reliability of a possible integrated approach to better characterize new molecules.

Regarding the *in vitro* toxicity assessment on the respiratory system very few literature was found for pharmaceutical compound. In this project I focused on the evaluation of well-known respiratory chemicals toxicant and irritant compounds on both a cell model and SmallAir™ model. TEER, LDH and viability test have been considered as end point. TEER and LDH showed not to be feasible parameters for predicting lung toxicity in the test system considered, while data obtained by the Resazurin viability test confirmed its reliability in the toxicity assessment. The viability results were also confirmed by the histology analysis. Furthermore, in the toxicity tests, the SmallAir™ model seemed to be less sensitive than A549 showing higher EC75 values. This property can be explained by the 3D structure physiological features such as cilia beating and mucus production that can protect the cells from the toxic effect.

For the permeability study, I focused on well-known inhalation compounds with very different permeability values (for example, low for Salbutamol and high for Budesonide) which resulted to be comparable in the two test systems considered. The most evident difference was observed with medium permeable compounds such as Digoxin. Results obtained in this study, indicate that the SmallAir™ model should express different efflux pumps on their surface compared to the standard Caco2 cell model. The exact type of transporters and their distribution and activity in the SmallAir™ test system have not been yet characterized, therefore tests conducted so far can only inform whether a compound is actively transported or not.

Regarding the different methods of compound application explored, more experiment are needed to optimize the instrument set up for the aerosol and powder treatment. If successful, these experiments should give results that, used in *in silico* predictions, can reflect the *in vivo* data, since they will take into consideration also the dissolution profile in the lung, which is one of the limits of the current predictions.

For the evaluation of the SmallAir™ model as a possible *in vitro* lung model for the assessment of inflammatory mediators, tissues were treated with TGF- β and Bleomycin. Results obtained with the treatment TGF- β confirm the activation of

Smad2 pathway. Unfortunately, results obtained in the measurement of cytokines LDH and ROS release after bleomycin treatment were not consistent with the literature. However only one experiment was conducted, therefore further experiments are suggested in order to confirm results obtained.

The SmallAir™ model was also evaluated as *in vitro* model for the assessment of the MCC. Results obtained in this project, showed that the SmallAir™ can be a promising model to assess the MCC *in vitro* after treatment with compound acting on ATP release and CFTR172inh, while further tests should be conducted to optimize the study design for the evaluation of the effect of different compound on cilia beating and MCC.

Finally, some integrations of *in vitro* data with *in silico* method were considered in order to establish an integrated strategy in the inhaled drug development. Unfortunately, so far no specific data base for the respiratory toxicity are commercially available, therefore in this project no integration of *in vitro* toxicity data with *in silico* approach was feasible.

MCC data were also used for the clearance simulation using the MPPD model. Result obtained showed that the deposition and the time of elimination of an inhaled compound can be significantly affected by the variation on MCC that the compound itself can cause. This indicates that such an assessment performed at the early stage of development can be useful in the evaluation of the pharmacokinetic profile of the compound of interest.

I am aware that tests performed so far are only a first step in the characterization of an *in vitro* lung model. However, overall these preliminary results can be considered promising. More compounds and conditions must be investigated, in order to validate a human relevant *in vitro* lung model to be applied in many fields of analysis, from permeability and transporters, to toxicity, formulation development, *in vitro* pharmacology etc. The organoid 3D tissues may represent a promising developing area to fill the gaps both in the drug discovery and the drug development of inhaled drugs testing models.

8 ACKNOWLEDGMENTS

I would like to express my utmost gratitude to my supervisor, Maria Grazia Romanelli for her patience and availability during my PhD study. My gratitude extends to my line manager and the management at Evotec Aptuit Verona for the opportunity to conduct my studies while working as Principal scientist. I would like to thank all the members in the PointBreath group, Dr. Annalisa Mercuri, Dr. Greta Baldan, Dr. Marco Pergher, Dr. Giulia Calusi, Dr. Madhurjya Neog, Dr. Viola Bigatto and Dr. Filippo Andreetta for the collaboration on the project. From the bottom of my heart I would like to say a big thank you to my friend Dr. Annalisa Mercuri, whose guidance and encouragement has been invaluable throughout this study. I also thank my Mentor Daisaku Ikeda, all my faith-mate and friends for their moral support. I cannot forget to thank Vezio Gambelli for all the unconditional support and understanding in these very intense years. Finally, I would like to express my gratitude to my parents Maria Grazia and Giampaolo and my sister Eleonora for their encouragement and inspiration all through my studies. Without their love it would be impossible for me to complete my study.

9 REFERENCES

- Agu, R. U., Ugwoke, M. I., Armand, M., Kinget, R., & Verbeke, N. (2001). The lung as a route for systemic delivery of therapeutic proteins and peptides. *Respiratory Research*, 2(4), 198–209. <https://doi.org/10.1186/rr58>
- Allen, T. E. H., Goodman, J. M., Gutsell, S., & Russell, P. J. (2014). Defining molecular initiating events in the adverse outcome pathway framework for risk assessment. *Chemical Research in Toxicology*, 27(12), 2100–2112. <https://doi.org/10.1021/tx500345j>
- Alvarado, A., & Arce, I. (2016). Metabolic Functions of the Lung, Disorders and Associated Pathologies. *Journal of Clinical Medicine Research*, 8(10), 689–700. <https://doi.org/10.14740/jocmr2668w>
- Anderson, Laube, Geller, Rubin, Ahrens, Atkins, Nikander, Fink, Hickey, Leach, MacIntyre, Smaldone, & Martonen. (2005). The expanding role of aerosols in systemic drug delivery, gene therapy, and vaccination: Discussion. *Respiratory Care*, 50(9), 1174–1176.
- Aufderheide, M., Heller, W. D., Krischenowski, O., Möhle, N., & Hochrainer, D. (2017). Improvement of the CULTEX® exposure technology by radial distribution of the test aerosol. *Experimental and Toxicologic Pathology*, 69(6), 359–365. <https://doi.org/10.1016/j.etp.2017.02.004>
- Aufderheide, M., Knebel, J. W., & Ritter, D. (2003). Novel approaches for studying pulmonary toxicity in vitro. *Toxicology Letters*, 140–141(v), 205–211. [https://doi.org/10.1016/S0378-4274\(02\)00512-X](https://doi.org/10.1016/S0378-4274(02)00512-X)
- Aufderheide, M., & Mohr, U. (2000). CULTEX - An alternative technique for cultivation and exposure of cells of the respiratory tract to airborne pollutants at the air/liquid interface. *Experimental and Toxicologic Pathology*, 52(3), 265–270. [https://doi.org/10.1016/S0940-2993\(00\)80044-5](https://doi.org/10.1016/S0940-2993(00)80044-5)
- Bal-Price, A., & Meek, M. E. (Bette. (2017). Adverse outcome pathways: Application to enhance mechanistic understanding of neurotoxicity. *Pharmacology and Therapeutics*, 179, 84–95. <https://doi.org/10.1016/j.pharmthera.2017.05.006>
- Baldan, G. (2017). *data on file*.
- Ballard, S. T., Trout, L., Mehta, A., & Inglis, S. K. (2002). Liquid secretion inhibitors reduce mucociliary transport in glandular airways. *American Journal of Physiology - Lung Cellular and Molecular Physiology*, 283(2 27-2). <https://doi.org/10.1152/ajplung.00277.2001>
- Baron, J., Burke, J. P., Guengerich, F. P., Jakoby, W. B., & Voigt, J. M. (1988). Sites for xenobiotic activation and detoxication within the respiratory tract: Implications for chemically induced toxicity. *Toxicology and Applied*

Pharmacology, 93(3), 493–505. [https://doi.org/10.1016/0041-008X\(88\)90053-1](https://doi.org/10.1016/0041-008X(88)90053-1)

Bartram, U., & Speer, C. P. (2004). The Role of Transforming Growth Factor β in Lung Development and Disease. *Chest*, 125(2), 754–765. <https://doi.org/10.1378/chest.125.2.754>

Bernhard, W. (2016). Lung surfactant: Function and composition in the context of development and respiratory physiology. *Annals of Anatomy*, 208, 146–150. <https://doi.org/10.1016/j.aanat.2016.08.003>

Bishop, E., Haswell, L., Adamson, J., Costigan, S., Thorne, D., & Gaca, M. (2019). An approach to testing undiluted e-cigarette aerosol in vitro using 3D reconstituted human airway epithelium. *Toxicology in Vitro*, 54(November 2017), 391–401. <https://doi.org/10.1016/j.tiv.2018.01.010>

Bitterle, E., Karg, E., Schroepel, A., Kreyling, W. G., Tippe, A., Ferron, G. A., Schmid, O., Heyder, J., Maier, K. L., & Hofer, T. (2006). Dose-controlled exposure of A549 epithelial cells at the air-liquid interface to airborne ultrafine carbonaceous particles. *Chemosphere*, 65(10), 1784–1790. <https://doi.org/10.1016/j.chemosphere.2006.04.035>

Bogdanffy, M. S., & Keller, D. A. (1999). Metabolism of xenobiotics by the respiratory tract. *Toxicology of the Lung*, 3.

Borghardt, J. M., Kloft, C., & Sharma, A. (2018). Inhaled Therapy in Respiratory Disease: The Complex Interplay of Pulmonary Kinetic Processes. *Canadian Respiratory Journal*, 2018. <https://doi.org/10.1155/2018/2732017>

Borghardt, J. M., Weber, B., Staab, A., & Kloft, C. (2015). Pharmacometric Models for Characterizing the Pharmacokinetics of Orally Inhaled Drugs. *AAPS Journal*, 17(4), 853–870. <https://doi.org/10.1208/s12248-015-9760-6>

Bustamante-Marin, X. M., & Ostrowski, L. E. (2017). Cilia and mucociliary clearance. *Cold Spring Harbor Perspectives in Biology*, 9(4). <https://doi.org/10.1101/cshperspect.a028241>

Byrne, A. J., Mathie, S. A., Gregory, L. G., & Lloyd, C. M. (2015). Pulmonary macrophages: Key players in the innate defence of the airways. *Thorax*, 70(12), 1189–1196. <https://doi.org/10.1136/thoraxjnl-2015-207020>

Castell, J. V., Donato, M. T., & Gómez-Lechón, M. J. (2005). Metabolism and bioactivation of toxicants in the lung. The in vitro cellular approach. *Experimental and Toxicologic Pathology*, 57(SUPPL. 1), 189–204. <https://doi.org/10.1016/j.etp.2005.05.008>

Cavarra, E., Carraro, F., Fineschi, S., Naldini, A., Bartalesi, B., Pucci, A., & Lungarella, G. (2004). Early response to bleomycin is characterized by different cytokine and cytokine receptor profiles in lungs. *American Journal of Physiology - Lung Cellular and Molecular Physiology*, 287(6 31-6), 1186–

1192. <https://doi.org/10.1152/ajplung.00170.2004>

- Chan, J. G. Y., Wong, J., Zhou, Q. T., Leung, S. S. Y., & Chan, H. K. (2014). Advances in device and formulation technologies for pulmonary drug delivery. *AAPS PharmSciTech*, *15*(4), 882–897. <https://doi.org/10.1208/s12249-014-0114-y>
- Chang, M. M. J., Shih, L., & Wu, R. (2008). Pulmonary Epithelium: Cell Types and Functions. *The Pulmonary Epithelium in Health and Disease*, 1–26. <https://doi.org/10.1002/9780470727010.ch1>
- Clippinger, A. J., Allen, D., Behrsing, H., BéruBé, K. A., Bolger, M. B., Casey, W., DeLorme, M., Gaça, M., Gehen, S. C., Glover, K., Hayden, P., Hinderliter, P., Hotchkiss, J. A., Iskandar, A., Keyser, B., Luettich, K., Ma-Hock, L., Maione, A. G., Makena, P., ... Jarabek, A. M. (2018). Pathway-based predictive approaches for non-animal assessment of acute inhalation toxicity. *Toxicology in Vitro*, *52*(April), 131–145. <https://doi.org/10.1016/j.tiv.2018.06.009>
- Clippinger, A. J., Allen, D., Jarabek, A. M., Corvaro, M., Gaça, M., Gehen, S., Hotchkiss, J. A., Patlewicz, G., Melbourne, J., Hinderliter, P., Yoon, M., Huh, D., Lowit, A., Buckley, B., Bartels, M., BéruBé, K., Wilson, D. M., Indans, I., & Vinken, M. (2018). Alternative approaches for acute inhalation toxicity testing to address global regulatory and non-regulatory data requirements: An international workshop report. *Toxicology in Vitro*, *48*(October 2017), 53–70. <https://doi.org/10.1016/j.tiv.2017.12.011>
- Cook, D., Brown, D., Alexander, R., March, R., Morgan, P., Satterthwaite, G., & Pangalos, M. N. (2014). Lessons learned from the fate of AstraZeneca's drug pipeline: A five-dimensional framework. *Nature Reviews Drug Discovery*, *13*(6), 419–431. <https://doi.org/10.1038/nrd4309>
- CORESTA. (2015). Routine Analytical Machine for E-Cigarette Aerosol Generation and Collection – Definitions and Standard Conditions. *CRM No. 81, 81*, 1–6. https://www.coresta.org/sites/default/files/technical_documents/main/CRM_81.pdf
- Csanády, G., Guengerich, F. P., & Bond, J. A. (1993). Comparison of the biotransformation of 1,3-butadiene and its metabolite, butadiene monoepoxide, by hepatic and pulmonary tissues from humans, rats and mice. *Carcinogenesis*, *14*(4), 783–784. <https://doi.org/10.1093/carcin/14.4.783>
- D. V. Carreno et al. (2013). LPS increase of ciliary beat frequency in respiratory ciliated cells. *The FASEB Journal*, *27*(1_supplment), 1215.1-1215.1.
- De Souza Xavier Costa, N., Ribeiro, G., Dos Santos Alemany, A. A., Belotti, L., Zati, D. H., Frota Cavalcante, M., Veras, M. M., Ribeiro, S., Kallás, E. G., Saldiva, P. H. N., Dolhnikoff, M., & Da Silva, L. F. F. (2017). Early and late

- pulmonary effects of nebulized LPS in mice: An acute lung injury model. *PLoS ONE*, 12(9), 1–16. <https://doi.org/10.1371/journal.pone.0185474>
- Ehrhardt, C., Laue, M., & Kim, K. (2008). Drug Absorption Studies. In *Drug Absorption Studies* (Issue January). <https://doi.org/10.1007/978-0-387-74901-3>
- Elbert, K. J., Schäfer, U. F., Schäfers, H. J., Kim, K. J., Lee, V. H., & Lehr, C. M. (1999). Monolayers of human alveolar epithelial cells in primary culture for pulmonary absorption and transport studies. *Pharmaceutical Research*, 16(5), 601–608. <https://doi.org/10.1023/a:1018887501927>
- Faber, S. C., & McCullough, S. D. (2018). Through the Looking Glass: In Vitro Models for Inhalation Toxicology and Interindividual Variability in the Airway. *Applied In Vitro Toxicology*, 4(2), 115–128. <https://doi.org/10.1089/aivt.2018.0002>
- Farr, S. J., & Otulana, B. A. (2006). Pulmonary delivery of opioids as pain therapeutics. *Advanced Drug Delivery Reviews*, 58(9–10), 1076–1088. <https://doi.org/10.1016/j.addr.2006.07.013>
- Fehrenbach, H. (2001). *FehrenbachH_RespiratoryResearch2001*.
- Florea, B. I., Cassara, M. L., Junginger, H. E., & Borchard, G. (2003). Drug transport and metabolism characteristics of the human airway epithelial cell line Calu-3. *Journal of Controlled Release*, 87(1–3), 131–138. [https://doi.org/10.1016/S0168-3659\(02\)00356-5](https://doi.org/10.1016/S0168-3659(02)00356-5)
- Forbes, B., Asgharian, B., Dailey, L. A., Ferguson, D., Gerde, P., Gumbleton, M., Gustavsson, L., Hardy, C., Hassall, D., Jones, R., Lock, R., Maas, J., McGovern, T., Pitcairn, G. R., Somers, G., & Wolff, R. K. (2011). Challenges in inhaled product development and opportunities for open innovation. *Advanced Drug Delivery Reviews*, 63(1–2), 69–87. <https://doi.org/10.1016/j.addr.2010.11.004>
- Forbes, B., Bäckman, P., Christopher, D., Dolovich, M., Li, B. V., & Morgan, B. (2015). In Vitro Testing for Orally Inhaled Products: Developments in Science-Based Regulatory Approaches. *AAPS Journal*, 17(4), 837–852. <https://doi.org/10.1208/s12248-015-9763-3>
- Forbes, B., & Ehrhardt, C. (2005). Human respiratory epithelial cell culture for drug delivery applications. *European Journal of Pharmaceutics and Biopharmaceutics*, 60(2), 193–205. <https://doi.org/10.1016/j.ejpb.2005.02.010>
- Forti, E., Bulgheroni, A., Cetin, Y., Hartung, T., Jennings, P., Pfaller, W., & Prieto, P. (2010). Characterisation of cadmium chloride induced molecular and functional alterations in airway epithelial cells. *Cellular Physiology and Biochemistry*, 25(1), 159–168. <https://doi.org/10.1159/000272060>

- Foster, K. A., Avery, M. L., Yazdanian, M., & Audus, K. L. (2000). Characterization of the Calu-3 cell line as a tool to screen pulmonary drug delivery. *International Journal of Pharmaceutics*, 208(1–2), 1–11. [https://doi.org/10.1016/S0378-5173\(00\)00452-X](https://doi.org/10.1016/S0378-5173(00)00452-X)
- Foster, K. A., Oster, C. G., Mayer, M. M., Avery, M. L., & Audus, K. L. (1998). Characterization of the A549 cell line as a type II pulmonary epithelial cell model for drug metabolism. *Experimental Cell Research*, 243(2), 359–366. <https://doi.org/10.1006/excr.1998.4172>
- Fröhlich, E. (2017). Toxicity of orally inhaled drug formulations at the alveolar barrier: Parameters for initial biological screening. *Drug Delivery*, 24(1), 891–905. <https://doi.org/10.1080/10717544.2017.1333172>
- Fröhlich, E., Mercuri, A., Wu, S., & Salar-Behzadi, S. (2016). Measurements of deposition, lung surface area and lung fluid for simulation of inhaled compounds. *Frontiers in Pharmacology*, 7(JUN), 1–10. <https://doi.org/10.3389/fphar.2016.00181>
- Fulcher, M. L., & Randell, S. H. (2013). Primary Mouse Small Intestinal Epithelial Cell Cultures. *Methods in Molecular Biology*, 945, 109–121. <https://doi.org/10.1007/978-1-62703-125-7>
- Garcia-Canton, C., Minet, E., Anadon, A., & Meredith, C. (2013). Metabolic characterization of cell systems used in in vitro toxicology testing: Lung cell system BEAS-2B as a working example. *Toxicology in Vitro*, 27(6), 1719–1727. <https://doi.org/10.1016/j.tiv.2013.05.001>
- Ge, V., Banakh, I., Tiruvoipati, R., & Haji, K. (2018). Bleomycin-induced pulmonary toxicity and treatment with infliximab: A case report. *Clinical Case Reports*, 6(10), 2011–2014. <https://doi.org/10.1002/ccr3.1790>
- Ghadiri, M., Young, P. M., & Traini, D. (2019). Strategies to enhance drug absorption via nasal and pulmonary routes. *Pharmaceutics*, 11(3), 1–20. <https://doi.org/10.3390/pharmaceutics11030113>
- Gizurason, S. (2015). The effect of cilia and the mucociliary clearance on successful drug delivery. *Biological and Pharmaceutical Bulletin*, 38(4), 497–506. <https://doi.org/10.1248/bpb.b14-00398>
- Gonda, I. (2000). The ascent of pulmonary drug delivery. *Journal of Pharmaceutical Sciences*, 89(7), 940–945. [https://doi.org/10.1002/1520-6017\(200007\)89:7<940::AID-JPS11>3.0.CO;2-B](https://doi.org/10.1002/1520-6017(200007)89:7<940::AID-JPS11>3.0.CO;2-B)
- Grellet, S., Momas, I., Seta, N., Bardet, G., & Achard, S. (2013). Reconstituted human airway epithelium 3D-model to assess the impact of indoor air pollutants on the inflammatory response. *Toxicology Letters*, 221, S112. <https://doi.org/10.1016/j.toxlet.2013.05.184>
- Groneberg, D. A., Eynott, P. R., Oates, T., Lim, S., Wu, R., Carlstedt, I.,

- Nicholson, A. G., & Chung, K. F. (2002). Expression of MUC5AC and MUC5B mucins in normal and cystic fibrosis lung. *Respiratory Medicine*, 96(2), 81–86. <https://doi.org/10.1053/rmed.2001.1221>
- Haagsman, H. P., & Diemel, R. V. (2001). Surfactant-associated proteins: Functions and structural variation. *Comparative Biochemistry and Physiology - A Molecular and Integrative Physiology*, 129(1), 91–108. [https://doi.org/10.1016/S1095-6433\(01\)00308-7](https://doi.org/10.1016/S1095-6433(01)00308-7)
- Haghi, M., Ong, H. X., Traini, D., & Young, P. (2014). Across the pulmonary epithelial barrier: Integration of physicochemical properties and human cell models to study pulmonary drug formulations. *Pharmacology and Therapeutics*, 144(3), 235–252. <https://doi.org/10.1016/j.pharmthera.2014.05.003>
- Hare, L. O. (1998). Lung Fibrosis Induced by Bleomycin: Structural Changes and Overview of Recent Advances. *ECM Journal*, 12(3), 487.
- Hartung, T., Luechtefeld, T., & Maertens, Alexandra and Kleensang, A. (2013). Food for thought: Integrated testing strategies for safety assessments. *Altex*, 30(1), 3–18. <http://www.scopus.com/inward/record.url?eid=2-s2.0-84876323285&partnerID=40&md5=6f48969fce1062ef68de9cd8007133e0>
- Hasani, A., Toms, N., O'Connor, J., Dilworth, J. P., & Agnew, J. E. (2003). Effect of salmeterol xinafoate on lung mucociliary clearance in patients with asthma. *Respiratory Medicine*, 97(6), 667–671. <https://doi.org/10.1053/rmed.2003.1498>
- Hein, S., Bur, M., Schaefer, U. F., & Lehr, C. M. (2011). A new Pharmaceutical Aerosol Deposition Device on Cell Cultures (PADD OCC) to evaluate pulmonary drug absorption for metered dose dry powder formulations. *European Journal of Pharmaceutics and Biopharmaceutics*, 77(1), 132–138. <https://doi.org/10.1016/j.ejpb.2010.10.003>
- Hiemstra, P. S., Grootaers, G., van der Does, A. M., Krul, C. A. M., & Kooter, I. M. (2018). Human lung epithelial cell cultures for analysis of inhaled toxicants: Lessons learned and future directions. *Toxicology in Vitro*, 47(September 2017), 137–146. <https://doi.org/10.1016/j.tiv.2017.11.005>
- Hoegger, M. J., Fischer, A. J., Mcmenimen, J. D., Ostedgaard, L. S., Tucker, A. J., Awadalla, M. A., Moninger, T. O., Michalski, A. S., Eric, A., Zabner, J., Stoltz, D. A., & Welsh, M. J. (2015). *HHS Public Access*. 345(6198), 818–822. <https://doi.org/10.1126/science.1255825>. Impaired
- Hofmann, W., & Asgharian, B. (2003). The effect of lung structure on mucociliary clearance and particle retention in human and rat lungs. *Toxicological Sciences*, 73(2), 448–456. <https://doi.org/10.1093/toxsci/kfg075>

- Hollenhorst, M. I., Richter, K., & Fronius, M. (2011). Ion transport by pulmonary epithelia. *Journal of Biomedicine and Biotechnology*, 2011. <https://doi.org/10.1155/2011/174306>
- Hong, K. U., Reynolds, S. D., Watkins, S., Fuchs, E., & Stripp, B. R. (2004). In vivo differentiation potential of tracheal basal cells: Evidence for multipotent and unipotent subpopulations. *American Journal of Physiology - Lung Cellular and Molecular Physiology*, 286(4 30-4), 643–649. <https://doi.org/10.1152/ajplung.00155.2003>
- Hou, S., Wu, J., Li, X., & Shu, H. (2015). Practical, regulatory and clinical considerations for development of inhalation drug products. *Asian Journal of Pharmaceutical Sciences*, 10(6), 490–500. <https://doi.org/10.1016/j.ajps.2015.08.008>
- Houtmeyers, E., Gosselink, R., Gayan-Ramirez, G., & Decramer, M. (1999). Effects of drugs on mucus clearance. *European Respiratory Journal*, 14(2), 452–467. <https://doi.org/10.1034/j.1399-3003.1999.14b35.x>
- Huang, P., Lazarowski, E. R., Tarran, R., Milgram, S. L., Boucher, R. C., & Stutts, M. J. (2001). Compartmentalized autocrine signaling to cystic fibrosis transmembrane conductance regulator at the apical membrane of airway epithelial cells. *Proceedings of the National Academy of Sciences of the United States of America*, 98(24), 14120–14125. <https://doi.org/10.1073/pnas.241318498>
- Huang, S., Boda, B., Vernaz, J., Ferreira, E., Wiszniewski, L., & Constant, S. (2017). Establishment and characterization of an in vitro human small airway model (SmallAir™). *European Journal of Pharmaceutics and Biopharmaceutics*, 118, 68–72. <https://doi.org/10.1016/j.ejpb.2016.12.006>
- Hughes, J. P., Rees, S. S., Kalindjian, S. B., & Philpott, K. L. (2011). Principles of early drug discovery. *British Journal of Pharmacology*, 162(6), 1239–1249. <https://doi.org/10.1111/j.1476-5381.2010.01127.x>
- Huh, D., Matthews, B. D., Mammoto, A., Montoya-Zavala, M., Yuan Hsin, H., & Ingber, D. E. (2010). Reconstituting organ-level lung functions on a chip. *Science*, 328(5986), 1662–1668. <https://doi.org/10.1126/science.1188302>
- ICRP, international commission on radiological protection. (1994). *Human Respiratory Tract Model for Radiological Protection* (pp. 1–3). ICRP Publication 66, Annals of the ICRP 24, 1–3. Elsevier Science, Oxford.
- Ingoglia, F., Visigalli, R., Rotoli, B. M., Barilli, A., Riccardi, B., Puccini, P., & Dall'Asta, V. (2015). Functional characterization of the organic cation transporters (OCTs) in human airway pulmonary epithelial cells. *Biochimica et Biophysica Acta - Biomembranes*, 1848(7), 1563–1572. <https://doi.org/10.1016/j.bbamem.2015.04.001>

- Jackson, G. R., Maione, A. G., Klausner, M., & Hayden, P. J. (2018). Prevalidation of an Acute Inhalation Toxicity Test Using the EpiAirway in Vitro Human Airway Model. *Applied In Vitro Toxicology*, 4(2), 149–158. <https://doi.org/10.1089/aivt.2018.0004>
- Ji, J., Hedelin, A., Malmlöf, M., Kessler, V., Seisenbaeva, G., Gerde, P., & Palmberg, L. (2017). Development of combining of human bronchial mucosa models with XposeALI® for exposure of air pollution nanoparticles. *PLoS ONE*, 12(1), 1–17. <https://doi.org/10.1371/journal.pone.0170428>
- Joo, N. S., Jeong, J. H., Cho, H. J., & Wine, J. J. (2016). Marked increases in mucociliary clearance produced by synergistic secretory agonists or inhibition of the epithelial sodium channel. *Scientific Reports*, 6(November), 1–12. <https://doi.org/10.1038/srep36806>
- Joseph, D., Puttaswamy, R. K., & Krovvidi, H. (2013). Non-respiratory functions of the lung. *Continuing Education in Anaesthesia, Critical Care and Pain*, 13(3), 98–102. <https://doi.org/10.1093/bjaceaccp/mks060>
- Karam, H., Hurbain-Kosmath, I., & Housset, B. (1995). Direct toxic effect of bleomycin on alveolar type 2 cells. *Toxicology Letters*, 76(2), 155–163. [https://doi.org/10.1016/0378-4274\(94\)03207-N](https://doi.org/10.1016/0378-4274(94)03207-N)
- Karra, N., Swindle, E. J., & Morgan, H. (2019). Drug delivery for traditional and emerging airway models. *Organs-on-a-Chip*, 1(December 2019), 100002. <https://doi.org/10.1016/j.ooc.2020.100002>
- Kolosova, I., Nethery, D., & Kern, J. A. (2011). Role of Smad2/3 and p38 MAP kinase in TGF- β 1-induced epithelial-mesenchymal transition of pulmonary epithelial cells. *Journal of Cellular Physiology*, 226(5), 1248–1254. <https://doi.org/10.1002/jcp.22448>
- Krewski, D., Acosta Jr, D., Andersen, M., Anderson, H., Bailar III, J. C., Boekelheide, K., Brent, R., Charnley, G., Cheung, V. G., Green Jr, S., Kelsey, K. T., Kerkvliet, N. I., Li, A. A., McCray, L., & Meyer, O. (2010). TOXICITY TESTING IN THE 21ST CENTURY: A VISION AND A STRATEGY Staff of Committee on Toxicity Testing and Assessment of Environmental Agents 1 R. Samuel McLaughlin Centre for Population Health Risk Assessment, Institute of Population HHS Public Access. *Toxicology and Environmental Health*, 13(0), 51–138. <https://doi.org/10.1080/10937404.2010.483176>
- Kunzmann, S., Ottensmeier, B., Speer, C. P., & Fehrholz, M. (2018). Effect of progesterone on Smad signaling and TGF- β /Smad-regulated genes in lung epithelial cells. *PLoS ONE*, 13(7), 1–13. <https://doi.org/10.1371/journal.pone.0200661>
- Labiris, N. R., & Dolovich, M. B. (2003). Pulmonary drug delivery. Part I: Physiological factors affecting therapeutic effectiveness of aerosolized

medications. *British Journal of Clinical Pharmacology*, 56(6), 588–599.
<https://doi.org/10.1046/j.1365-2125.2003.01892.x>

Lacroix, G., Koch, W., Ritter, D., Gutleb, A. C., Larsen, S. T., Loret, T., Zanetti, F., Constant, S., Chortarea, S., Rothen-Rutishauser, B., Hiemstra, P. S., Frejafon, E., Hubert, P., Gribaldo, L., Kearns, P., Aublant, J. M., Diabaté, S., Weiss, C., De Groot, A., & Kooter, I. (2018). Air-Liquid Interface in Vitro Models for Respiratory Toxicology Research: Consensus Workshop and Recommendations. *Applied In Vitro Toxicology*, 4(2), 91–106.
<https://doi.org/10.1089/aivt.2017.0034>

Låg, M., Westly, S., Lerstad, T., Bjørnsrud, C., Refsnes, M., & Schwarze, P. E. (2002). Cadmium-induced apoptosis of primary epithelial lung cells: Involvement of Bax and p53, but not of oxidative stress. *Cell Biology and Toxicology*, 18(1), 29–42. <https://doi.org/10.1023/A:1014467112463>

Lenzer, J., York, N., & Abergavenny, R. D. (2006). *Inhaled insulin is approved in Europe and United States Study shows that tobacco firms covertly hired scientists*. 332(February), 2006.

Lieber, M., Todaro, G., Smith, B., Szakal, A., & Nelson-Rees, W. (1976). A continuous tumor-cell line from a human lung carcinoma with properties of type II alveolar epithelial cells. *International Journal of Cancer*, 17(1), 62–70. <https://doi.org/10.1002/ijc.2910170110>

Liu, X., Jin, L., Upham, J. W., & Roberts, M. S. (2013). The development of models for the evaluation of pulmonary drug disposition. *Expert Opinion on Drug Metabolism and Toxicology*, 9(4), 487–505.

Lombry, C., Edwards, D. A., Préat, V., & Vanbever, R. (2004). Alveolar macrophages are a primary barrier to pulmonary absorption of macromolecules. *American Journal of Physiology - Lung Cellular and Molecular Physiology*, 286(5 30-5), 1002–1008.
<https://doi.org/10.1152/ajplung.00260.2003>

Loret, T., Rogerieux, F., Trouiller, B., Braun, A., Egles, C., & Lacroix, G. (2018). Predicting the in vivo pulmonary toxicity induced by acute exposure to poorly soluble nanomaterials by using advanced in vitro methods. *Particle and Fibre Toxicology*, 15(1), 1–20. <https://doi.org/10.1186/s12989-018-0260-6>

Manford, F., Tronde, A., Jeppsson, A. B., Patel, N., Johansson, F., & Forbes, B. (2005). Drug permeability in 16HBE14o- airway cell layers correlates with absorption from the isolated perfused rat lung. *European Journal of Pharmaceutical Sciences*, 26(5), 414–420.
<https://doi.org/10.1016/j.ejps.2005.07.010>

Mathias, N. R., Timoszyk, J., Stetsko, P. I., Megill, J. R., Smith, R. L., & Wall, D. A. (2002). Permeability characteristics of Calu-3 human bronchial epithelial

- cells: In vitro-in vitro correlation to predict lung absorption in rats. *Journal of Drug Targeting*, 10(1), 31–40.
<https://doi.org/10.1080/10611860290007504>
- Mathias, N. R., Yamashita, F., & Lee, V. H. L. (1996). Respiratory epithelial cell culture models for evaluation of ion and drug transport. *Advanced Drug Delivery Reviews*, 22(1–2), 215–249. [https://doi.org/10.1016/S0169-409X\(96\)00420-6](https://doi.org/10.1016/S0169-409X(96)00420-6)
- Matute-Bello, G., Downey, G., Moore, B. B., Groshong, S. D., Matthay, M. A., Slutsky, A. S., & Kuebler, W. M. (2011). An official american thoracic society workshop report: Features and measurements of experimental acute lung injury in animals. *American Journal of Respiratory Cell and Molecular Biology*, 44(5), 725–738. <https://doi.org/10.1165/rcmb.2009-0210ST>
- Melis, N., Tauc, M., & Giuliano, S. (2014). *Revisiting CFTR inhibition : CFTR inh -172 and GlyH-101*. April. <https://doi.org/10.1111/bph.12726>
- Miller, A. J., & Spence, J. R. (2017). In vitro models to study human lung development, disease and homeostasis. *Physiology*, 32(3), 246–260. <https://doi.org/10.1152/physiol.00041.2016>
- Moeller, A., Ask, K., Warburton, D., Gauldie, J., & Kolb, M. (2008). The bleomycin animal model: A useful tool to investigate treatment options for idiopathic pulmonary fibrosis? *International Journal of Biochemistry and Cell Biology*, 40(3), 362–382. <https://doi.org/10.1016/j.biocel.2007.08.011>
- Moore, B. B., & Hogaboam, C. M. (2008). Murine models of pulmonary fibrosis. *American Journal of Physiology - Lung Cellular and Molecular Physiology*, 294(2), 152–160. <https://doi.org/10.1152/ajplung.00313.2007>
- Mortensen, N. P., & Hickey, A. J. (2014). Targeting inhaled therapy beyond the lungs. *Respiration*, 88(5), 353–364. <https://doi.org/10.1159/000367852>
- Mossman, B. T., Borm, P. J., Castranova, V., Costa, D. L., Donaldson, K., & Kleeberger, S. R. (2007). Mechanisms of action of inhaled fibers, particles and nanoparticles in lung and cardiovascular diseases. *Particle and Fibre Toxicology*, 4, 1–10. <https://doi.org/10.1186/1743-8977-4-4>
- Mülhopt, S., Dilger, M., Diabaté, S., Schlager, C., Krebs, T., Zimmermann, R., Buters, J., Oeder, S., Wäscher, T., Weiss, C., & Paur, H. R. (2016). Toxicity testing of combustion aerosols at the air-liquid interface with a self-contained and easy-to-use exposure system. *Journal of Aerosol Science*, 96, 38–55. <https://doi.org/10.1016/j.jaerosci.2016.02.005>
- NCRP, national council on radiation protection and measurements. (1997). *Deposition, Retention and Dosimetry of Inhaled Radioactive Substances*. NCRP Report No. 125. National Council on Radiation Protection and Measurements, Bethesda, MD.

- Nicod, L. P. (2005). Lung defences: An overview. *European Respiratory Review*, 14(95), 45–50. <https://doi.org/10.1183/09059180.05.00009501>
- Noah, T. L., Yankaskas, J. R., Carson, J. L., Gambling, T. M., Cazares, L. H., McKinnon, K. P., & Devlin, R. B. (1995). Tight junctions and mucin mRNA in BEAS-2B cells. *In Vitro Cellular & Developmental Biology - Animal: Journal of the Society for In Vitro Biology*, 31(10), 738–740. <https://doi.org/10.1007/BF02634112>
- Oberdörster, G. (1992). Pulmonary deposition, clearance and effects of inhaled soluble and insoluble cadmium compounds. *IARC Scientific Publications*, 118, 189–204.
- OECD. (2013). *Guidance Document on Developing and Assessing Adverse Outcome Pathways*. 184.
- OECD. (2016). Users' Handbook supplement to the Guidance Document for developing and assessing Adverse Outcome Pathways. *Env/Jm/Mono(2016) 12, 1*(OECD Series on Adverse Outcome Pathways No. 1), 63. <https://doi.org/10.1787/5jlv1m9d1g32-en>
- Oesch, F., Fabian, E., & Landsiedel, R. (2019). Xenobiotica-metabolizing enzymes in the lung of experimental animals, man and in human lung models. In *Archives of Toxicology* (Vol. 93, Issue 12). Springer Berlin Heidelberg. <https://doi.org/10.1007/s00204-019-02602-7>
- Palumbo, P., Picchini, U., Beck, B., Van Gelder, J., Delbar, N., & DeGaetano, A. (2008). A general approach to the apparent permeability index. *Journal of Pharmacokinetics and Pharmacodynamics*, 35(2), 235–248. <https://doi.org/10.1007/s10928-008-9086-4>
- Park, K. S., Wells, J. M., Zorn, A. M., Wert, S. E., Laubach, V. E., Fernandez, L. G., & Whitsett, J. A. (2006). Transdifferentiation of ciliated cells during repair of the respiratory epithelium. *American Journal of Respiratory Cell and Molecular Biology*, 34(2), 151–157. <https://doi.org/10.1165/rcmb.2005-0332OC>
- Patton, J. S., & Byron, P. R. (2007). Inhaling medicines: Delivering drugs to the body through the lungs. *Nature Reviews Drug Discovery*, 6(1), 67–74. <https://doi.org/10.1038/nrd2153>
- Patton, J. S., Fishburn, C. S., & Weers, J. G. (2004). The lungs as a portal of entry for systemic drug delivery. *Proceedings of the American Thoracic Society*, 1(4), 338–344. <https://doi.org/10.1513/pats.200409-049TA>
- Plopper, C. G. (1996). Structure and Function of the Lung. Respiratory. In T. C. Jones, D. L. Dungworth, & U. Mohr (Eds.), *Respiratory System. Monographs on Pathology of Laboratory Animals*. Springer, Berlin, Heidelberg.

- Plopper, C. G., Mariassy, A. T., & Lollini, L. O. (1983). Structure as revealed by airway dissection. A comparison of mammalian lungs. *American Review of Respiratory Disease*, *128*(2 II Suppl.), 4–7.
<https://doi.org/10.1164/arrd.1983.128.2P2.S4>
- Pomari, L. (2019). *An investigation into the use of in vitro lung models as transport model*. Universita' degli studi di Padova.
- Raut, A., Dhapare, S., Venitz, J., & Sakagami, M. (2020). Pharmacokinetic profile analyses for inhaled drugs in humans using the lung delivery and disposition model. *Biopharmaceutics and Drug Disposition*, *41*(1–2), 32–43.
<https://doi.org/10.1002/bdd.2210>
- Ren, H., Birch, N. P., & Suresh, V. (2016). An optimised human cell culture model for alveolar epithelial transport. *PLoS ONE*, *11*(10), 1–22.
<https://doi.org/10.1371/journal.pone.0165225>
- Rogers, A. V., Dewar, A., Corrin, B., & Jeffery, P. K. (1993). Identification of serous-like cells in the surface epithelium of human bronchioles. *European Respiratory Journal*, *6*(4), 498–504.
- Rose, M. C., & Voynow, J. A. (2006). Respiratory tract mucin genes and mucin glycoproteins in health and disease. *Physiological Reviews*, *86*(1), 245–278.
<https://doi.org/10.1152/physrev.00010.2005>
- Rozycki, H. J. (2014). Potential contribution of Type I alveolar epithelial cells to chronic neonatal lung disease. *Frontiers in Pediatrics*, *2*(MAY), 1–7.
<https://doi.org/10.3389/fped.2014.00045>
- Sakagami, M. (2006). In vivo, in vitro and ex vivo models to assess pulmonary absorption and disposition of inhaled therapeutics for systemic delivery. *Advanced Drug Delivery Reviews*, *58*(9–10), 1030–1060.
<https://doi.org/10.1016/j.addr.2006.07.012>
- Salomon, J. J., Muchitsch, V. E., Gausterer, J. C., Schwagerus, E., Huwer, H., Daum, N., Lehr, C. M., & Ehrhardt, C. (2014). The cell line NCI-H441 is a useful in vitro model for transport studies of human distal lung epithelial barrier. *Molecular Pharmaceutics*, *11*(3), 995–1006.
<https://doi.org/10.1021/mp4006535>
- Satir, P., & Christensen, S. T. (2007). Overview of Structure and Function of Mammalian Cilia. *Annual Review of Physiology*, *69*(1), 377–400.
<https://doi.org/10.1146/annurev.physiol.69.040705.141236>
- Schanker, L. S., Mitchell, E. W., & Brown, R. A. (1986). Species comparison of drug absorption from the lung after aerosol inhalation or intratracheal injection. *Drug Metabolism and Disposition: The Biological Fate of Chemicals*, *14*(1), 79–88. <http://europepmc.org/abstract/MED/2868870>
- Scheffer, G. L., Pijnenborg, A. C. L. M., Van der Valk, P., Scheper, R. J., Smit, E.

- F., Müller, M., Postma, D. S., Timens, W., & De Vries, E. G. E. (2002). Multidrug resistance related molecules in human and murine lung. *Journal of Clinical Pathology*, 55(5), 332–339. <https://doi.org/10.1136/jcp.55.5.332>
- Scheffler, S., Dieken, H., Krischenowski, O., Förster, C., Branscheid, D., & Aufderheide, M. (2015). Evaluation of e-cigarette liquid vapor and mainstream cigarette smoke after direct exposure of primary human bronchial epithelial cells. *International Journal of Environmental Research and Public Health*, 12(4), 3915–3925. <https://doi.org/10.3390/ijerph120403915>
- Schipper, N. G. M., & Verhoef, J.C. & Merkus, F. W. H. M. (1991). The Nasal Mucociliary Clearance: Relevance to Nasal Drug Delivery. *Pharm Res*, 8, 807–814.
- Seidal, K., Jorgensen, N., Elinder, C. G., Sjogren, B., & Vahter, M. (1993). Fatal cadmium-induced pneumonitis. *Scandinavian Journal of Work, Environment and Health*, 19(6), 429–431. <https://doi.org/10.5271/sjweh.1450>
- Sembeni, B. (2020). *Caratterizzazione di un modello in vitro 3D di tessuto respiratorio per la valutazione della tossicità e del movimento ciliare*. ALMA MATER STUDIORUM- Università di Bologna.
- Shlyonsky, V., Goolaerts, A., Van Beneden, R., & Sariban-Sohraby, S. (2005). Differentiation of epithelial Na⁺ channel function: An in vitro model. *Journal of Biological Chemistry*, 280(25), 24181–24187. <https://doi.org/10.1074/jbc.M413823200>
- Shrestha, J., Razavi Bazaz, S., Aboulkheyr Es, H., Yaghobian Azari, D., Thierry, B., Ebrahimi Warkiani, M., & Ghadiri, M. (2020). Lung-on-a-chip: the future of respiratory disease models and pharmacological studies. *Critical Reviews in Biotechnology*, 40(2), 213–230. <https://doi.org/10.1080/07388551.2019.1710458>
- Sibille, Y., & Reynolds, H. Y. (1990). Macrophages and polymorphonuclear neutrophils in lung defense and injury. *The American Review of Respiratory Disease*, 141(2), 471–501. <https://doi.org/10.1164/ajrccm/141.2.471>
- Sivars, K. B., Sivars, U., Hornberg, E., Zhang, H., Brändén, L., Bonfante, R., Huang, S., Constant, S., Robinson, I., Betts, C. J., & Aberg, P. M. (2018). A 3D human airway model enables prediction of respiratory toxicity of inhaled drugs in vitro. *Toxicological Sciences*, 162(1), 301–308. <https://doi.org/10.1093/toxsci/kfx255>
- Smetanová, L., Štětínová, V., Svoboda, Z., & Květina, J. (2011). CACO-2 CELLS , BIOPHARMACEUTICS CLASSIFICATION SYSTEM (BCS) AND BIOWAIVER. *Acta Medica*, 54(1), 3–8. <https://doi.org/10.14712/18059694.2016.9>

- Srinivasan, B., Kolli, A. R., Esch, M. B., Abaci, H. E., Shuler, M. L., & Hickman, J. J. (2015). TEER Measurement Techniques for In Vitro Barrier Model Systems. *Journal of Laboratory Automation*, 20(2), 107–126. <https://doi.org/10.1177/2211068214561025>
- Stanke, F. (2015). The Contribution of the Airway Epithelial Cell to Host Defense. *Mediators of Inflammation*, 2015. <https://doi.org/10.1155/2015/463016>
- Tagaya, E., Yagi, O., Sato, A., Arimura, K., Takeyama, K., Kondo, M., & Tamaoki, J. (2016). Pulmonary Pharmacology & Therapeutics Effect of tiotropium on mucus hypersecretion and airway clearance in patients with COPD *. *Pulmonary Pharmacology & Therapeutics*, 39, 81–84. <https://doi.org/10.1016/j.pupt.2016.06.008>
- Tang, Y., Xuan, Y., Qiao, G., Ou, Z., He, Z., Zhu, Q., Liao, M., & Yin, G. (2019). MDM2 promotes epithelial–mesenchymal transition through activation of Smad2/3 signaling pathway in lung adenocarcinoma. *OncoTargets and Therapy*, 12, 2247–2258. <https://doi.org/10.2147/OTT.S185076>
- Tay, Z. W., Chandrasekharan, P., Zhou, X. Y., Yu, E., Zheng, B., & Conolly, S. (2018). In vivo tracking and quantification of inhaled aerosol using magnetic particle imaging towards inhaled therapeutic monitoring. *Theranostics*, 8(13), 3676–3687. <https://doi.org/10.7150/thno.26608>
- Tollefsen, K. E., Scholz, S., Cronin, M. T., Edwards, S. W., de Knecht, J., Crofton, K., Garcia-Reyero, N., Hartung, T., Worth, A., & Patlewicz, G. (2014). Applying Adverse Outcome Pathways (AOPs) to support Integrated Approaches to Testing and Assessment (IATA). *Regulatory Toxicology and Pharmacology*, 70(3), 629–640. <https://doi.org/10.1016/j.yrtph.2014.09.009>
- Tronde, A. (2002). *Pulmonary Drug Absorption: In vitro and in vivo investigations of drug absorption across the lung barrier and its relation to drug physiochemical properties*. ACTA Universitatis Upsaliensis. Comprehensive Summaries of Uppsala Dissertations from the Faculty of Pharmacy 275.
- Upadhyay, S., & Palmberg, L. (2018). Air-liquid interface: Relevant in vitro models for investigating air pollutant-induced pulmonary toxicity. *Toxicological Sciences*, 164(1), 21–30. <https://doi.org/10.1093/toxsci/kfy053>
- Urso, R., Blardi, P., & Giorgi, G. (2002). A short introduction to pharmacokinetics. *European Review for Medical and Pharmacological Sciences*, 6(2), 33–44.
- van de Waterbeemd, H., & Gifford, E. (2003). ADMET in silico modelling: towards prediction paradise? *Nature Reviews Drug Discovery*, 2(3), 192–204. <https://doi.org/10.1038/nrd1032>

- Van Winkle, L. S., & Fanucchi, M. V. (2009). *Cellular and molecular characteristics of basal cells in airway epithelium Lung epithelium resistance View project Conifer seed germination and dormancy View project*. 2148(July). <https://doi.org/10.1080/01902140120740>
- Velaga, S. P., Djuris, J., Cvijic, S., Rozou, S., Russo, P., Colombo, G., & Rossi, A. (2018). Dry powder inhalers: An overview of the in vitro dissolution methodologies and their correlation with the biopharmaceutical aspects of the drug products. *European Journal of Pharmaceutical Sciences*, 113(August 2017), 18–28. <https://doi.org/10.1016/j.ejps.2017.09.002>
- Wan, H., Winton, H. L., Soeller, C., Stewart, G. A., Thompson, P. J., Gruenert, D. C., Cannell, M. B., Garrod, D. R., & Robinson, C. (2000). Tight junction properties of the immortalized human bronchial epithelial cell lines Calu-3 and 16HBE14o-. *European Respiratory Journal*, 15(6), 1058–1068. <https://doi.org/10.1034/j.1399-3003.2000.01514.x>
- Wang, J., Edeen, K., Manzer, R., Chang, Y., Wang, S., Chen, X., Funk, C. J., Cosgrove, G. P., Fang, X., & Mason, R. J. (2007). Differentiated human alveolar epithelial cells and reversibility of their phenotype in vitro. *American Journal of Respiratory Cell and Molecular Biology*, 36(6), 661–668. <https://doi.org/10.1165/rcmb.2006-0410OC>
- Wang, S., & Hubmayr, R. D. (2011). Type I alveolar epithelial phenotype in primary culture. *American Journal of Respiratory Cell and Molecular Biology*, 44(5), 692–699. <https://doi.org/10.1165/rcmb.2009-0359OC>
- Weibel, E. R. (2017). Lung morphometry: the link between structure and function. *Cell and Tissue Research*, 367(3), 413–426. <https://doi.org/10.1007/s00441-016-2541-4>
- Widdicombe, J. H. (2002). Regulation of the depth and composition of airway surface liquid. *Journal of Anatomy*, 201(4), 313–318. <https://doi.org/10.1046/j.1469-7580.2002.00098.x>
- Willis, B. C., & Borok, Z. (2007). TGF- β -induced EMT: Mechanisms and implications for fibrotic lung disease. *American Journal of Physiology - Lung Cellular and Molecular Physiology*, 293(3). <https://doi.org/10.1152/ajplung.00163.2007>
- Willoughby, J. A. (2015). Predicting Respiratory Toxicity Using a Human 3D Airway (EpiAirway™) Model Combined with Multiple Parametric Analysis. *Applied In Vitro Toxicology*, 1(1), 55–65. <https://doi.org/10.1089/aivt.2014.0003>
- Winton, H. L., Wan, H., Cannell, M. B., Gruenert, D. C., Thompson, P. J., Garrod, D. R., Stewart, G. A., & Robinson, C. (1998). Cell lines of pulmonary and non-pulmonary origin as tools to study the effects of house dust mite proteinases on the regulation of epithelial permeability. *Clinical*

and *Experimental Allergy*, 28(10), 1273–1285.
<https://doi.org/10.1046/j.1365-2222.1998.00354.x>

- Wittekindt, O. H. (2017). Tight junctions in pulmonary epithelia during lung inflammation. *Pflugers Archiv European Journal of Physiology*, 469(1), 135–147. <https://doi.org/10.1007/s00424-016-1917-3>
- Wittmann, C., Chockley, P., Singh, S. K., Pase, L., Lieschke, G. J., & Grabher, C. (2012). Hydrogen peroxide in inflammation: Messenger, guide, and assassin. *Advances in Hematology*, 2012. <https://doi.org/10.1155/2012/541471>
- Wong, M. H., & Johnson, M. D. (2013). Differential Response of Primary Alveolar Type I and Type II Cells to LPS Stimulation. *PLoS ONE*, 8(1), 1–13. <https://doi.org/10.1371/journal.pone.0055545>
- Worth, A. P., & Blaauboer, B. J. (2018). Integrated Approaches to Testing and Assessment. In *The History of Alternative Test Methods in Toxicology* (Issue 1). Elsevier Inc. <https://doi.org/10.1016/B978-0-12-813697-3.00032-9>
- Wright, J. L., Cosio, M., & Churg, A. (2008). Animal models of chronic obstructive pulmonary disease. *American Journal of Physiology - Lung Cellular and Molecular Physiology*, 295(1). <https://doi.org/10.1152/ajplung.90200.2008>
- Yang, H., Sun, L., Li, W., Liu, G., & Tang, Y. (2018). In Silico Prediction of Chemical Toxicity for Drug Design Using Machine Learning Methods and Structural Alerts. *Frontiers in Chemistry*, 6(February), 1–12. <https://doi.org/10.3389/fchem.2018.00030>
- Yilmaz, Y., Williams, G., Walles, M., Manevski, N., Krähenbühl, S., & Camenisch, G. (2018). Comparison of Rat and Human Pulmonary Metabolism Using Precision-cut Lung Slices (PCLS). *Drug Metabolism Letters*, 13(1), 53–63. <https://doi.org/10.2174/1872312812666181022114622>
- Zavala, J. (2016). Assessment of Biological Responses of EpiAirway™ 3-D Cell Constructs vs. A549 Cells for Determining Toxicity of Ambient Air Pollution. *Inhal Toxicol*, 28(6), 251–259.
- Zi, Z., Chapnick, D. A., & Liu, X. (2014). *NIH Public Access*. 586(14), 1921–1928. <https://doi.org/10.1016/j.febslet.2012.03.063>. Dynamics